

**Expression analysis and functional studies of Bone
Morphogenetic Protein and Activin Membrane-Bound
Inhibitor (BAMBI) in hepatocellular carcinoma**

PhD thesis

Presented by:

M.Sc. Tatjana Dediulia

In December 2019

Supervisor:

Prof. Dr. Steven Dooley

Dissertation

submitted to the

Combined Faculty of Natural Sciences and Mathematics

of the Ruperto Carola University Heidelberg, Germany

for the degree of

Doctor of Natural Sciences

Presented by

M.Sc. Tatjana Dediulia

Born in: Klaipeda, Lithuania

Oral examination:

**Expression analysis and functional studies of Bone
Morphogenetic Protein and Activin Membrane-Bound
Inhibitor (BAMBI) in hepatocellular carcinoma**

Referees: Prof. Dr. Stefan Wöfl

Prof. Dr. Steven Dooley

*For my parents,
my grandparents and
my husband*

TABLE OF CONTENT

| | |
|--|-----------|
| TABLE OF CONTENT | I |
| ABBREVIATIONS | VI |
| SUMMARY | X |
| ZUSAMMENFASSUNG | XI |
| 1 INTRODUCTION..... | 1 |
| 1.1 Hepatocellular carcinoma | 1 |
| 1.1.1 Background..... | 1 |
| 1.1.2 Histological and molecular changes in HCC..... | 2 |
| 1.1.3 The influence of the liver's microenvironment..... | 2 |
| 1.1.4 Clinical classification of HCC..... | 4 |
| 1.1.5 Molecular classification of HCC..... | 6 |
| 1.2 TGF- β signalling pathway | 8 |
| 1.2.1 TGF- β and signalling components..... | 8 |
| 1.2.2 Canonical TGF- β signalling | 9 |
| 1.2.3 Non-canonical TGF- β signalling | 11 |
| 1.2.4 TGF- β signalling in liver cells | 11 |
| 1.2.5 TGF- β in cancer | 12 |
| 1.2.6 TGF- β signalling regulators (TSRs)..... | 14 |
| 1.3 TGF- β signalling regulation by BAMBI (BMP and activin membrane-bound inhibitor) | 15 |
| 1.3.1 The role of BAMBI in carcinogenesis..... | 17 |
| 1.4 Aims of this study | 18 |
| 2 MATERIALS AND METHODS | 20 |
| 2.1 Materials..... | 20 |
| 2.1.1 Instruments | 20 |
| 2.1.2 Chemicals | 21 |
| 2.1.3 Cell culture | 22 |
| 2.1.3.1 Cell lines | 22 |
| 2.1.3.2 Cell culture reagents and additives | 23 |
| 2.1.3.3 Materials for RNA interference, transfection and adenoviral infection technology | 24 |
| 2.1.3.4 Reagents for Caspase3 assay | 25 |

| | | |
|----------|--|----|
| 2.1.4 | Materials for DNA and RNA work | 26 |
| 2.1.4.1 | Kits, buffers and reagents for RNA isolation, reverse transcription and cDNA synthesis | 26 |
| 2.1.4.2 | Primers for SYBR Green real time PCR..... | 27 |
| 2.1.5 | Materials for SDS-PAGE gel electrophoresis and immunoblot analysis..... | 28 |
| 2.1.5.1 | Buffers and solutions for protein lysis and determination of concentration | 28 |
| 2.1.5.2 | Buffers, reagents and materials for SDS-PAGE gel electrophoresis and immunoblot | 29 |
| 2.1.5.3 | Antibodies, buffers and reagents for protein detection | 30 |
| 2.1.5.4 | Antibodies, buffers and reagents for immunohistochemistry (IHC) | 33 |
| 2.1.6 | Materials for bacterial transformation and plasmid purification | 33 |
| 2.2 | Methods | 34 |
| 2.2.1 | Cell culture | 34 |
| 2.2.1.1 | Cell culture..... | 34 |
| 2.2.1.2 | Cryopreservation of cell lines | 34 |
| 2.2.1.3 | Mycoplasma detection | 34 |
| 2.2.2 | Cell culture experiments..... | 35 |
| 2.2.2.1 | Detection of Smad3/Smad4 reporter activity | 35 |
| 2.2.2.2 | Detection of Smad3/Smad4 reporter activity upon BAMBI infection | 36 |
| 2.2.2.3 | shRNA knockdown of BAMBI..... | 36 |
| 2.2.2.4 | Lentiviral production..... | 37 |
| 2.2.2.5 | Stable BAMBI shRNA knockdown cell lines establishment | 37 |
| 2.2.2.6 | BAMBI over-expression (adenoviral and lentiviral constructs) | 38 |
| 2.2.2.7 | Wound assay | 38 |
| 2.2.2.8 | Counting assay | 39 |
| 2.2.2.9 | Caspase3 assay | 39 |
| 2.2.2.10 | Migration assay..... | 40 |
| 2.2.2.11 | Invasion assay | 41 |
| 2.2.3 | Patient and mouse samples | 41 |
| 2.2.4 | mRNA isolation and expression analysis..... | 42 |
| 2.2.4.1 | RNA isolation from cell cultures using TRIzol® reagent | 42 |

| | | |
|----------|---|-----------|
| 2.2.4.2 | Tissue homogenization using Precellys Evolution Tissue Homogenizer.... | 43 |
| 2.2.4.3 | RNA isolation using InviTrap® Spin Universal RNA Mini Kit..... | 43 |
| 2.2.4.4 | Preparation of whole cell and nuclear RNA..... | 43 |
| 2.2.4.5 | RNA gel electrophoresis | 44 |
| 2.2.4.6 | RNA analysis using Agilent RNA 6000 Nano kit..... | 44 |
| 2.2.4.7 | Reverse transcription | 45 |
| 2.2.4.8 | SYBR® Green real time PCR analysis..... | 45 |
| 2.2.4.9 | Evaluation of real time PCR results..... | 46 |
| 2.2.5 | SDS-PAGE gel electrophoresis and immunoblots analysis | 46 |
| 2.2.5.1 | Protein lysates of cultured cells..... | 46 |
| 2.2.5.2 | Determination of protein concentration..... | 46 |
| 2.2.5.3 | Samples preparation for immunoblot..... | 47 |
| 2.2.5.4 | Preparation of SDS-polyacrylamide gels and gel electrophoresis | 47 |
| 2.2.5.5 | Western blot transfer..... | 48 |
| 2.2.5.6 | Immunodetection of proteins..... | 49 |
| 2.2.6 | Bacterial transformation and plasmid purification | 49 |
| 2.2.6.1 | Bacterial transformation using One Shot® TOP10 Competent Cells | 49 |
| 2.2.6.2 | Plasmids purification using HiSpeed® Plasmid Purification Midi kit..... | 49 |
| 2.2.7 | Immunohistochemistry of paraffin embedded samples..... | 50 |
| 2.2.8 | Statistical Analysis | 51 |
| 2.2.8.1 | Statistical analysis of experimental work | 51 |
| 2.2.8.2 | Analysis of publicly available HCC data | 51 |
| 3 | RESULTS | 54 |
| 3.1 | BAMBI expression meta-analysis in publicly available data sets from HCC patient cohorts and mice models | 54 |
| 3.1.1 | BAMBI is significantly upregulated in more than 70% of HCC patients from different cohorts and aetiologies..... | 54 |
| 3.1.2 | BAMBI expression in chemically-induced liver carcinogenesis (DEN) and genetic (MDR2-KO) mice models..... | 55 |
| 3.1.3 | Correlation with clinical-pathological data..... | 58 |
| 3.2 | Expression analysis of BAMBI in HCC cell lines | 60 |

| | | |
|----------|---|-----------|
| 3.2.1 | BAMBI is expressed differently in in HCC cell lines with early (epithelial phenotype) <i>versus</i> late (mesenchymal phenotype) TGF- β signature | 60 |
| 3.2.2 | BAMBI antibody evaluation and protein expression in HCC cell lines..... | 62 |
| 3.2.2.1 | BAMBI antibody evaluation..... | 62 |
| 3.2.2.2 | BAMBI mRNA accumulation in the nucleus of HLE cells..... | 63 |
| 3.2.2.3 | Confirmation of ectopic BAMBI protein expression and effects in HLE cells..... | 65 |
| 3.3 | Selection between TGF- β - and BMP-signalling pathways | 66 |
| 3.3.1 | BAMBI expression upon cytokine treatment in Hep3B and HLE cells..... | 66 |
| 3.3.2 | Correlation of BAMBI expression with TGF- β - and BMP-target genes in HCC patients cohorts..... | 67 |
| 3.3.3 | Effects of BAMBI modulation on SMAD3 activity in Hep3B and HLE cells.... | 68 |
| 3.4 | BAMBI protein expression in paraffin-embedded HCC patient tissues..... | 72 |
| 3.4.1 | BAMBI is upregulated in 50% of HCC tissue samples..... | 72 |
| 3.4.2 | BAMBI is upregulated in 76% of samples in an HCC Tissue Microarray (TMA) . 73 | |
| 3.4.3 | Presence and/or absence of BAMBI impacts on pSMAD2 staining | 77 |
| 3.5 | BAMBI effects on proliferation and apoptosis in HLE and Hep3B cells | 78 |
| 3.5.1 | Proliferation changes following BAMBI up- or downregulation | 78 |
| 3.5.2 | BAMBI blocks the apoptotic effect of TGF- β signalling | 81 |
| 3.6 | BAMBI modulation effects on migration and invasion in HLE and Hep3B..... | 84 |
| 3.6.1 | HLE cells with BAMBI overexpression display enhanced migration..... | 84 |
| 3.6.2 | Invasion increases upon BAMBI overexpression in HLE cells | 89 |
| 3.7 | Influence of BAMBI modulation on other signalling pathways | 92 |
| 4 | DISCUSSION | 95 |
| 4.1 | Upregulated BAMBI expression in human hepatocellular carcinoma tissues and mice models | 95 |
| 4.2 | BAMBI expression correlation with clinical-pathological characteristics of HCC patients..... | 96 |
| 4.3 | Differential BAMBI expression in HCC cell lines | 96 |
| 4.4 | BAMBI effects on apoptosis..... | 97 |
| 4.5 | BAMBI effects on proliferation, migration and invasion | 97 |
| 4.6 | BAMBI in cholangiocarcinoma..... | 98 |

| | | |
|-----|---|------------|
| 4.7 | BAMBI, a potential therapeutic target for personal HCC therapies..... | 100 |
| | REFERENCES | 101 |
| | LIST OF FIGURES | 115 |
| | LIST OF TABLES..... | 117 |
| | DECLARATION..... | 118 |
| | ACKNOWLEDGEMENT | 119 |

ABBREVIATIONS

| | |
|--------------------|---|
| °C | Degree Celsius |
| AASLD | American Association for the Study of Liver Disease |
| ACTB | Beta actin |
| Ad | Adenovirus |
| AFB1 | Aflatoxin B1 |
| AFP | Alpha-fetoprotein |
| AJCC | American Joint Committee on Cancer |
| AKT | Alpha serine/threonine-protein kinase |
| ALK | Activin receptor-like kinase |
| AMH | Anti-Müllerian hormone |
| AML1 | Acute myeloid leukemia 1 protein |
| AP | Alkaline phosphatase |
| AP1 | Activator protein 1 |
| APS | Ammonium persulfate |
| APTT | Activated partial thromboplastin time |
| ARE | Activin response element |
| BAMBI | Bone morphogenetic protein and activin membrane-bound inhibitor |
| BCL2 | B-cell lymphoma |
| BCL9-2 | B-cell lymphoma 9-2 protein |
| BCLC | Barcelona-Clinic Liver Cancer |
| BDEC | Bile duct epithelial cells |
| BDL | Bile duct-ligated |
| BIM | Bcl-2 interacting mediator of cell death |
| BMP | Bone morphogenetic protein |
| BMPR | BMP receptor |
| BSA | Bovine serum albumin |
| Cas3 | Caspase 3 |
| CCA | Cholangiocarcinoma |
| CCL4 | Carbon tetrachloride |
| CD | Cluster of differentiation |
| CDC42 | Cell division control protein 42 |
| CDK | Cyclin dependent kinase |
| cDNA | Complementary DNA |
| c-Jun | Transcription factor AP-1 |
| CLD | Chronical liver disease |
| cm | Centimeter |
| c-Myc | Cellular homologue of myelocytomatosis |
| ColA1 | Collagen A1 |
| CTGF | Connective tissue growth factor |
| DAB | 3,3'-Diaminobenzidine |
| DAP | Death-associated protein |
| DAXX | Death associate protein 6 |
| ddH ₂ O | Double distilled water |
| DEN | Diethyl nitrosamine |
| DEPC | Diethyl pyro carbonate |
| DMEM | Dulbecco's modified eagle medium |

| | |
|--------------|--|
| DMSO | Dimethyl sulfoxide |
| DNA | Deoxyribonucleic acid |
| dNTP | Deoxyribonucleide |
| DTT | Dithiothreitol |
| e.g. | "exempli gratia" (for example) |
| EASL | European Association for Study of the Liver |
| ECM | Extracellular matrix |
| EGF | Epidermal growth factor |
| EGFP | Enhanced green fluorescent protein |
| EMT | Epithelial-mesenchymal transition |
| EpCAM | Epithelial cell adhesion molecule |
| ERK | Extracellular signal-regulated kinase |
| FBS | Fetal bovine serum |
| g | Gram |
| GAPDH | Glyceraldehyde 3-phosphate dehydrogenase |
| GDF | Growth and differentiation factor |
| GEO | Gene Expression Omnibus |
| GFP | Green fluorescent protein |
| GSE | Genomic Spatial Event |
| h | Hour |
| H3B | Hep3B cell line |
| H3B Mock | Hep3B cells infected with pLV empty vector |
| H3B shBAMBI | Hep3B cells infected with pLV-shRNA against BAMBI |
| HAMP | Hepcidin |
| HBeAb | Hepatitis B antibody |
| HBeAg | Hepatitis B antigen |
| HBSS | Hank's buffered salt solution |
| HBV | Hepatitis B virus |
| HCC | Hepatocellular carcinoma |
| HCl | Hydrochloric acid |
| HCV | Hepatitis C virus |
| HEK293T | Human embryonic kidney 293 cell line with SV40 T-antigen |
| HGF | Hepatocyte growth factor |
| Hh | Hedgehog |
| HLE BAMBI | HLE cells infected with overexpression pLV BAMBI |
| HLE Mock | HLE cells infected with pLV empty vector |
| HSC | hepatic stellate cells |
| ICAT | Inhibitor of β -catenin-TCF |
| iCOD | Integrated Clinical Omics Database |
| ID1 | Inhibitor of DNA binding 1 |
| IHC | Immunohistochemistry |
| IKK α | I κ B kinase α |
| IL | Interleukin |
| IP | Immunoprecipitation |
| iRNA | Interfering RNA |
| ISH | In situ hybridization |
| I-Smad | Inhibitory Smad |
| IUCC | International Union for Cancer Control |

| | |
|----------------|--|
| JAK | Tyrosine-protein kinase |
| JIS | Japan Integrated Staging |
| JNK | Stress-activated protein kinase |
| KCl | Potassium chloride |
| kDa | Kilo Daltons |
| L | Liter |
| LAP | Latency associated protein |
| LCSGJ | Liver Cancer Study Group of Japan |
| LSEC | Liver sinusoidal endothelial cells |
| LTBP | Latent TGF- β binding protein |
| LV | Lentivirus |
| M | Molar |
| mA | Milliampere |
| MAD1 | Myc oncogene antagonist |
| MAPK | Mitogen-activated protein kinase |
| MCL1 | Myeloid leukemia cell differentiation protein |
| MDR2-KO | Multidrug resistance gene 2 knockout |
| mg | Milligram |
| MH | Mad Homology |
| min | Minute |
| ml | Milliliter |
| mM | Millimolar |
| mm | Millimeter |
| MMP | Matrix metalloproteinase |
| MOI | Multiplicity of infection |
| mRNA | Messenger RNA |
| NaCl | Sodium chloride |
| NaOH | Sodium hydroxide |
| NASH | Non-alcoholic steatohepatitis |
| NF κ B | Nuclear factor NF-kappa-B |
| ng | Nanogram |
| NL | Normal liver |
| nm | Nanometer |
| OS | Overall survivor |
| p | p-value |
| PAI-1/SERPINE1 | Plasminogen activator inhibitor-1 |
| PAK | Serine/threonine protein kinase |
| Par | Polarity protein |
| PCNA | Proliferating cell nuclear antigen |
| PET | Polyethylene terephthalate |
| PI3K | Phosphoinositide 3-kinase |
| PIC | Protease inhibitor, Complete |
| pLV | Lentiviral plasmid |
| pM | Picomolar |
| pP38 | 38 kDa phosphoprotein |
| PPIA | Peptidyl prolyl isomerase A |
| PT | Prothrombin time |
| qRT-PCR | Quantitative real-time polymerase chain reaction |

| | |
|-----------------------|--|
| <i>r</i> | Pearson correlation coefficient |
| Rac1 | Ras-related C3 botulinum toxin substrate 1 |
| RhoA | Ras homolog gene family, member A |
| RIN | RNA integrity number |
| RNA | Ribonucleic acid |
| ROS | Reactive oxygen species |
| rpm | Rotations per minute |
| rRNA | Ribosomal RNA |
| rS18 | Ribosomal protein 18 40S small ribosomal subunit |
| R-Smad | Receptor Smad |
| RT | Room temperature |
| s | Second |
| SBE | Smad binding element |
| SD | Standard deviation |
| SDS | Sodium dodecyl sulfate |
| SE | Standard error |
| shRNA | Short hairpin RNA |
| siRNA | Small interfering RNA |
| SMAD | Mothers against decapentaplegic |
| Sp-1 | Stimulation protein 1 |
| ST | Surrounding tissue |
| STAT | Signal transducer and activator of transcription |
| TAK1 | TGF- β -associated kinase 1 |
| TDGF1/Cripto | Teratocarcinoma-Derived Growth Factor 1 |
| TGF- α | Transforming growth factor alpha |
| TGF- β | Transforming growth factor beta |
| TGF- β 1 | Transforming growth factor beta isoform 1 |
| TGF- β 2 | Transforming growth factor beta isoform 2 |
| TIF1 γ /TRIM33 | Transcription intermediate factor 1 γ |
| TLR4 | Toll-like receptor 4 |
| TMA | Tissue microarray |
| TNF | Tumor necrosis factor |
| TRAF6 | TNF receptor associated factor 6 |
| TSR | TGF- β signalling regulator |
| TTR | Time to recurrence |
| T β RI/TGFBRI | TGF- β receptor 1 |
| T β RII/TGFBRII | TGF- β receptor 2 |
| V | Volt |
| VEGF | Vascular endothelial growth factor |
| Wnt | Wingless-type MMTV integration site family |
| xg | Earth's gravitational force |
| α SMA | Alpha-smooth muscle actin |
| μ g | Microgram |
| μ l | Microliter |
| μ M | Micromolar |

SUMMARY

Hepatocellular carcinoma (HCC) is a complex disease with a poor prognosis which has increased the survival rates on account to the improvement in patient stratification and the introduction of new targeted therapies. However, there is still an urgent need for early diagnostic markers and personalized treatments in order to enhance the survival and reduce HCC's recurrence. BAMBI, a transmembrane glycoprotein that regulates several biological activities through TGF- β signalling inhibition, was shown to have increased expression levels in colorectal, gastric and ovarian cancers where it correlated with metastasis, invasion and poor prognosis. Although in HCC BAMBI was reported to be upregulated, no molecular and functional studies were done so far to unravel its participation in hepatocarcinogenesis.

Our meta-analysis in publicly available HCC data cohorts confirmed BAMBI overexpression in 78% of HCC patients (n=803) being upregulated and also present in cirrhotic samples and the tumour stroma. Further, BAMBI expression was also confirmed in MDR2-KO and DEN mice. Parallel to these results, the immunohistochemical (IHC) staining of a human HCC tissue microarray revealed the upregulation in 76% of patients with positive staining for BAMBI in the surrounding tissues. In HCC cell lines, BAMBI expression appeared only in the cells that present early TGF- β signature (Hep3B, HepG2 and HUH7), which corresponds to an epithelial phenotype and less aggressiveness. BAMBI knockdown in Hep3B cells produced a strong TGF- β -mediated apoptosis and reduced cell proliferation. In less differentiated HLE cells with low intrinsic BAMBI expression, BAMBI overexpression enhanced proliferation, migration and invasion *in vitro*. Immunoblot assays additionally show BAMBI expression dependent modulation of ERK1/2, NF κ B, Wnt/ β -catenin, AKT and JNK/p38 MAPK pathways.

In conclusion, we report that bone morphogenetic protein and activin membrane-bound inhibitor (BAMBI) is upregulated in livers of HCC patients and differently expressed in HCC cell models. High BAMBI expression is blocking TGF β -mediated apoptosis and increases proliferation in epithelial HCC cells, and reduces proliferation, migration and invasion with impact on Wnt/ β -catenin, ERK1/2, AKT, NF κ B and JNK/p38 MAPK pathways in mesenchymal HCC. The activation of these functions depends on the TGF- β signature stage and cell context. We postulate BAMBI as a potential target in personalized therapies for human hepatocellular carcinoma.

ZUSAMMENFASSUNG

Das Hepatozelluläre Karzinom (HCC) ist eine komplexe Erkrankung, die häufig mit schlechter Prognose einhergeht. In den letzten Jahren haben sich die Überlebensraten aufgrund verbesserter Stratifizierung von Patienten und Einführung neuer zielgerichteter Therapien erhöht. Es besteht immer noch ein dringender Bedarf an frühen diagnostischen Markern und personalisierten Behandlungen, um die Überlebensraten von Patienten zu erhöhen und das Wiederauftreten von HCC zu reduzieren. BAMBI, ein Transmembranglycoprotein, das mehrere biologische Aktivitäten durch die Hemmung von TGF- β -Signalen reguliert, zeigt bei Darm-, Magen- und Ovarialkarzinomen eine erhöhte Expression, die mit Metastasen, Invasion und schlechter Prognose korreliert. Obwohl gezeigt wurde, dass BAMBI in HCC hochreguliert ist, wurden bisher keine molekularen und funktionellen Studien durchgeführt, um die Beteiligung an der Hepatokarzinogenese aufzuklären.

Unsere Meta-Analyse von öffentlich zugänglichen HCC-Datenkohorten bestätigt, dass BAMBI bei 78% der HCC-Patienten (n = 803) überexprimiert ist. Eine Hochregulation war auch in zirrhotischen und Stromaprobe vorherrschend. Ferner konnte eine erhöhte BAMBI-Expression in MDR2-KO- und DEN-Mäusen bestätigt werden. Parallel zu diesen Ergebnissen, zeigten immunohistologische Färbungen von BAMBI in menschlichen HCC-Geweben die Überexpression bei 76% aller Patienten. In HCC-Zelllinien konnte eine erhöhte BAMBI-Expression nur in Zellen mit „früher TGF- β -Signatur“ (Hep3B, HepG2 und HUH7) gezeigt werden, was einem epithelialen-Phänotyp und einer geringeren Aggressivität entspricht. Ein funktionales Herunterregulieren von BAMBI in Hep3B-Zellen induzierte eine starke TGF- β -vermittelte Apoptose und verringerte die Zellproliferation. In weniger differenzierten HLE-Zellen verstärkte eine BAMBI-Überexpression die Proliferation, Migration und Invasion in vitro. Auf Proteinebene konnten Veränderungen der ERK1/2, AKT, NF κ B und JNK/p38 MAPK Signalwege durch die Modulation von Bambi demonstriert werden.

Zusammenfassend konnten wir ausführlich zeigen, dass BAMBI in vitro in verschiedenen HCC Zelllinien mit unterschiedlichem Phänotyp auch unterschiedliche Funktionen ausübt, von der Blockierung der TGF β -vermittelten Apoptose bis hin zu zunehmender Proliferation, Migration und Invasion, die mit Veränderungen der Signalkaskaden von Wnt / β -Catenin, ERK1 / 2-, AKT-, NF κ B- und JNK / p38-MAPK einhergeht. Die Aktivierung dieser Funktionen hängt vom „TGF- β -Signatur-Stadium“ und dem Zellkontext ab. Durch unsere Ergebnisse postulieren wir BAMBI als potentielles Zielprotein für personalisierte Therapien hepatozelluläre Karzinom.

1 INTRODUCTION

1.1 Hepatocellular carcinoma (HCC)

1.1.1 Background

Liver cancer is the fifth most common type of cancer worldwide and includes cholangiocarcinoma, hepatoblastoma and hepatocellular carcinoma (HCC) as the primary liver cancers [1]. The rate of annually diagnosed cases ranges from 500.000 to 1.000.000, resulting in 600.000 deaths per year due to HCC's scarce survival rate [2, 3]. The major risk factors for HCC include cirrhosis, chronic HBV or HCV infection, exposure to mycotoxin aflatoxin B1 (AFB1) and non-alcoholic steatohepatitis (NASH). There are also some less common causes, such as hereditary hemochromatosis, alpha1-antitrypsin deficiency, autoimmune hepatitis, obesity and diabetes [4-6]. Usually, HCC appears late in life following a progressive chronic liver disease lasting years or even decades. The different subtypes and phenotypes of HCC suggest that it might originate from different cell types of the liver, including the progenitor cells, and not only from hepatocytes, as was the accepted opinion in the past [7-9].

Hepatocytes make up the main population of liver cells and perform the major part of the metabolic duties, but they are not the only ones present in this complex network forming the liver. Other non-hepatocyte cell types include stromal cells, such as hepatic stellate cells (HSC) and fibroblasts, which produce the extracellular matrix (ECM) and have a structural role; immune cells, mainly macrophages or Kupffer cells and some inflammation-recruited leukocytes; epithelial cells or cholangiocytes in the bile ducts; endothelial cells such as liver sinusoidal endothelial cells (LSEC) lining the blood vessels; and liver progenitor cells, which are able to produce both hepatocyte and non-hepatocyte cells [7-9]. All of them may have a function in the initiation and progression of HCC, leading to a highly interconnected process in which malignant cells develop and are maintained.

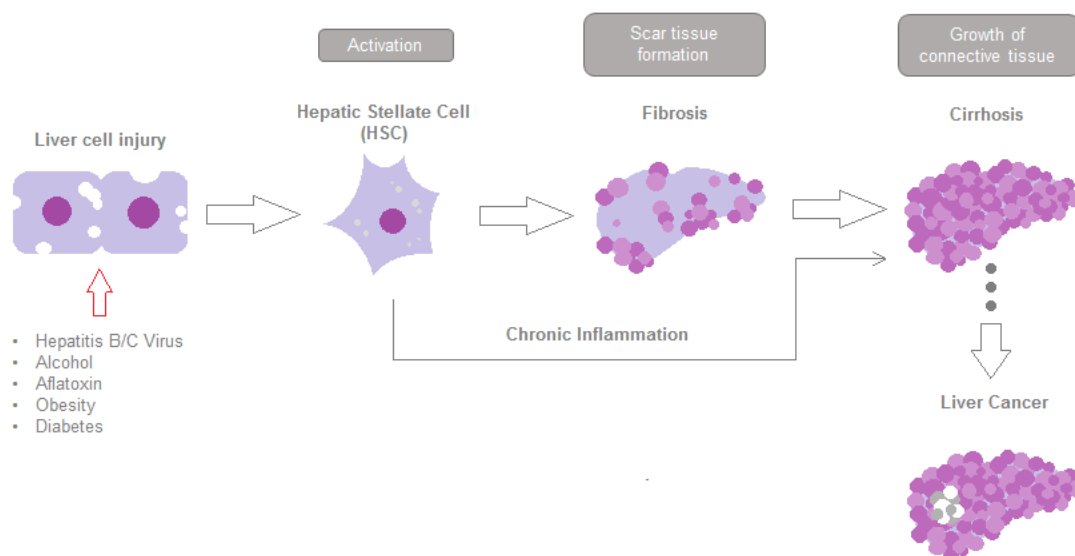


Figure 1.1 Schematic representation of liver cancer formation (adapted from the Proteintech blog). Following liver damage, the quiescent HSCs become activated and transform into highly proliferative myofibroblast-like cells. After this activation, fibrogenesis starts, leading to cirrhotic liver and liver cancer.

1.1.2 Histological and molecular changes in HCC

The histological appearance of HCC is greatly variable; therefore, tumour cells are identified based on (1) a high nuclear-to-cytoplasmic ratio, (2) prominent nuclei and nucleoli, (3) nuclear irregularity, (4) moderate eosinophilia and (5) granular cytoplasm. The progression of HCC is associated with histological dedifferentiation from well, moderately or poorly differentiated morphology [10, 11]. Other signs of HCC progression are changes in subcellular organelles (fewer and smaller mitochondria) and higher amounts of endoplasmic reticulum and free ribosomes [12, 13].

At the molecular level, several alterations in the DNA genome have been discovered in HCC. These alterations include DNA mutations in oncogenes and tumour suppressor genes, and changes in the number of chromosomal copies [14-16]. Epigenetic alterations have been seen in several HCC-driving pathways, e.g., CpG methylation in the promoter genes of the JAK/STAT pathway. The activating phosphorylation of the STAT3 transcription factor has been reported in a high percentage of HCC tumours and is associated with cell differentiation, proliferation, and apoptosis [17-19]. An excess of cytokine signalling, e.g., IL-6, can activate this pathway without any molecular alterations, supporting the hypothesis that the liver microenvironment can stimulate HCC development and progression [20, 21].

One of the typical differentially expressed pathways in HCC is the Wnt, which has been reported as upregulated in 90% of the cases. This pathway regulates the expression of genes associated with proliferation, metabolism and ECM remodelling, such as c-Myc, c-Jun, cyclin D1 and matrix metalloproteinases (MMPs). Even though the functional extent of this pathway is very broad, it may collaborate with the p53 tumour suppressor gene [22, 23]. Another alteration occurs in the Hedgehog (Hh) signalling pathway, which has been found to be upregulated in 60% of the tumours. Hh is involved in embryonic tissue development and its inhibition produces a decrement in the proliferation and an increment in the apoptosis of HCC cell lines with Hh overexpression [24, 25]. However, changes in these pathways alone are not enough to develop HCC.

The list of molecular alterations is long and still incomplete. Some of the carcinogenic pathways are very complex and have not been characterised completely, adding more difficulty to the study of HCC development, since most of them are interconnected. Commonly, these pathways result in the upregulation of genes involved in the cell cycle and in proliferation and escape from apoptosis, allowing faster tumour growth and overcoming the cell cycle checkpoints.

Considering the heterogeneity of HCC subtypes, large gene panels have been used to assess the risks of HCC initiation, progression and recurrence. Single genes or pathways are no longer useful, and the results of transcriptome analysis have shown heterogeneous molecular profiles that might lead to a variety of curative responses [26].

1.1.3 The influence of the liver's microenvironment

The microenvironment (also referred to as stroma in cancer) is a complex system consisting of the extracellular matrix (ECM), proteins and proteoglycans, small signalling molecules and soluble factors (cytokines and chemokines) and a variety of cell types

such as immune cells, endothelial cells and fibroblasts. The microenvironment's main duty is to modulate the epithelium cell fate and to serve as a barrier to cell transformation. The dynamic communication with the epithelium modulates cell growth and apoptosis, and maintains the polarity and differentiation of the epithelial cells. Drastic changes, such as the recruitment and activation of microenvironment cells and the remodelling of ECM, occur in this system during cancer formation. Moreover, tumour-stroma crosstalk can influence the tumour cells' phenotype and promote selective pressure for tumour initiation, progression and metastasis [21, 27].

The liver microenvironment is a highly interconnected network that drives key factors such as chronic inflammation, tissue remodelling, genetic alterations and alterations in cellular signalling [28]. For example, human exposure to mycotoxin aflatoxin B1 (AFB1) has been associated with mutations in the tumour suppressor gene p53, which suppresses the G1 checkpoint arrest and leads to a higher mutation rate [29]. Consequently, the derived genetic diversity increases DNA mutations and is postulated to decrease the effects of chemotherapeutics.

Chronic inflammation contributes to HCC initiation and progression, but its causes are diverse, including HBV/HCV infection and ethanol consumption [30]. The continuous production of ROS, such as hydrogen peroxide, hydroxyl radicals and superoxide radicals, by immune-mediated cell death due to chronic HBV and HCV infection or ethanol consumption results in increased oxidative stress, which can promote the proliferation of hepatocytes and lead to a large number of DNA mutations [31, 32]. The shortening of telomeres as a consequence of this proliferation is associated with chromosomal instability and progression to HCC [33].

Another characteristic is the altered cytokine expression, which produces an excess of ECM formation by hepatic stellate cells. This tissue remodelling manifests as fibrosis and later as cirrhosis. The process involves different cell types such as stromal cells (fibroblasts and HSCs), immune cells (macrophages) and tumour cells. All these factors change the balance between ECM degradation and synthesis, leading to ECM accumulation [34, 35]. An excess of ECM is classified as fibrosis, which can progress to cirrhosis once the excess starts to enclose entire liver lobules. Cirrhosis is present in the majority (up to 80%) of HCC patients, suggesting that the accumulation of ECM is one of the main drivers of HCC progression [6]. The hypoxia resulting from the altered blood flow activates the response of both tumour and non-tumour cells through upregulation of angiogenic factors, such as the vascular endothelial growth factor (VEGF). HSCs and liver endothelial cells stimulate vascular growth as a response to the VEGF, creating the chaotic angiogenesis characteristic in tumours. This angiogenesis is not sufficient to relieve the hypoxia; therefore, areas of hypoxia pockets still exist, which leads to even greater angiogenesis [36-38]. This process is also related to chemotherapy resistance, as it means that reduced amounts of active agents reach the HCC tumours.

Last but not least, an important factor in HCC progression is the altered crosstalk between hepatocytes and stromal cells. Altered stromal cells have been reported to drive HCC development through TGF- β secretion, which leads to activation of oncogenic pathways in the tumour cells when implanted in p19ARF-knockout mice [39, 40]. There are some known pathways involved in tumour-initiated alterations in ECM interactions, such as downregulation of cadherins (E-cadherin), upregulation of MMP activity and epithelial-mesenchymal transition (EMT) [41-43]. For example, an altered Hh pathway

induces the activation of HSCs and hepatic progenitor cells driving the fibrogenic process and thereby stimulating tumour progression [44].

All these facts support the hypothesis that the microenvironment is a major player in HCC initiation and progression. Hence, it should be taken into account and should be further investigated.

1.1.4 Clinical classification of HCC

One of the main functions of cancer classification is to facilitate prognosis and selection of the best treatment for the patients. Although many established classifications exist, just a few of them include molecular data. This is the case for HCC classifications, where so far no molecular data has been included and these classifications are mostly used for clinical management of HCC.

A perfect staging system should be as simple and quick as possible, with the aim being to assess the prognosis and enable better therapeutic decisions. In order to be used on a large scale, the system must be reproducible and transportable to other populations related to the one used to develop the staging system [45].

The Okuda staging system suggested by Okuda *et al.* [46] in 1984 divides patients into two dimensional groups depending on the volume of the tumour (< or > 50% occupancy of the liver) and the liver function parameters (albumin >or< 3 g/dL, bilirubin <or> 3 mg/dL and ascites 0/1). Despite having been in use for almost two decades, it has been hardly able to discriminate small tumours with <50% occupancy and does not include several variables that have been identified over the years. The TNM staging algorithm developed by the American Joint Committee on Cancer (AJCC) and the International Union for Cancer Control (IUCC) includes criteria that have been regularly updated since 1977. This system assesses primary tumour features (T), the presence or absence of nodal involvement (N) and distant metastasis (M). Some other characteristics may be included, such as the histologic grade (G) and the fibrosis score (F), without any effect on staging [49]. The TNM is a good example of an inadequate staging system as a prediction model because it is only able to assess the extension of the tumour. Other scores successfully take into account not only the tumour characteristics but also the liver function. The Cancer of the Liver Italian Program (CLIP) score incorporates the Child-Pugh stage, tumour morphology (uninodular, multinodular, massive), extension in the liver, AFP levels and the presence or absence of portal vein thrombosis. This system distinguishes patients into six categories and has been validated on Japanese, Canadian, German and Korean patients, performing better than other scores [50]. The main problem is that it is unable to identify the early stages, which are responsive to surgical or percutaneous therapies. Several investigators have suggested that the CLIP score is superior to contemporary systems but should be improved, including the performance status [45].

One of the most frequently applied systems is the Barcelona-Clinic Liver Cancer (BCLC) classification, which is considered the standard HCC system by the American Association for the Study of Liver Disease (AASLD) and the European Association for Study of the Liver (EASL). The BCLC system takes into account the size and extent of the primary tumour as well as liver function and physiological factors, and incorporates

the Okuda stage and the Child-Pugh score [47, 48]. The tumour stages are linked to treatment strategies and have four classification groups: early, intermediate, advanced and end-stage. The early stage encompasses patients whose survival rate five years after resection, transplantation or percutaneous treatments is 50% to 70%. The tumour status in this stage is defined by the size of the main nodule and its multi-centricity, including single nodules ≤ 2 cm in size, single ones 2-5 cm in size and three nodules ≤ 3 cm in size. These are well-differentiated HCCs that show bile ducts and portal veins without invasion of any other structure. The intermediate stage includes multinodular tumours without an invasive pattern with a median of 16 months of survival, which could be expanded to 19-20 months using chemoembolization. The advanced stage classifies patients with symptomatic tumours and vascular invasion whose survival is only six months. Finally, the end-stage includes patients presenting Okuda stage III (3-4 factors present, such as tumour size $>50\%$ of the liver, ascites, albumin <3 g/dL, bilirubin >3 mg/dL) with a median survival of 3-4 months [47]. Even though it is widely used and accepted, the BCLC score is not a perfect classification system. Patients classified under the intermediate stage can vary from those with small tumours to those in which almost the whole liver is replaced by the tumour, but without vascular invasion or compromised liver function. Those characteristics would upgrade the patients to the advanced stage. Consequently, the old classifications have been combined and new ones have been developed in order to complete the BCLC and other systems or to overcome their lacks or deficiencies.

761 HCC patients from France, Belgium and Canada were used to develop the GRETCH (Groupe d'Etude et de Traitement du Carcinome Hépatocellulaire) score, which includes five prognostic factors (Karnofsky index, bilirubin, alkaline phosphatase, AFP > 35 pg/L and portal obstruction) that divide the patients into four groups. This system is not widely used due to its lack of validation [52]. Many other prognostic scores have been developed from Asian cohorts. For example, the Tokyo score [53] arose from 403 Japanese patients after percutaneous ablation. It includes four parameters (albumin, bilirubin, size and number of tumours) that separate the patients into three groups. Despite its good predictive power, which is even better than the BCLC, it poorly fits to advanced stages because it was derived from early-HCC patients. In 2003, the Liver Cancer Study Group of Japan (LCSGJ) argued that the CLIP score did not provide an accurate prognosis for early-stage patients and proposed the Japan Integrated Staging (JIS) score [51]. This system integrates the TNM and the Child-Pugh scores. It was developed using a cohort of 722 Japanese patients and produced a better survival prognosis than CLIP, particularly in early-stage patients. However, the JIS score has not been validated in Western populations and still lacks the integration of biomarkers. The Chinese University Prognostic Index (CUPI) [54] for HCC produces three classes of risk based on survival. It was developed on a cohort of 926 Chinese patients using the TNM score and including total bilirubin, ascites, AP, AFP and asymptomatic disease status. Since all the patients were mono-ethnic and presented HBV infection, the transportability of this score is highly affected.

Many studies have investigated the power of prediction of all these different staging scores and systems, showing conflicting results. In separate studies, the BCLC presented the best predictive power when compared with the TNM, CUPI, GRETCH, CLIP, JIS, Okuda and Tokyo scores, on a cohort of 244 U.S. American patients and 1717 treatment-naïve Asian patients [55, 56].

However, other studies showed that the CLIP had the best long-term prognostic capacity in a mixed-HCC cohort of patients presenting early to advanced stages, while the BCLC was more useful for predicting the survival of treated patients [57, 58].

In conclusion, HCC have a heterogeneous nature, which makes it difficult to establish a universally accepted staging system. Characteristics such as the location of the tumour or its proximity to major vessels are not taken into account. Additionally, the deterioration time of the underlying liver disease is difficult to calculate since patients can be stable for a long period of time before suffering from liver failure. Moreover, most prognostic models are unreliable due to time-varying predictors. Finally, risk factors and the complex tumour biology of HCC are not integrated by any of these systems.

1.1.5 Molecular classification of HCC

Gene expression profiling has shed new light on the pathogenesis of HCC and its heterogeneous origins. Apparently, there are some common molecular subclasses associated with prognosis that may be enriched in subsets of HCC according to the aetiology of the liver disease. According to this information, the biology of tumours could play a key role in staging and also impact the response to therapies [59-61].

Preliminary studies have shown that tumours could be classified depending on their molecular biology. Several molecular signatures arisen to predict recurrence and cancer outcomes. In 2008, Coulouarn *et al.* [62] studied the TGF- β gene expression signature to improve the prognosis and diagnosis predictions of HCC. They hypothesised that since TGF- β can act both as a tumour suppressor and as a tumour promotor, the identification of a gene signature linked to this pathway could lead to the identification of more homogeneous and clinically relevant groups in liver cancer patients. They found specific TGF- β -responsive genes in primary mouse hepatocytes upon TGF- β stimulation and successfully demonstrated that the TGF- β gene expression signature could discriminate between TGF- β -positive and TGF- β -negative human HCC in a cohort consisting of 139 patients. In addition, they discovered two subsets of tumours within TGF- β -positive HCCs that expressed either early or late TGF- β -responsive genes. This result was further validated in a 104 HCC cohort and HCC cell lines identifying them by their invasion capacity. Late-signature patients presented higher recurrence and less survival time compared to early TGF- β signature patients. Furthermore, similar results were obtained in lung adenocarcinoma patients, suggesting that this signature could be generally applied in the molecular prognosis of cancer.

Another study established a 153-gene molecular signature from 67 HCC samples, which allowed classifying metastatic patients and identifying survival-related genes [63]. Different studies tried to identify recurrence-related genes, finding a 12-gene signature that predicted aggressive behaviour and a 20-gene signature that independently could predict recurrence in Japanese patients [64, 65].

As a result of several molecular analyses and through integration of genomic, transcriptomic and epigenomic profiling from many tumours, two molecular subtypes of HCC have been established: a proliferation class and a non-proliferation class [66-68].

As indicated by its name, the proliferation class presents the activation of cell proliferation and survival pathways such as PI3K/AKT/mTOR, Ras/MAPK and MET. In this class, the HCC patients can be divided into two further subclasses (S1 and S2), which share the activation of E2F1 and the inactivation of TP53, but also present different molecular changes. The S1 subclass is characterised by the activation of the TGF- β and Wnt pathways, while the S2 subclass or progenitor cell group mainly presents AFP, IGF2, and EPCAM overexpression and IFN-related gene downregulation. In general, the proliferation class has been associated with aggressiveness, larger tumour size and poor histological differentiation, as well as HBV aetiology and poor outcomes [67, 68].

The non-proliferative or less aggressive class (S3) is still highly heterogeneous and characterised by more differentiated tumours, normal liver function and the activation of several metabolism, detoxification and protein synthesis pathways. It has been theorised that this class could be divided into three subclasses, but so far only one (S3) has been clearly defined [66, 69]. Canonical Wnt signalling pathway activation due to CTNNB1 mutation [70] and TERT promotor mutations are distinctive of this class. Patients in this class correlated with better outcomes and were associated with alcohol and HCV aetiologies.

The molecular information provided so far has helped to identify the dysregulation of multiple pathways and their heterogeneous involvement across HCC and will benefit the design of personalised targeted therapies. Furthermore, the genetic expression of pre-cancerous stages, which usually present cirrhosis or chronic hepatitis, could help to predict the outcome. Besides, many studies have shown the involvement of the tumour microenvironment (TME) in HCC development [71, 72], but very few studies have targeted the different cell populations or the stroma for better clarification. In line with these studies, a new molecular classification of HCC based on immune status has arisen: immune class, immune intermediate class and immune excluded class [73]. The immune class (30% of HCC) shows high levels of immune cell infiltration, PD1 and PD-L1 expression, IFN γ signalling activation and no CTNNB1 mutations. Just like the proliferative class, the immune class is divided into two subclasses: the active immune class, with an adaptive T-cell response, and the exhausted immune class, with TGF- β regulated gene expression involved in immunosuppression and T-cell debilitation. CTNNB1 mutations and T-cell exclusion from the TME are characteristics of the immune excluded class, which overlaps with the non-proliferative class. The immune intermediate stage comprises about 45% of all HCC cases and its definition is less clear. An enhancement in chromosomal aberrations, such as copy number variation and mutations, and a decrement of immune cell infiltration are some characteristics of this class [73].

Currently, earlier detection of HCC at the curative stage is improving the outcome of patients undergoing liver transplantation, but the curative response varies due to the heterogeneous aetiology and molecular profiles of HCC patients [47, 74]. This represents a challenge in the search for better early diagnosis of molecular markers and personalised treatments. Potentially curative therapies such as surgical resection, transplantation and percutaneous ablation are only available to patients with limited progression of the disease (around one third of the cases). The patients die from liver

failure and most of them are diagnosed at advanced disease stages [67]. There is a need for further analysis of the molecular landscape in order to translate current knowledge into predictive and/or prognostic biomarkers, with the ultimate goal being to improve clinical management and achieve better patient outcomes as a result.

1.2 TGF- β signalling pathway

1.2.1 TGF- β and signalling components

Transforming growth factor beta (TGF- β) family comprises more than 30 secreted polypeptides, which can be divided into two subgroups: the TGF- β subfamily, which includes TGF- β isoforms 1-3, activins and Nodal; and the bone morphogenetic protein (BMP) subfamily, which consists of BMPs, growth and differentiation factors (GDFs) and the anti-Müllerian hormone (AMH). These molecules act by binding to specific receptors located on the surface of the cell membrane. The members of the TGF- β family participate in many processes such as cell growth, apoptosis, differentiation, angiogenesis, immunoreactions, matrix remodelling and migration. Therefore, they execute relevant functions during embryogenesis, control of the immune system, angiogenesis and tissue homeostasis, along with the development and progression of different diseases. In the liver, they stimulate the activation of perisinusoidal cells, induce the growth of normal fibroblasts and inhibit hepatocyte proliferation [75, 76].

TGF- β s are secreted as inactive molecules that should be activated by cleavage prior to their specific receptor binding. In the case of TGF- β 1 (used in this study; see Figure 1.2), it is synthesised as a 391 amino acid precursor containing a signal sequence, a pro-region and a N-terminal 112 amino acid sequence that includes the TGF- β monomer [77, 78]. A homodimeric pro-peptide is formed after the cleavage of the signal sequence, and once the dimer pro-region is cut off, it stays associated with the mature TGF- β dimer, forming the latency associated protein (LAP). This LAP protein is covalently bound to the latent TGF- β binding protein (LTBP) involved in the association of the TGF- β -LAP complex with the extracellular matrix (ECM). This is the inactive status of the TGF- β 1 isoform that prevents it from driving its biological functions. The activation of the complex is mainly done by several proteases (e.g., plasmin [79]) as well as by non-proteolytical proteins (e.g., thrombospondin [80] and integrins [81]) and some environmental factors like a mildly acidic pH [82].

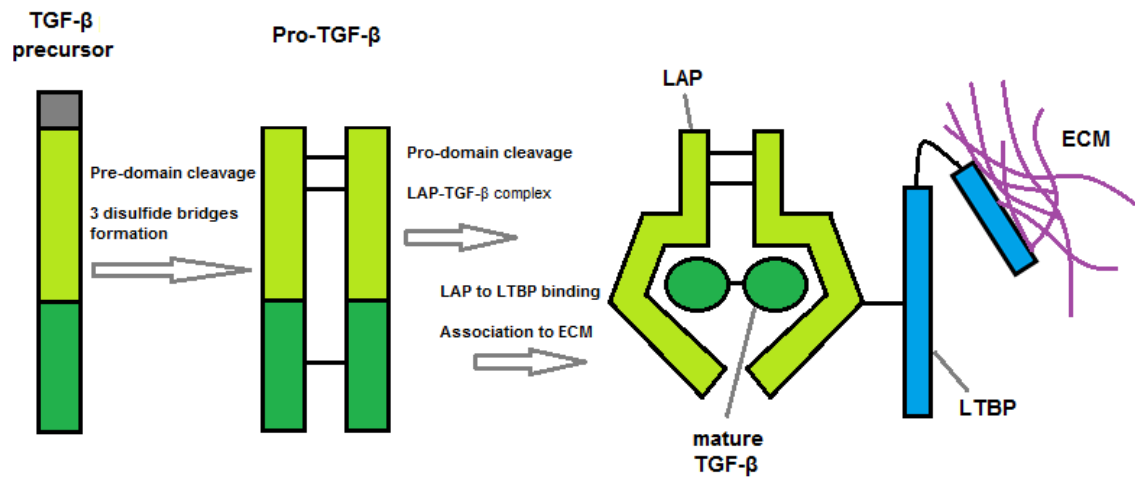


Figure 1.2 TGF-β1 production (based on [83, 84])

The signalling of activated TGF-β occurs via the ligand-induced heteromeric complex formation of distinct type I (TGF-β receptor 1; TβRI) and type II (TGF-β receptor 2; TβRII) cell surface serine/threonine kinase receptors. The TGF-β mature dimers bind to TβRII, resulting in the recruitment of two TβRI between two type II receptors (Figure 1.3) [85]. These receptors have a similar structure, consisting of an extracellular ligand binding domain, a transmembrane region and a C-terminal intracellular domain with a serine/threonine kinase. The type I receptor is phosphorylated by the constitutively active type II receptor and propagates the signal through the phosphorylation of specific receptor-regulated (R)-Smad proteins [86].

Five type II and seven type I receptors modulate the signal of the whole TGF-β superfamily. The cytokines bind specifically to a certain combination of type I and II receptors. The predominant TβRI is the activin receptor-like kinase 5 (ALK5) [87], but other TβRII-TβRI interactions have been reported in different cell types. For example, ALK1 in endothelial cells and ALK2 and 3 in epithelial cells were found binding to TGF-β in an ALK5-dependent manner, activating R-Smad1, 5 and 8 instead of Smad2 and 3, which are the main signalling mediators for TGF-β (see chapter 1.2.2) [88, 89].

1.2.2 Canonical TGF-β signalling

The canonical intracellular TGF-β signalling superfamily is mediated by transcriptional co-regulators or Smad proteins. There are eight of these proteins, which can be grouped into receptors or R-Smads (Smad1, 2, 3, 5 and 8), inhibitors or I-Smads (Smad6 and 7), and a common signalling partner or Co-Smad (Smad4). Structurally, R- and Co-Smads have two conserved domains at the amino-terminal and carboxyl-terminal ends named Mad Homology 1 and 2 (MH1 and MH2), respectively. The inhibitory Smads have a conserved MH2 domain but their N-terminal regions are weakly similar to the MH1 domain [90, 91]. As explained in chapter 1.2.1, after ligand binding, the heterotrimeric receptor complex transfers the signal into the cell through R-Smad-specific phosphorylation. Smad2 and Smad3 are mainly activated by TGF-β via two serine residues phosphorylation in their serine-X-serine (SXS) C-terminal motif. Once activated,

all the R-Smads associate with the common mediator (Co)-Smad4 by binding two R-Smads to one Smad4 protein in order to form a heterotrimeric transcription factor [92]. These complexes then translocate to the nucleus where they regulate the transcription of many genes (Figure 1.3).

A specific palindromic DNA sequence (5'-GTCTAGAC-3') or, as it is commonly called, a Smad binding element (SBE), is recognised by Smad3/Smad4. Smad2 lacks the capacity to bind to DNA; therefore, the Smad2/Smad4 complex needs to associate with DNA binding proteins in order to activate an activin response element (ARE) [91, 93]. Since the SBE is a very short sequence, which reduces Smad3's binding affinity, it is usually close to the recognition sites of Smad-interacting factors that increase the binding efficiency. For example, Sp-1 (stimulation protein 1) activates several TGF- β target genes via association with Smad2 and/or Smad3, such as Smad7, PAI-1 (plasminogen activator inhibitor-1) [94] and Collagen (ColA1) [95].

As their name implies, the Inhibitory (I)-Smads, Smad6 and Smad7, efficiently inhibit TGF- β signalling. Their expression is enhanced as a negative feedback mechanism [76]. While Smad6 mainly inhibits BMP subfamily signalling, Smad7 can interfere with both TGF- β and BMP signalling [96, 97]. There are, of course, other proteins that are capable of antagonising TGF- β signalling, such as Ski and SnoN, which prevent the association between the co-activator p300 and the Smad-DNA binding complex [98, 99]. The duration and intensity of TGF- β signalling is regulated by a broad spectrum of mechanisms.

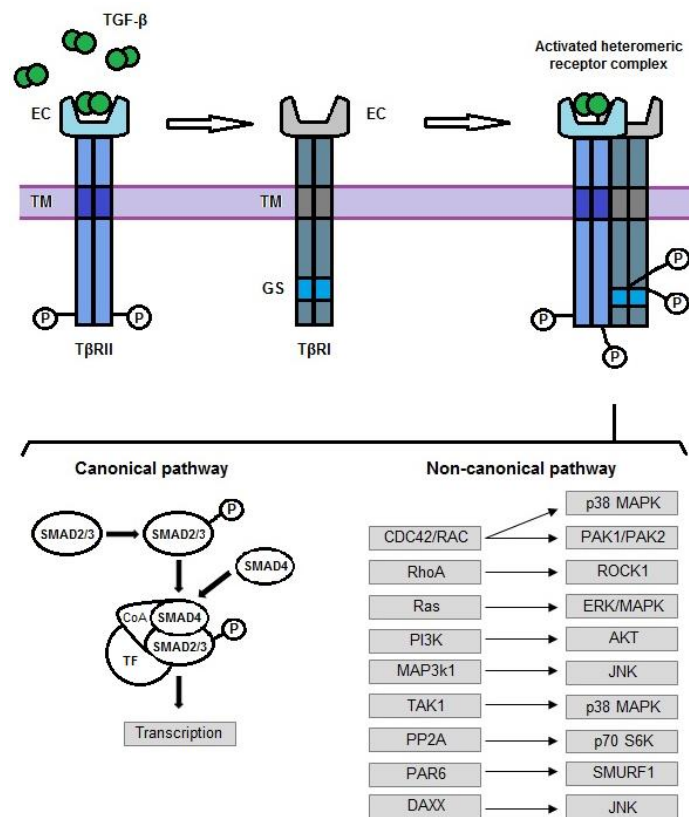


Figure 1.3 Canonical and non-canonical TGF- β signalling (modified from [76, 84, 121, 123]). EC = Extracellular domain, TM = Transmembrane domain, GS = Serine-rich region or GS box, CoA = Co-activator, TF = Transcription factor.

Finally, different factors collaborate to ensure cell-type- and context-specific target gene expression, creating a very intricate system. The fact that TGF- β can crosstalk with other signalling pathways increases the complexity of the signalling and the difficulty of unravelling all the participating elements.

1.2.3 Non-canonical TGF- β signalling

In addition to the canonical Smad signalling pathway, there are several (R)-Smad-dependent but Smad4-independent signalings in response to TGF- β . The identification of the transcription intermediate factor 1 γ (TIF1 γ or TRIM33) supports the fact that Smad4 is not essential for all TGF- β -regulated responses. TIF1 γ competes with Smad4 for Smad2/3 interaction, being also able to act as a Smad4 inhibitor [100]. In keratinocytes, Smad2/3 binds to I κ B kinase α (IKK α), consequently controlling Myc oncogene antagonist MAD1 expression and keratinocyte differentiation [101]. On the other hand, the TGF- β receptor complex can interact with the IL1R-TRAF6-TAK1 (interleukin 1/TNF receptor associated factor 6/TGF- β -associated kinase 1) receptor-effector module, inducing the activation of JNK and p38 mitogen-activated protein kinase (MAPK). These proteins are responsible for stress signals and are involved in TGF- β -induced apoptosis and EMT (epithelial-mesenchymal transition) [102]. In epithelial cells, T β RII releases Par6 from the Par6-T β RI complex by phosphorylation, allowing Par6 to dissolve the tight junctions during EMT [103]. Other studies found that PI3K/Akt signalling can participate in TGF- β -mediated survival response or EMT in epithelial cells [104]. The TGF- β receptor can also engage the Rho-ROCK1 signalling module as well as the CDC42/Rac1-PAK2 complex involved in the regulation of actin and stress fibre formation, linking them to EMT (RhoA) and alterations of the actin cytoskeleton (CDC42) [105-108].

Additionally, TGF- β canonical signalling can be modified by cross-talking pathways through phosphorylation of the linker regions in R-Smads. These regions are less conserved within different Smads, which opens up the possibility for specific regulation. Smad2 and 3 linker phosphorylation is mediated by cyclin-dependent kinases (CDK) 2 or 4, which consequently decreases p15 expression and the growth arrest [109]. Finally, there are other mechanisms that regulate R-Smads, e.g., blocking the activated Smad3 from shuttering into the nucleus (see chapter 1.2.6).

1.2.4 TGF- β signalling in liver cells

In chronic liver disease (CLD), the primary target of TGF- β are the hepatic stellate cells (HSCs) contributing to their activation and fibrogenesis [110]. After their activation and transdifferentiation into myofibroblasts, there is a TGF- β -mediated stimulatory growth effect [111]. In this cell type, several TGF- β -direct target genes, such as type (I) procollagen and plasminogen activator inhibitor (PAI1), have been identified. On the other hand, the transcriptional activation of myofibroblast markers α -smooth muscle actin (α SMA) and connective tissue factor (CTGF) has been found to be regulated in a TGF- β -independent manner, with the TGF- β being necessary for stress-fibre formation and organisation [112]. Many studies point to Smad3 as the main mediator of the fibrogenic response of HSCs [113, 114]. In addition, HSC migration and disease progression has

been associated with Smad3 linker phosphorylation by p38/JNK/MAPK [115, 116] (chapter 1.2.3).

In hepatocytes, TGF- β induces growth arrest via interaction of Sp1 transcriptional factors with Smad proteins, enhancing the expression of the cyclin-dependent kinase (CDK) inhibitor p21 [117]. TGF- β mRNA was found in non-parenchymal cells but not in hepatocytes in the regenerating and normal liver, suggesting the existence of a paracrine regulatory system that includes TGF- β and controls hepatocyte replication [118]. Hepatocyte apoptosis has also been found induced by TGF- β via the adaptor protein Daxx, which is associated with the Fas receptor that mediates JNK activation and programmed cell death. Moreover, the induced death-associated protein (DAP) kinase and the expression of the pro-apoptotic protein BIN upon TGF- β stimulation are able to produce hepatocyte apoptosis [119].

In other cell types, such as BDEC, immune cells and liver sinusoidal endothelial cells, the effect of TGF- β has been investigated less thoroughly. TGF- β might trigger cytostatic and tumorigenic effects on BDEC. In addition, since TGF- β plays a role as a differentiation factor for regulatory T cells and Th17 cells, an inhibition effect on inflammation is expected [120]. Finally, TGF- β has an impact as a proangiogenic factor in the branched sinusoid network in the context of regeneration, cirrhosis and carcinogenesis [83].

1.2.5 TGF- β in cancer

The overexpression of TGF- β 1 has been associated with colon, oesophageal, breast, lung, gastric, hepatocellular and pancreatic cancers, where it is usually correlated with tumour progression, metastasis, angiogenesis and poor prognosis. In human HCC, high amounts of this cytokine were detected in malignant hepatocytes, identifying them as the source of the overexpression. TGF- β plays a significant role in cancer by acting as a tumour suppressor initially and as a tumour promotor in later stages. It maintains tissue homeostasis and blocks tumour progression, regulating cell proliferation, differentiation, survival as well as the cellular microenvironment (the importance of the microenvironment was explained in chapter 1.1.3). In theory, all human cell types can respond to TGF- β . Different disruptions of TGF- β signalling in different contexts enable malignant cells to avoid and/or modify the suppressive effects of this pathway. In this context, TGF- β signalling promotes proliferation and invasion, immune escape and metastasis of cancer cells (Figure 1.4) [121 -124].

In order to elude the tumour-suppressive effects of TGF- β , malignant cells inactivate core components of the pathway such as TGF- β receptors. It seems that the transcriptional repression of T β RII is responsible for most of the tumour-associated TGF- β resistance [125]. Another scheme are down-stream alterations that affect just the tumour-suppressive arm of the pathway. In this case, cancer cells can benefit from the remaining TGF- β functions, increasing the potential for tumour progression. For example, TGF- β -induced epithelial-mesenchymal transition (EMT) contributes to tumour dissemination and invasion by conferring motility to the cells [166]. EMT-undergoing cells have been located in the invasion front in human carcinomas, suggesting that the large amount of TGF- β and other cytokines at this location may induce EMT. In addition, TGF- β could be

involved in distal metastasis promotion, considering that high levels of TGF- β immunostaining have been associated with metastasis in infiltrated breast carcinoma [167]. Due to TGF- β implications in cancer, there is a growing interest in the development of anti-TGF- β therapies [121, 168]. The immunosuppressive effects of TGF- β in cancers such as glioma, melanoma, and renal cell carcinoma evolved into TGF- β pathway inhibitor compounds development and production. The problem of these strategies is that the side effects could be disastrous, considering that the blockage may cause tumour-specific benefits, such as autoimmune reactions, chronic inflammation, activation of compensatory mechanisms and progression of premalignant lesions [169, 170]. For these reasons, it is essential to unravel the TGF- β mechanisms and pro-tumorigenic effects in different tumour types and stages of progression in order to develop personalised and more effective therapies.

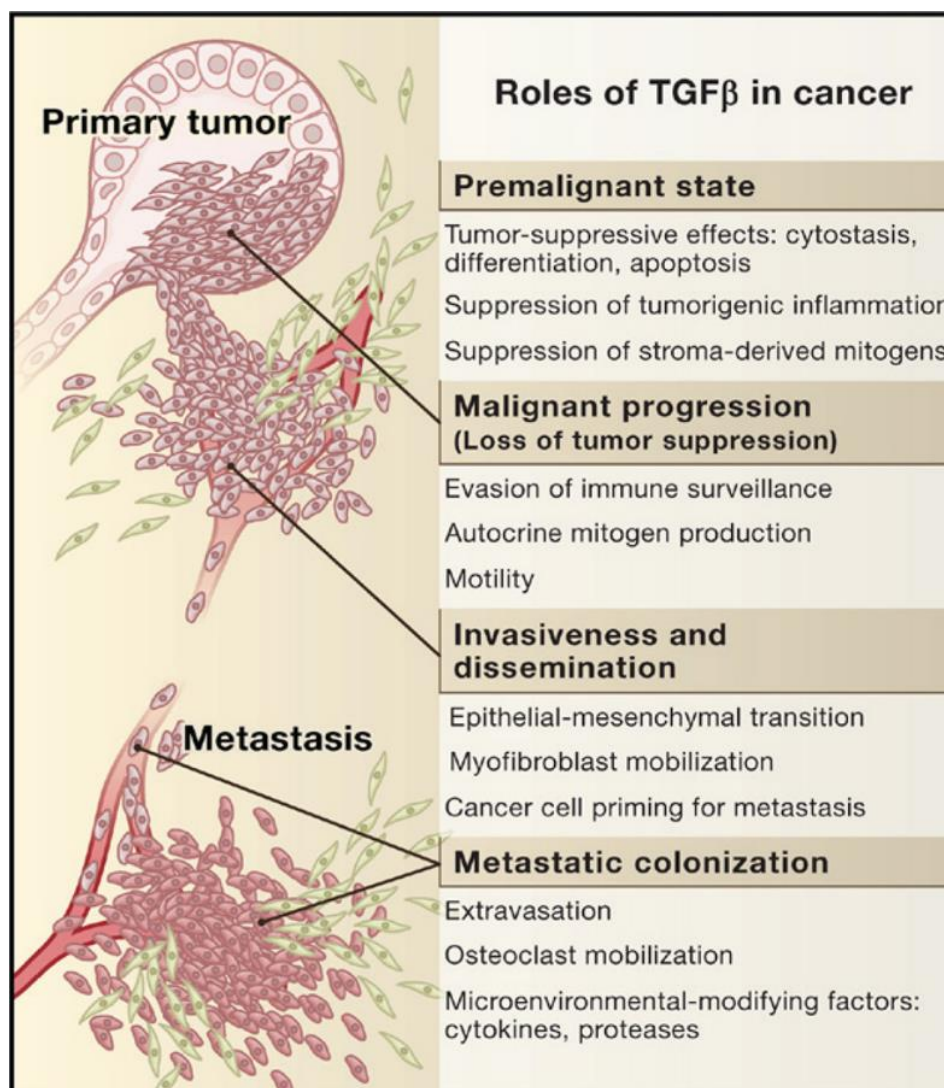


Figure 1.4 The ambiguous role of TGF- β in cancer (taken from [122])

1.2.6 TGF- β signalling regulators (TSRs)

As described in previous chapters of this thesis, the TGF- β signalling pathway modulates a broad range of important cell processes and regulates the expansion of epithelial and neural tissues, the immune system and wound repair. Hence, this pathway is controlled by multiple positive and negative regulators that ensure the functional activity of TGF- β in an appropriate time and cell context.

Ligand trap proteins restrict TGF- β family members from accessing membrane receptors. As explained in chapter 1.2.1, the latent TGF- β -binding proteins (LTBP 1-4) sequester TGF- β and anchor it to the extracellular matrix by forming a complex with latency-associated protein (LAP). BMPs can also get trapped by other sets of proteins, such as noggin, chordin, gremlin, follistatin, DAN/Cerberus and Bmper. Follistatin expression has been implicated in hepatocellular carcinoma and breast cancer bone metastasis [126, 127]. On the other hand, Gremlin-1 has been linked to skin basal cell carcinoma, among other cancers [128].

I-Smads (chapter 1.2.2), Smad6 and Smad7, are two inhibitors of TGF- β signalling, with Smad7 being one of the most potent antagonists of the TGF- β family members. Smad7 participates in a negative feedback loop since it is induced by TGF- β members and blocks the pathway by recruiting Smurf E3 ubiquitin ligases (Smurf1 and 2) to the activated receptors. As a result, they are targeted for degradation via proteasomal and lysosomal pathways [129]. Smad6, which preferably blocks BMP signalling, competes with Smad4 for complex formation with phosphorylated Smad1 [130].

The regulation of I-Smads has been pointed out as a mechanism used by other pathways to crosstalk with TGF- β /Smad signalling. For example, interferon γ uses the JAK1/STAT1 pathway and the tumour necrosis factor- α and interleukin-1 through NF- κ B/RelA to enhance the expression of I-Smads and, therefore, negatively regulate TGF- β signalling [131, 132]. Other molecules such as AMSH, a protein implicated in interleukin signalling, compete for the interaction with I-Smads and promote TGF- β signalling through I-Smad inhibition [133].

The Smad pathway can also be modulated by proto-oncogene activity. The activation of ERK by EGF, HGF or activated Ras inhibits the ligand-induced nuclear accumulation of R-Smads [134]. Another example is how the ectopic expression of c-Myc makes cells insensitive to the anti-proliferative effect of TGF- β [135]. In leukaemia, the fusion product of Ev1-1 and AML1 proteins interacts with Smad3 and blocks its transcriptional activity by avoiding DNA binding or by recruiting the CtBP repressor [136]. Smad3 activity can also be suppressed by c-Jun and Jun B inducing its disassociation from the DNA [137].

Several membrane-associated proteins regulate TGF- β -induced receptor activation. For example, Cripto/TDGF1, a member of the epidermal growth factor-Cripto/frl/cryptic family, can attach to the outer cell membrane through a glycosylphosphatidylinositol anchor, where it functions as a co-receptor for nodal signalling during embryogenesis. Cripto has been found overexpressed in breast, pancreatic, lung, colon and bladder cancers [138]. The inhibition of the ligand-receptor interaction of activins and TGF- β by Cripto contributes to their pro-tumorigenic activity [139, 140]. On the other hand, the BAMBI (bone morphogenetic protein and activin membrane-bound inhibitor) is capable

of inhibiting activin A, TGF- β , and BMP signalling by associating with TGF- β family receptors (this will be further explained in chapter 1.3).

The implication of a broad number of TGF- β signalling regulatory mechanisms and molecules in fibrogenesis and carcinogenesis has increased the interest of the scientific community in searching for potential regulators that may be markers for tumour progression and/or prognosis as well as possible therapeutic targets (see chapter 1.4).

1.3 TGF- β signalling regulation by BAMBI (BMP and activin membrane-bound inhibitor)

BAMBI (bone morphogenetic protein and activin membrane-bound inhibitor) was first found by Onichtchouk *et al.* in 1999 [141] during a screening of BMP4 signalling components. The novel *Xenopus* complementary DNA, whose expression pattern was similar to BMP4, showed 89% similarity in its amino-acid sequence and 83% identity to the *nma* human gene, without its function being known at that time. BAMBI encodes a 260-amino acid transmembrane glycoprotein that is evolutionarily conserved in vertebrates from *Xenopus* to *Homo sapiens*, and is highly homologous to type I receptors of the TGF- β family. Unlike the known TGF- β receptors, BAMBI lacks the serine/threonine-kinase domain necessary for R-Smad phosphorylation and the consequent signalling transduction.

Using *Xenopus* embryonic explants and whole embryo assays, Onichtchouk *et al.* [141], proved BAMBI's ability to antagonise activin and BMP4 signalling during embryonic development. The embryos showed a dorsoanteriorised phenotype with enlarged heads when injected with BAMBI mRNA, and suffered from gastrulation defects at higher injection doses. In this study, it was found that the BAMBI mode of action is ligand-independent. In order to prove this, the researchers used a construction (BAMBIDN) without the extracellular domain, which did not affect the endogenous BMP signalling and even reversed the blocking effects of wild-type BAMBI. Moreover, the co-expression of BAMBI with constitutively active type I receptors in mouse embryonic carcinoma P19 cells reduced the activation of reporter genes. These results suggest that BAMBI does not interfere with ligand binding in order to block TGF- β signalling. Furthermore, the co-immunoprecipitation assays demonstrated the interaction between BAMBI and all type I receptors (BMP2/4 type I receptors, BMPR-IA and BMPR-IB, also known as ALK3 and ALK6; the orphan receptor ALK1; T β RI or ALK5; activin type I receptor ActR-IB or ALK4), except ALK2 (the putative BMP7 receptor) as well as the interaction with type II receptors, i.e., T β RII and ActR-II.

The fact that BAMBI was only able to bind TGF- β 1 when co-expressed with T β RII indicates that it is incorporated into complexes with this receptor. The decrease of T β RI/T β RII complex formation upon BAMBI overexpression confirmed this hypothesis. On the other hand, reduced levels of phosphorylated T β RI revealed the ability of BAMBI to interact with surface receptors. This prevents the formation of active receptor complexes by inhibiting the dimerization of T β RI (Figure 1.5).

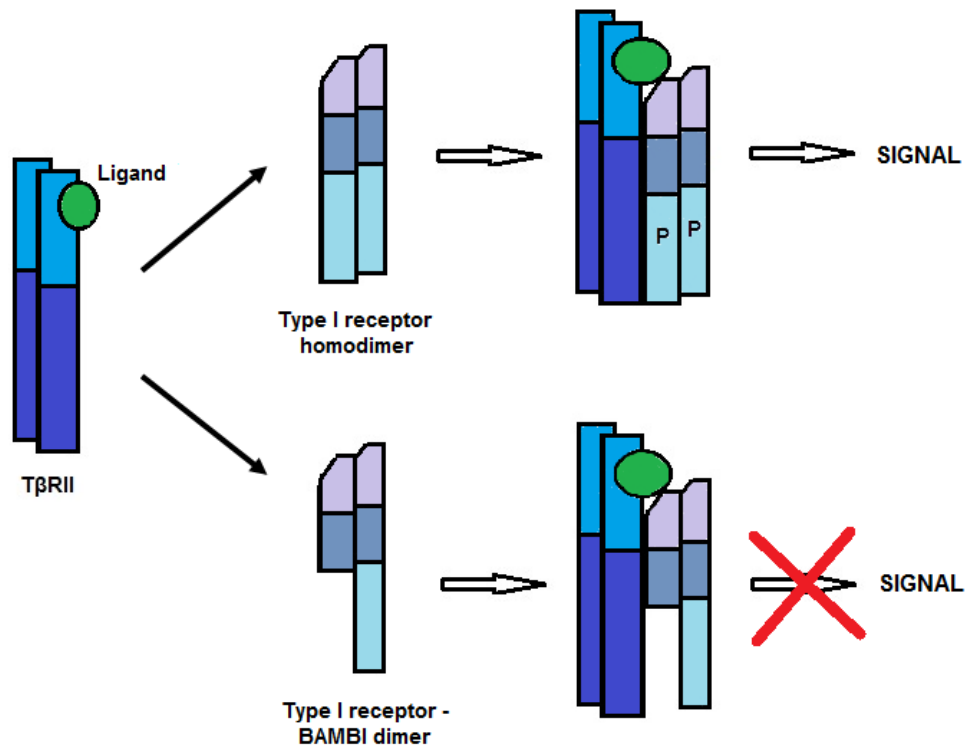


Figure 1.5 BAMBI silencing mechanism (adapted from [141])

BAMBI has been shown to co-express with BMP4 during the embryo development of zebrafish, *Xenopus*, birds, and mice, being its expression induced by BMP4 [141-143]. TGF- β and Wnt signalling can also induce BAMBI expression [144]. Lin *et al.* [145] proved the Wnt signalling promotion by human BAMBI by enhancing the interaction between Frizzled5 (Wnt receptor) and Dishevelled2 (a downstream mediator), proving that BAMBI might integrate different signalling pathways.

Despite BAMBI's role during embryogenesis, the genetic elimination of BAMBI in mice resulted in normal development, growth and survival, but showed a vascular phenotype with prominent endothelial cells in myocardial and glomerular capillaries, larger glomerular capillaries and enhanced glomerular endothelial hypertrophy [146]. Further studies conducted on these mice revealed BAMBI's role in the modulation of endothelial biology and angiogenesis by activation of TGF- β signalling through Smad1/5 and ERK1/2 phosphorylation.

In the liver, BAMBI was found to be expressed in primary human hepatocytes, endothelial cells of blood vessels, cholangiocytes and HSC [147], but its expression decreased in activated HSC [148, 186]. Mainly, the analysis of BAMBI expression focused on HSC because its mRNA expression did not appear in hepatocytes, Kupffer cells or primary human monocytes [147, 148].

1.3.1 The role of BAMBI in carcinogenesis

Human BAMBI or NMA has been found abnormally increased in many high-grade carcinomas leading to the proliferation and metastasis of tumour cells [149, 150]. In contrast to these results, it was also found to be downregulated in metastatic melanoma cell lines and in a subset of high-grade bladder cancer [151, 152]. BAMBI's function in carcinogenesis has not been completely revealed and the mechanisms by which BAMBI drives its effects are not fully understood.

As explained in chapter 1.3, human BAMBI inhibits TGF- β and BMP-mediated signalling by blocking the phosphorylation of R-Smads and therefore deactivates cell growth arrest. Yan *et al.* [150] suggested a mechanism where BAMBI is able to synergise with Smad7 to drive this inhibition effects by forming a ternary complex with ALK5 and Smad7 and, hence, to block the interaction with R-Smads. Zhang *et al.* [153] explored this association between BAMBI and Smad7 through microarray-based immunohistochemistry in 276 gastric cancer tissues and 263 tumour-adjacent tissues. They concluded that gastric cancer with the combined expression of BAMBI and Smad7 correlated with more invasion and metastasis, and was associated with less survival time, suggesting that both molecules may cooperate to promote malignant progression. Another interesting link between BAMBI and Smads has been found in ovarian cancer, where elevated nuclear staining of BAMBI was seen in TGF- β -treated cells, indicating its co-translocation with Smads into the nucleus [154]. In ovarian tumour tissue, BAMBI was overexpressed and localised mainly to the cytoplasmic compartment and uniformly distributed within the tumour. However, there was no significant impact on recurrence or overall survival, nor any evidence of increased metastatic potential as found in colorectal cancer [154].

On the other hand, BAMBI has been shown to interact with the Wnt/ β -catenin signalling pathway, a mediator of many developmental processes that is involved in tumorigenesis (discussed in chapter 1.1.2). Wnt/ β -catenin enhanced expression promotes proliferation and tumorigenesis in tumour tissues. The disruption of the Wnt/ β -catenin signalling cascade has shown anticancer properties [155]. In fact, Liu *et al.* [156] demonstrated that BAMBI knock-down in gastric cancer cell lines downregulated β -catenin expression, reducing the aggressiveness of these cells. They proposed that high levels of BAMBI may induce epithelial-mesenchymal transition and metastasis by contributing to β -catenin upregulation.

Another study of osteosarcoma cells found that BAMBI overexpression affected β -catenin intracellular expression and resulted in higher levels of invasion and proliferation [157]. Using RNA interference against BAMBI, the invasion and cell motility of osteosarcoma cells could be blocked, confirming BAMBI's role in the pathogenesis of osteosarcoma. Interestingly, MMP-2 expression was associated with that of BAMBI, and MMP-2 and MMP-9 activities were improved, as proved by zymography assay. Furthermore, evidence linking the Wnt pathway to the progression of human osteosarcoma was provided, considering that the levels of the cyclin-dependent kinases (CDKs) CDK2 and CDK6 were increased in cells with BAMBI overexpression.

In addition, Fritzmann *et al.* [149], discovered an outstanding link between BAMBI expression and the regulation of metastasis by performing and analysing a colorectal cancer expression profile. In their study, BAMBI acted as a downstream target of Wnt/ β -catenin that mediated the loss of TGF- β signalling sensitivity and led to metastasis in

human colorectal adenocarcinoma cell lines. In this context, BCL9-2, a coactivator of Wnt/ β -catenin signalling, was found to be a key player in metastasis formation by controlling BAMBI and TGF- β effects.

Bringing some controversy to the role of BAMBI in carcinogenesis, a subset of high-grade bladder cancer showed epigenetic silencing of the BAMBI gene [152]. The methylation of BAMBI was significantly correlated with high-grade and invasive tumours, enhanced apoptosis and reduced cell motility when overexpressed in bladder cancer cell lines. It seems that in this case, BAMBI acted by blocking the tumour-promoting and enhancing the tumour-suppressing effects of TGF- β signalling. Therefore, the tumour cells found a way to proceed with their malignant evolution through epigenetic silencing of BAMBI expression.

In a study more closely related to the liver, Sekiya *et al.* [144] found that the inhibitor of β -catenin-TCF (ICAT) was able to suppress the expression of BAMBI, while β -catenin could activate BAMBI transcription. Furthermore, its expression was elevated in most colorectal and hepatocellular carcinomas compared to non-cancerous tissues. They suggest that BAMBI overexpression mediated by β -catenin is used by tumour cells to escape the growth inhibitory effects of TGF- β signalling in colorectal cancer. Moreover, BAMBI appeared to be exclusively expressed in hepatic stellate cells (HSCs), and endotoxin-induced toll-like receptor 4 (TLR4) signalling was able to downregulate its expression through NF- κ B p50. This led to enhanced TGF- β signalling and therefore confirmed the crucial role of BAMBI in inflammation-mediated progression of liver fibrosis [158, 159]. Furthermore, adiponectin controls the expression of BAMBI in HSC, as shown by Wanninger *et al.* [147]. In the context of fatty liver, lower levels of BAMBI in the liver of patients with NAFLD occurred due to low circulating levels of adiponectin. In line with this finding, NASH patients presented even lower levels of BAMBI [147]. Besides, differentiation in primary human preadipocytes induced by FGF-1 decreased BAMBI expression in a PI3K-dependent manner, establishing BAMBI as a critical adipogenic effector of FGF-1 [160].

Finally, despite all the studies done on different cancers, the function of BAMBI in HCC has not been unravelled yet and the mechanisms that BAMBI uses to drive its effects have not been fully discovered. However, all the evidence presented demonstrates the importance of BAMBI and TGF- β signalling in carcinogenesis, and consequently exposes it as a feasible therapeutic opportunity. Targeted inhibition of BAMBI may restore sensitivity to TGF- β -mediated growth inhibition and apoptosis.

1.4 Aims of this study

Hepatocellular carcinoma (HCC) is a complex disease with a poor prognosis. However, its survival rates have increased thanks to improvement in patient stratification and the introduction of new targeted therapies. Some of the most relevant improvements in HCC management have resulted from meta-analyses and cohort studies providing new guidelines for clinical practice. Despite all these improvements, there is still an urgent need for early diagnostic markers and personalised treatments of HCC in order to enhance the survival of patients and reduce the recurrence of the disease.

Our group has been studying the TGF- β signalling pathway in liver diseases for years. TGF- β has a major impact on disease progression and hepatocarcinogenesis [111, 112, 161-164, 190]. Therefore, this project started with a large list of TGF- β signalling regulators (TSRs) identified via RNAi screen in HaCat cells, using the Smad binding element (SBE) luciferase as a read-out [165] (Table 1.1).

Since high-throughput omics technologies have been widely applied and have provided large amounts of data, we wanted to reuse this data for a screening among the candidates (Table 1.1) in order to translate the findings to liver cancer and to dissect the relevant mechanisms that facilitate TGF- β -related hepatocarcinogenesis. With this approach, we wanted to find new useful candidates for prediction or as therapeutic targets.

In this study, the bone morphogenetic protein and activin membrane-bound inhibitor (BAMBI) is identified as a potential therapeutic target, and an analysis of its functions in HCC is presented. In addition, an attempt is made to discover the mechanisms used by BAMBI to drive its effects.

| | | | | | | | |
|----------------|------------------|----------------|------------------|---------------|-------------------------------|---------------|--------------------|
| Acan | Bmp3 | Col10a1 | Fstl1 | Inha | Norrin | Ski | Tgfbrap1 |
| Acvr1 | Bmp4 | Col2a1 | Gdf1 | Inhba | Nov | Smad6 | TIEG |
| Acvr1b | Bmp5 | CRIM1 | Gdf10 | Inhbb | NR4A1 | Smad7 | Timp1 |
| Acvr1c | Bmp6 | CRIM2 | Gdf11 | Lefty1 | PIN1 | SMOC1 | Timp3 |
| Acvr2a | Bmp7 | Criptic | Gdf15 | Lefty2 | PPiα | Smurf1 | TMEPAI |
| Acvr2b | Bmp8a | Ctgf | Gdf2 | LRP1 | PPM1A | Smurf2 | Traf4 |
| Acvr11 | Bmp8b | CTHRC1 | Gdf3 | Ltbp1 | PRDC | SnoN | TrkC |
| Adams4 | Bmper | CV2 | Gdf5 | Ltbp2 | RGMA | Sox9 | Twisted |
| Adams5 | Bmpr1a | CYLD | Gdf6 | Ltbp3 | Rgmb | SPARC | UCH37 |
| Amh | Bmpr1b | CYR61 | Gdf7 | Ltbp4 | RGMc/HF E2/HJV | SPP24 | USAG-1 |
| Amhr2 | Bmpr2 | DAND5 | Gdf9 | MED12 | RGMd | SPTB | USP15 |
| AnXA1 | Cd109 | Decorin | Grem1 | Mgp | RNF12 | Tdgf1 | USP4 |
| Arkadia | CD133 | DPT | Gusb | Mmp13 | Ror2 | Tgfb1 | Vasorin |
| Aspn | Cer1 | ELAC2 | Hepcidine | Mstn | Runx2 | Tgfb2 | VE Cadherin |
| Bambi | Chrd | Eng | Hsp90ab1 | Nbl1 | Sclerostin | Tgfb3 | Wisp1 |
| Bmp10 | Chrdl1 | ERRg | Id1 | Nedd4L | Sdc4 | Tgfb1 | Wisp2 |
| Bmp15 | Chrdl2 | Fn1 | Igf1 | Nodal | Serpine1 | Tgfb2 | Wisp3 |
| Bmp2 | c-Kit/KIT | Fst | Igf1r | Nog | SK/DKK1 | Tgfb3 | Yap1 |

Table 1.1 TGF- β signalling regulator (TSR) candidates

2 MATERIAL AND METHODS

2.1 Materials

2.1.1 Instruments

| | |
|---|---|
| Agarose gel electrophoresis system | Peqlab Biotechnology (Erlangen, Germany) |
| PerfectBlue™ Mini&Midi System | |
| Blotting module, Tetra Blotting Module | Bio-Rad Laboratories (Munich, Germany) |
| Blotting module, XCell II™ Blot Module | Life Technologies (Frankfurt, Germany) |
| Cell culture incubator, HERA cell | Kendro Laboratory (Hanau, Germany) |
| Centrifuges | |
| Biofuge Primo R | Heraeus Holding (Solingen, Germany) |
| Biofuge Fresco | Heraeus Holding (Solingen, Germany) |
| Electrophoresis module, Mini-Protean | Bio-Rad Laboratories (Munich, Germany) |
| Electrophoresis module, | Life Technologies (Frankfurt, Germany) |
| XCell SureLock® Mini-Cell | |
| Gel casting system for immunoblot, Mini-Protean | Bio-Rad Laboratories (Munich, Germany) |
| Image reader, LAS 1000 | Fujifilm (Billingham, United Kingdom) |
| Inverted light-microscope, Leica DMI8 | Leica Biosystems (Wetzlar, Germany) |
| Laminar flow hood, HA 2472 GS | Heraeus Holding (Solingen, Germany) |
| Luminescent image analyser, FUSION SL™ AdvanceMulti- | Peqlab Biotechnology (Erlangen, Germany) |
| Imaging system | |
| Microplate reader, Tecan infinite M200 | Tecan Group Ltd. (Männedorf, Switzerland) |
| NanoQuant plate | Tecan Group Ltd. (Männedorf, Switzerland) |
| PCR Thermocycler, PeqStar Universal 96 well | Peqlab Biotechnology (Erlangen, Germany) |
| Real time PCR, Stratagene MX 3005 P system | Agilent Technologies (Waldbronn, Germany) |
| Rotation microtome RM 2165 | Leica Biosystems (Wetzlar, Germany) |

| | |
|--|-------------------------------------|
| Tissue homogenizer, Precellys Evolution | Peqlab (Erlangen, Germany) |
| Upright light-microscope, LAS X Widefield Systems | Leica Biosystems (Wetzlar, Germany) |

2.1.2 Chemicals

| | |
|---|--|
| Acrylamide/Bis Solution, 37.5:1 (30% w/v) | Serva (Heidelberg, Germany) |
| Ammonium persulfate (APS) | Sigma-Aldrich (St. Louis, Missouri, USA) |
| Bovine serum albumin, Fraction V | Serva (Heidelberg, Germany) |
| Bromophenol Blue, sodium salt | Applichem (Darmstadt, Germany) |
| CHAPS | Sigma-Aldrich (St. Louis, Missouri, USA) |
| Chloroform | Sigma-Aldrich (St. Louis, Missouri, USA) |
| <i>p</i> -Coumaric acid | Sigma-Aldrich (St. Louis, Missouri, USA) |
| Deoxycholic acid, sodium salt | Serva (Heidelberg, Germany) |
| 3,3'-Diaminobenzidine (DAB) | Sigma-Aldrich (St. Louis, Missouri, USA) |
| Diethyl pyrocarbonate (DEPC), 99% | Sigma-Aldrich (St. Louis, Missouri, USA) |
| Dimethyl sulfoxide (DMSO), 99.5% | Sigma-Aldrich (St. Louis, Missouri, USA) |
| Dithiothreitol (DTT) | Sigma-Aldrich (St. Louis, Missouri, USA) |
| ECL substrate (electrochemiluminescence) | Amersham (Freiburg, Germany) |
| EDTA, disodium salt | Applichem (Darmstadt, Germany) |
| Ethanol, 99% | Merck Group (Darmstadt, Germany) |
| Formaldehyde | Sigma-Aldrich (St. Louis, Missouri, USA) |
| Formamide | Merck Group (Darmstadt, Germany) |
| GelRed™ | GeneOn (Ludwigshafen, Germany) |
| Glycerol | Sigma-Aldrich (St. Louis, Missouri, USA) |
| Glycine | Merck Group (Darmstadt, Germany) |
| HEPES, 99.5% | Sigma-Aldrich (St. Louis, Missouri, USA) |
| Hydrochloric acid (HCl), 1 N | Merck Group (Darmstadt, Germany) |
| Hydrogen peroxide solution, 1 M | Merck Group (Darmstadt, Germany) |
| Isopropanol | Merck Group (Darmstadt, Germany) |
| Luminol | Sigma-Aldrich (St. Louis, Missouri, USA) |

| | |
|--|--|
| Methanol | Merck Group (Darmstadt, Germany) |
| β -Mercaptoethanol | Merck Group (Darmstadt, Germany) |
| MOPS, buffer grade | Applichem (Darmstadt, Germany) |
| Nonident P40 | Roche (Mannheim, Germany) |
| Ponceau S Red | Sigma-Aldrich (St. Louis, Missouri, USA) |
| Potassium chloride (KCl) | Sigma-Aldrich (St. Louis, Missouri, USA) |
| SDS (sodium dodecyl sulfate), ultra-pure | Carl Roth (Karlsruhe, Germany) |
| Sodium acetate trihydrate | Merck Group (Darmstadt, Germany) |
| Sodium hydroxide (NaOH), 1 N | Merck Group (Darmstadt, Germany) |
| Sodium chloride (NaCl) | Carl Roth (Karlsruhe, Germany) |
| TEMED (N,N,N',N'-Tetramethylethylene-diamine) | Sigma-Aldrich (St. Louis, Missouri, USA) |
| Trypan blue solution | Sigma-Aldrich (St. Louis, Missouri, USA) |
| Tris(hydroxymethyl)amino methane (Tris base) | Sigma-Aldrich (St. Louis, Missouri, USA) |
| Tween-20 | Sigma-Aldrich (St. Louis, Missouri, USA) |
| Universal-Agarose "Seakem LE" | Lonza Group (Cologne, Germany) |
| Urea | Sigma-Aldrich (St. Louis, Missouri, USA) |

2.1.3 Cell culture

2.1.3.1 Cell lines

For the cell culture experiments, six different liver cancer cell lines and HEK293T were used.

| | |
|-------|---|
| HepG2 | Epithelial HepG2 cells established from the tumour tissue of a 15 years old male from Argentina. The cells were described not to harbour a hepatitis B virus genome [171]. |
| Hep3B | This cell line was isolated from an 8 years old black male from USA. This cell line contains integrated a 2.3 kb hepatitis B virus genome fragment and, when injected into nude mice, forms tumours with hepatocellular characteristics [171, 172]. |
| HUH6 | These are epithelial like cells derived from a hepatoblastoma of a Japanese infant [173]. |

| | |
|-------------|--|
| FLC-4 | This is a mutant of the HCC cell line JHH-4, which was established from a 51 years old Japanese male with HCC of Edmondson's type III. FLC-4 cells show similar morphological and biological properties of its parental cell line JHH-4, which forms tumours in nude mice. FLC-4 are well differentiated cells and secrete liver-specific proteins [174, 175]. |
| HLE and HLF | HLE and HLF were obtained from a hepatoma (non-differentiated) of a 68 years old patient. While HLE cells have an epithelial-like morphology, HLF cells resemble fibroblasts but they appear to have originated from hepatoma cells. Unlike HLF, HLE produce α -fetoprotein but only HLF cells form tumours upon transplantation into the cheek pouch of adult hamsters treated with cortisone acetate [176]. |
| HEK293T | This cell line is a highly transfectable derivative of human embryonic kidney 293 cells, and contains the SV40 T-antigen. It is competent to replicate vectors carrying the SV40 region of replication and it has been widely used for retroviral production, gene expression and protein production [177, 178]. |

HepG2, Hep3B, HLE and HLF cell lines (originally purchased from Japanese Collection of Research Bioresources Cell Bank) were kindly provided by the SFB/TTR77 project funded by the Deutsche Forschungsgemeinschaft. Prof. Michael Kern (Institute of Pathology, Cologne, Germany) provided the FLC-4 and HUH6 cell lines.

2.1.3.2 Cell culture reagents and additives

| | |
|--|---|
| Dulbecco's Modified Eagle Medium (DMEM), with 25nM HEPES, 4.5g glucose, w/o L-glutamine | Lonza Group (Cologne, Germany) |
| L-glutamine, 200 mM | PAA Laboratories (Cölbe, Germany) |
| Penicillin/ Streptomycin | Lonza Group (Cologne, Germany) |
| Fetal Bovine Serum (FBS) | Gibco (Life Technologies, Frankfurt, Germany) |
| Hank's Buffered Salt Solution (HBSS) | Sigma Aldrich (St. Louis, USA) |
| 10x-Trypsin EDTA | Sigma Aldrich (St. Louis, USA) |
| Human recombinant TGF- β 1 | Peptidech (Hamburg, Germany) |
| Human recombinant TGF- β 2 | Peptidech (Hamburg, Germany) |
| Human recombinant IL-6 | Peptidech (Hamburg, Germany) |
| Human recombinant BMP6 | Peptidech (Hamburg, Germany) |
| Human recombinant BMP9 | R&D (Minneapolis, USA) |

2.1.3.3 Materials for RNA interference, transfection and adenoviral infection technology

Reagents for transfection

| | |
|--|---|
| Lipofectamine® 2000 Transfection Reagent | Invitrogen (Darmstadt, Germany) |
| Metafectene® PRO | Biontex Laboratories (München, Germany) |
| Opti-MEM Reduced Serum Medium | Gibco (Life Technologies, Frankfurt, Germany) |

Plasmids

| | |
|------------------------------|---|
| mBAMBI pLV-puro | gift from Prof. Peter ten Dijke (Leiden University Medical Center, Leiden, Netherlands) |
| pLV-puro empty vector | gift from Prof. Peter ten Dijke (Leiden University Medical Center, Leiden, Netherlands) |
| mBAMBI c-Flag pLV-puro | gift from Prof. Peter ten Dijke (Leiden University Medical Center, Leiden, Netherlands) |
| c-Flag pLV-puro empty vector | gift from Prof. Peter ten Dijke (Leiden University Medical Center, Leiden, Netherlands) |
| pEGFP-N3-hBAMBI | from PhD Takeaki Oda (Institute of Molecular and Cellular Biosciences, University of Tokyo) |
| REV | gift from Prof. Peter ten Dijke (Leiden University Medical Center, Leiden, Netherlands) |
| GAG | gift from Prof. Peter ten Dijke (Leiden University Medical Center, Leiden, Netherlands) |
| VSV | gift from Prof. Peter ten Dijke (Leiden University Medical Center, Leiden, Netherlands) |
| shRNA 8751 | gift from Prof. Peter ten Dijke (Leiden University Medical Center, Leiden, Netherlands) |
| shRNA 8752 | gift from Prof. Peter ten Dijke (Leiden University Medical Center, Leiden, Netherlands) |

| | |
|------------|---|
| shRNA 8753 | gift from Prof. Peter ten Dijke (Leiden University Medical Center, Leiden, Netherlands) |
| shRNA 8754 | gift from Prof. Peter ten Dijke (Leiden University Medical Center, Leiden, Netherlands) |
| pEGFP-C1 | Takara Bio Inc. (Shiga, Japan) |

Adenoviruses

| | |
|--------------------------------|--|
| Ad(CAGA) ₉ -MLP-Luc | described in [96] |
| Ad-PL-DEST-BRE | described in [179] |
| Ad-CMV-GFP | Cat. N°1060 Vector Biolabs (Philadelphia, USA) |
| Ad-h-BAMBI | ADV-201955, Vector Biolabs (Philadelphia, USA) |

Reagents for reporter assay

| | |
|--------------------------|-----------------------------|
| Reporter Lysis Buffer 5x | Promega (Mannheim, Germany) |
| Luciferase Assay Reagent | Promega (Mannheim, Germany) |

2.1.3.4 Reagents for Caspase 3 assays

Caspase3 cell lysis buffer

| | |
|--------|-------------|
| 50ml | 100mM HEPES |
| 13.3ml | 750mM NaCl |
| 0.1g | 0.1% CHAPS |
| 0.1ml | mM EDTA |
| 0.1ml | 1M DTT |

Add ddH₂O until 100ml

Caspase3 assay buffer

| | |
|--------|--------------|
| 50ml | 100mM HEPES |
| 13,3ml | 750mM NaCl |
| 0,1g | 0.1% CHAPS |
| 0.1ml | mM EDTA |
| 1ml | 1M DTT |
| 10ml | 10% Glycerol |

Add ddH₂O until 100ml

Caspase3 fluorometric substrate

AC-DEVD-AFC substrate

Biomol (Hamburg, Germany)

5mg of substrate dissolved in 5ml DMSO, aliquoted and stored at -20°C protected from light

2.1.4 Materials for RNA work**2.1.4.1 Kits, buffers and reagents for RNA isolation, reverse transcription and cDNA synthesis**

| | |
|--|---|
| InviTrap® Spin Universal RNA Mini Kit | Stratec Molecular (Berlin, Germany) |
| TRIzol® Reagent | Invitrogen (Darmstadt, Germany) |
| RevertAid H Minus Reverse Transcriptase (200 U/μL) | Thermo scientific (Waltham, Massachusetts, USA) |
| 5x Reaction buffer | Thermo scientific (Waltham, Massachusetts, USA) |
| Oligo(dT)18 Primer | Thermo scientific (Waltham, Massachusetts, USA) |
| Random Hexamer Primer | Thermo scientific (Waltham, Massachusetts, USA) |
| dNTPs for cDNA Probe Synthesis (10 mM) | Thermo scientific (Waltham, Massachusetts, USA) |

DEPC-water

1 ml Diethyl pyrocarbonate (DEPC) in 1 L ddH₂O; incubated at RT overnight with a shaker; autoclaved.

20x MOPS (RNA running buffer)

400mM MOPS

100mM Sodium acetate trihydrate

20mM EDTA, disodium salt

In DEPC water, pH 7.0

RNA loading buffer

50% Formamide

22mM Formaldehyde

5% 20x MOPS

10% Glycerol

In DEPC water; addition of 1 spatula tip of bromophenol blue

Natrium-acetate buffer

96.92g Tris
 54.4g Natrium-acetate
 80ml 0.5M EDTA

Prepared in 1L of DEPC water and adjusted to pH 7.8

0.5 EDTA

116.07g EDTA, disodium salt

Dissolved in 1L DEPC water and adjusted to pH7.5

Buffer A

1ml 1M HEPES
 1ml 1M KCl
 20µl 0.5M EDTA
 0.0154g DTT

Dissolve in 100ml of DEPC water

2.1.4.2 Primers for SYBR Green real time PCR

| Gene name | Forward | Reverse | Species |
|--------------|------------------------|-------------------------|---------|
| BAMBI | CGCCACTCCAGCTACATCTT | TGCTTGCAAGAGAGTCCAGG | human |
| <i>Bambi</i> | CGAAGCCTCAGGACAAGGAA | AGCAGCACCAAGATCAGTCC | mouse |
| ID1 | GTGGCCATCTCGCGCT | TGTCGTAGAGCAGCACGTTT | human |
| MMP9 | CAGGTGTGGGTGTACACAGG | GTTCAACTCACTCCGGGAAC | human |
| PCNA | CTGAGGGCTTCGACACCTAC | TCACTCCGTCTTTTGACAG | human |
| p21 | GTGGCCTTGTCGCTGTCTT | GCGCTTGGAGTGATAGAAATCTG | human |
| PAI1 | GAAATGTCAGATGCGTGCC | GTCTCAGGCGGCCACAAG | human |
| rS18 | AAACGGCTACCACATCCAAG | CCTCCAATGGATCCTCGTT | human |
| HPRT1 | CCTGGCGTCGTGATTAGTGA | CGAGCAAGACGTCAGTCCT | human |
| <i>Ppai</i> | GAGCTGTTTGACAGACAAAGTC | CCCTGGCACATGAATCCTGG | mouse |

Table 2.1 Primer sets for gene specific SYBR Green real time PCR.

2x SYBR® Green Master Mix

Applied Biosystems (Foster City, CA, USA)

2.1.5 Materials for SDS-PAGE gel electrophoresis and immunoblot analysis

2.1.5.1 Buffers and solutions for protein lysis and determination of concentration

RIPA buffer (Cell lysis buffer)

| | |
|------------|--------------------------------|
| 1.815g | Tris base |
| 4.383g | Sodium chloride (NaCl) |
| 6ml | Nonident P40 |
| 0.279g | EDTA, sodium salt |
| 0.3g | SDS |
| 1.6g | Deoxycholic acid, sodium salt |
| 1pill/50ml | Protease inhibitor (see below) |

Adjusted with ddH₂O to 300ml, pH 7.2, stored at -20°C;

Addition of 50µl phosphatase inhibitor cocktail 2 (see below) per 5ml of complete RIPA buffer immediately prior use.

8M UREA lysis buffer

| | |
|---------|--------------------------------|
| 24ml | 8M Urea |
| 5ml | Glycerol |
| 2.5ml | 20% SDS |
| 0.25ml | 1M DTT |
| 0.333ml | 1.5M Tris, pH 6.8 |
| 1 pill | Protease inhibitor (see below) |

Adjusted with ddH₂O to 50ml, stored at -20°C;

Addition of 50µl phosphatase inhibitor cocktail 2 (see below) per 5ml of complete Urea buffer immediately prior use.

| | |
|--|--|
| Protease inhibitor, Complete (PIC) | Roche (Mannheim, Germany) |
| Phosphatase inhibitor cocktail 2 | Sigma Aldrich (St. Louis, Missouri, USA) |
| Bovine serum albumin, Fraction V (BSA) | Merck (Darmstadt, Germany) |
| Protein Assay, DC | Bio-Rad (Munich, Germany) |

2.1.5.2 Buffers, reagents and materials for SDS-PAGE gel electrophoresis and immunoblot

10x Lämmli buffer

144g Glycine
30.34g Tris base
100ml 10% SDS

Adjusted with ddH₂O to 1L.

1x Lämmli buffer

100ml 10x Lämmli buffer
900ml ddH₂O

20x NuPAGE® MOPS SDS Running Buffer Life Technologies (Frankfurt, Germany)

1x NuPAGE® MOPS SDS Running Buffer

50ml 20x NuPAGE® MOPS SDS Running Buffer
950ml ddH₂O

NuPAGE® LDS Sample Buffer (4X) Life Technologies (Frankfurt, Germany)

NuPAGE® Novex® 4-12% Bis-Tris Gels, 1.5 mm, 15 well Life Technologies (Frankfurt, Germany)

6M UREA loading buffer (1x)

378.55 mg Tris pH 6.8
18 g Urea
1 g SDS
1 spatula tip Bromophenol blue
5 ml Glycerol

Dissolve Tris in 20 ml of ddH₂O and adjust the pH to 6.8 with HCl; add Urea, SDS and let dissolve with gentle shaking; add one spatula tip of bromophenol blue, then Glycerol and gently homogenize; adjust the volume to 50ml with ddH₂O, make 950µl aliquots and store at -20°C. Add 50 µl of β-mercaptoethanol per 950 µl of loading buffer before using.

10x Wet transfer buffer (stock)

30.27 g Tris
144.13 g Glycine

Dissolve in 900ml of ddH₂O and adjust to 1L with ddH₂O.

1x Wet transfer buffer (work solution)

100 ml 10x Wet transfer stock buffer

200 ml Methanol

Filled up with ddH₂O to 1L.

20x NuPAGE® Transfer Buffer Life Technologies (Frankfurt, Germany)

1x NuPAGE® Transfer Buffer (work solution)

50 ml 20x NuPAGE® Transfer Buffer

200 ml Methanol

Filled up with ddH₂O to 1L.

Protein ladder, PageRuler Plus prestained Fermentas (St. Leon-Rot, Germany)

Nitrocellulose membranes, 0.2 µm pore size Whatmann (Maidstone, England)

Chromatography paper, 3MM Chr Whatmann (Maidstone, England)

Sponge blotting pads Invitrogen (Darmstadt, Germany)

2.1.5.3 Antibodies, buffers and reagents for protein detection**10x TBS**

12.1 g Tris base

87.66 g Sodium chloride (NaCl)

Dissolved in 800 ml of ddH₂O, adjusted to pH 7.6 and filled up with ddH₂O to 1L.

TBST (0.005%)

100 ml 10x TBS

900 ml ddH₂O

5 ml Tween-20

Dissolve with a magnetic shaker.

Ponceau S Red Sigma-Aldrich (St. Louis, Missouri, USA)

SuperSignal™ West Dura Extended Duration Substrate Thermo scientific (Waltham, Massachusetts, USA)

Western Lightning® Plus-ECL Substrate PerkinElmer (Rodgau, Germany)

ECL solution

10 ml 0.1 M Tris-HCl buffer (pH 8.5)
50 µl 250 mM Luminol
22 µl 90 mM p-Coumaric acid
3 µl Hydrogen peroxide solution 30%

Fresh preparation for each use/prior use

Stripping buffer (62.5 mM Tris, 2% SDS, pH 6.7)

7.57 mg Tris base
2 g SDS

Dissolve Tris and SDS in 800 ml of ddH₂O; adjust pH to 6.7 and then the volume to 1L with ddH₂O; add 40 µl of β-mercaptoethanol per 100 ml of stripping buffer prior use.

| Primary antibodies | | | | |
|------------------------------|---------|---------------------|-----------|----------|
| Epitope (target) | Species | Company | Cat.No | Dilution |
| Phospho-Smad2 (S465/467) | Rabbit | Cell Signalling | 3101L | 1:1000 |
| Phospho-Smad3 (S423/425) | Rabbit | Epitomics/Biomol | 1881-1 | 1:1000 |
| Smad2 | Rabbit | Cell Signalling | 5339 | 1:1000 |
| Smad3 | Rabbit | Cell Signalling | 9513 | 1:1000 |
| Smad2/3 | Rabbit | Cell Signalling | 5678s | 1:1000 |
| Phospho-P38 (Thr180/Tyr182) | Rabbit | Cell Signalling | 9211 | 1:1000 |
| P38 | Rabbit | Cell Signalling | 9212 | 1:1000 |
| BAMBI | Rabbit | Prestige Antibodies | HPA010866 | 1:1000 |
| BAMBI | Mouse | R&D Systems | AF921-SP | 1:2000 |
| TWSG1 | Rabbit | Abcam | ab183890 | 1:1000 |
| Phospho-Stat3 (Tyr705) | Rabbit | Cell Signalling | 9145 | 1:1000 |
| Stat3 | Rabbit | Santa Cruz Biotech. | sc-482 | 1:1000 |
| Phospho-Smad1/5/8 (S463/465) | Rabbit | EMD Millipore | AB3848 | 1:1000 |
| Smad1 | Rabbit | Cell Signalling | 9743 | 1:1000 |
| E-Cadherin | Rabbit | Cell Signalling | 3195S | 1:1000 |
| Anti-active-beta-Catenin | Mouse | EMD Millipore | 05-665 | 1:1000 |
| Bcl-2 | Rabbit | Cell Signalling | 2870 | 1:1000 |
| Phospho-Bcl2 (Thr56) | Rabbit | Cell Signalling | 2875 | 1:1000 |
| Mcl1 | Rabbit | Cell Signalling | 4572 | 1:1000 |
| c-Myc | Mouse | Santa Cruz Biotech. | sc-70464 | 1:500 |
| Cleaved Caspase3 | Rabbit | Cell Signalling | 9664 | 1:1000 |
| NFkB p50 | Mouse | Santa Cruz Biotech. | sc-8414 | 1:1000 |
| NFkB p65 | Rabbit | Santa Cruz Biotech. | sc-372 | 1:1000 |
| Phospho-Akt (S473) | Rabbit | Cell Signalling | 4060 | 1:1000 |
| Akt | Rabbit | Cell Signalling | 9272 | 1:1000 |
| GAPDH (FL-335) | Rabbit | Abcam | ab9485 | 1:1000 |
| Phospho-TAK1 | Rabbit | Cell Signalling | 9339 | 1:1000 |
| TAK1 | Rabbit | Cell Signalling | 4505 | 1:1000 |
| GFP | Rabbit | EMD Millipore | AB10145 | 1:1000 |
| Flag M2 | Mouse | Sigma-Aldrich | F3165 | 1:1000 |
| GAPDH | Mouse | EMD Millipore | MAB374 | 1:10000 |
| CTGF | Goat | Santa Cruz Biotech. | sc-14939 | 1:1000 |
| p-Erk(E-4) | Mouse | Santa Cruz Biotech. | sc-7383 | 1:1000 |
| Erk 1/2 | Mouse | Santa Cruz Biotech. | sc-135900 | 1:1000 |
| VEGF | Rabbit | Santa Cruz Biotech. | sc-152 | 1:1000 |
| Phospho-c-Jun (S63) | Rabbit | Cell Signalling | 9261S | 1:1000 |
| TIMP1 | Rabbit | Santa Cruz Biotech. | sc-5538 | 1:1000 |
| PCNA | Mouse | Santa Cruz Biotech. | sc-25280 | 1:1000 |
| Secondary antibodies | | | | |
| Anti-rabbit IgG-HRP | Goat | Santa Cruz Biotech. | sc-2301 | 1:10000 |
| Anti-mouse IgG-HRP | Goat | Santa Cruz Biotech. | sc-2005 | 1:5000 |
| Anti-goat IgG-HRP | Donkey | Santa Cruz Biotech. | sc-2033 | 1:3000 |

Table 2.2 Primary and secondary antibodies used for immunoblot analysis. The antibodies were obtained from Cell Signalling (Danvers, MA, USA), Santa Cruz Biotechnology (Santa Cruz, California, USA), Sigma-Aldrich (St. Louis, Missouri, USA), Epitomics (Burlingame, California, USA), Abcam (Cambridge, UK) or R&D Systems (Minneapolis, USA).

LB Agar

1L LB medium

15g/L Agar

Add agar before autoclaving; cool to 55°C and add the antibiotic before pouring into petri dishes; store at 4°C until use

HiSpeed Plasmid Midi Kit

Qiagen (Hilden, Germany)

2.2 Methods

2.2.1 Cell culture

All cell culture work was performed under sterile conditions using a laminar flow hood and following the safety instructions.

2.2.1.1 Cell culture

Six different hepatocellular carcinoma cell lines (chapter 2.1.3.1) were maintained in complete normal growth medium. Cells were cultured in filter cap tissue culture flasks at 37°C in a humidified incubator with 5% CO₂. The growth medium comprised high glucose DMEM medium, 2mM L-glutamine, 1% penicillin (100 IU/ml)/streptomycin (100 µg/ml) and 10% FBS. Cells were subcultured at 80-90% of confluency. For that, after washing with HBSS and detaching with 1x Trypsin-EDTA the cells were collected in complete growth medium (always double amount of medium than 1x Trypsin-EDTA). An appropriate amount of cells was used for further culturing or experiments. In case of experiments, cell numbers were determined using a Neubauer chamber. The viability of the cells was identified using Trypan blue solution.

2.2.1.2 Cryopreservation of cell lines

Cells of a low passage number were collected (chapter 2.2.1.1) in growth medium, spun down (1200 rpm, 5 min, room temperature) and resuspended in ice cold growth medium supplemented with 10% dimethyl sulfoxide (DMSO) or FBS with 10% of DMSO. Cells were put in cryotubes, kept in CoolCell devise at -80°C for 6-8 h and finally stored in liquid nitrogen. The cryopreserved cells were thawed at regular intervals to perform experiments within a similar passage range. To thaw, the cells in cryotubes were warmed very quickly to 37°C in a water bath and transferred to warm complete medium, spun down (1200 rpm, 5 min, and RT) and resuspended in growth medium.

2.2.1.3 Mycoplasma detection

All cell cultures used in this study were tested for mycoplasma contamination at a low passage number, using the Promokine PCR Mycoplasma Test Kit I/C according to manufacturer's protocol. Briefly, 1 ml of cell culture supernatant was spun at 500xg for

5 min to pellet the cellular debris. Then the supernatant was centrifuged at 14000 rpm for 15 min in a new tube and the resulted pellet was resuspended in 100 μ l of DNA free water after decanting. The sample was incubated at 95°C for 5 min and briefly centrifuged (5 s) before adding to the PCR mixture. The test is a PCR (polymerase chain reaction) based detection of mycoplasma 16S RNA and includes an internal and a positive control to ensure a successful PCR. Positive and negative controls were used together with the samples to perform a PCR with the following conditions: 1 cycle at 95°C for 2 min, 40 cycles at 94°C for 30 s, 55°C for 30 s, 72°C for 40 s and cooled down to 4-8°C. PCR products were detected as described in 2.2.4.5. Mycoplasma negative samples resulted in one signal (internal control, 479bp), while contaminated samples or the positive control showed a second signal at 270bp (Figure 2.1).



Figure 2.1 PCR for detection of mycoplasma contamination. Four examples of tested HCC cell lines' supernatants are shown together with the positive (Co+) and negative (Co-) controls.

2.2.2 Cell culture experiments

If not stated otherwise, cell line experiments were conducted in starvation medium (growth medium with 0.5% FBS) and with final confluency below 70-80%. The cells were stored in the cell culture incubator between the working steps. All experiments were performed within a passage number 14-30 after thawing cryopreserved cells (chapter 2.2.1.2).

2.2.2.1 Detection of Smad3/Smad4 reporter activity

In order to detect TGF- β induced Smad3/Smad4 transcriptional activity, an adenoviral construct carrying nine CAGA sequence repetitions within the firefly luciferase promoter region (Ad(CAGA)₉-MLP-Luc, described in [76]) was used for a luciferase promoter assay (hereafter named CAGA-Luc assay). 100000 cell/well were allowed to attach to 24 wells cell culture plate for 3 h. Cells were then infected with the adenovirus for 8 h (10 MOI) before changing the medium to starvation. The next day, medium was replaced with fresh starvation medium with or without 5 ng/ml of TGF- β 1, and the cells were disrupted after washing with HBSS in passive lysis buffer 1 or 16 h post-treatment. Each condition was performed in triplicates. Cell lysates were transferred to white microtiter 96 wells plate (30 μ l/well; 3 wells/condition). After adding the luciferase substrate (50 μ l/well), the luciferase activity was quantified by capturing luminescence with a microplate reader. The obtained values were first normalized to protein concentration (also measured in triplicates for each condition; described in chapter 2.2.5.2) of the same sample, and afterwards, treated samples were normalized to untreated controls.

2.2.2.2 Detection of Smad3/Smad4 reporter activity upon Ad-Bambi infection

Prior the CAGA-Luc, described in chapters 2.2.2.1, an adenoviral infection with h-Ad-Bambi (Vector Biolabs) construct was performed in order to assess the changes in the reporter's activity upon Bambi overexpression. Two methods were tested: sequential infection and co-infection. In the sequential infection, the cells were infected with Bambi adenovirus overnight (10 MOI) and let to recover for 6 h on the next day before infecting with the CAGA-Luc. During the co-infection, both virus Ad-Bambi and CAGA-Luc were mixed in the starvation medium at 10 MOI each virus and used to infect the cells for 8 h (afterwards the procedure was the same for both type of infection as described in chapter 2.2.2.1).

2.2.2.3 shRNA knockdown of BAMBI

HepG2 and Hep3B cells (300000 cells/well) were cultured overnight in a 6-wells plate, before changing the medium to one without antibiotics and transfecting them with shRNA8751 and shRNA8752 constructs against BAMBI and pEGFP plasmid as control (to monitor the efficiency of the transfection). The transfection was performed according to manufacturer's protocol of Metafectine[®] reagent. Briefly, two mixes were done separately: mix A with 140 μ l of OPTIMEM and 8 μ l of Metafectine, and mix B with 140 μ l OPTIMEM and 1.5 μ g shRNA (different tube for each shRNA and the pEGFP control). Then both were incubated for 5 min at RT before combining them in one tube and incubating for another 20 min (at RT). After the incubation, 280 μ l of the final mix was added to the corresponding wells and the plate were incubated overnight before changing to fresh medium. Controls were treated with the same mixture but without shRNA or pEGFP. The efficiency of the transfection was monitored by counting the green fluorescent cells in the pEGFP control under the microscope. After 72 h, the knockdown efficiency was studied by immunoblot after disrupting the cells in RIPA buffer (chapter 2.2.5) and with qRT-PCR (chapter 2.2.4.6) after extracting the RNA with TRIzol[®] reagent (chapter 2.2.4.3).

2.2.2.4 Lentiviral production

HEK293T cells (300000 cells/well) were plated in a 6 wells plate and let to grow overnight before changing the medium to fresh DMEM without antibiotics and FBS. Four plasmids co-transfection procedure was used to produce lentivirus from shRNA8751, shRNA8752, pLK0.1 empty vector, c-Flag-Bambi and c-Flag-pLV control. The transfection was performed following the same steps as described in chapter 2.2.2.5 with a difference in the mix B where the Metafectine was combined with a mix of the packaging plasmids (0.3 µg REV + 0.75 µg GAG + 0.45 µg VSV) and 1.5 µg of lentiviral plasmid (shRNA8751 / shRNA8752 / pLK0.1 empty vector / c-Flag-Bambi / c-Flag-pLV control). After overnight incubation, the medium was changed to fresh one and harvested on the next day. The collected medium was spun down at 2000 rpm during 10 min and the supernatant containing the virus was filtered through a sterile 0.45 µm filter (Acrodisc syringe filters cat# 4184, PALL Life Science). The virus was aliquoted and stored at -80°C or used directly to infect the target cells.

2.2.2.5 Stable BAMBI shRNA knockdown cell lines establishment

Hep3B cells (300000 cells/well) were plated in 6 wells plates and infected with 250 µl of the shRNA8751, shRNA8752 and pLK0.1 empty vector viruses (chapter 2.2.2.6) per well. On the next day the medium was changed to a fresh one containing 1 µg of Puromycin in order to select the infected cells. Once the control cells (without infection) were all dead due to Puromycin treatment, the selection was over and the knockdown efficiency was assessed by immunoblot and qRT-PCR.

In order to assess a better knockdown efficiency, the cell cloning by serial dilution in 96 well plate protocol (Corning) was used. Briefly, after detaching and counting the cells, 20000 cells/ml suspension was used as a starting point of the serial dilutions in the 96 wells plate filled with 100 µl of fresh DMEM medium. The 1:2 dilution were performed as shown in the diagram:

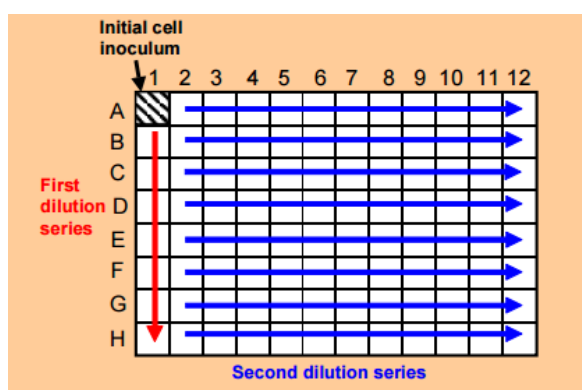


Figure 2.2 Figure from Corning protocol (<https://catalog2.corning.com>). After adding 200 µl of cell suspension to well A1, 100 µl was quickly transferred from the first well to well B1. This 1:2 dilutions were repeated down the entire column discarding the 100 µl from H1. After adding 100 µl of fresh medium to each well in column 1, 100 µl from the column A1→ H1 were quickly transferred to the next column (A2 → H2) using a 8-channel micropipette. This 1:2 dilutions were repeated across the entire plate discarding the last 100 µl from the last column (A12 → H12). Again the final volume in each well was brought to 200 µl by adding 100 µl of fresh medium to each well.

The plate were incubated at 37°C in a humidified CO₂ incubator and checked for clones by microscopy. After 4-5 days the clones were ready to transfer to 12 wells plates and start the selection with Puromycin. The knockdown efficiency was studied with a qRT-PCR after extracting the RNA with TRIzol[®]. All the clones were expanded, cryopreserved and stored at -80°C before transferred to liquid nitrogen.

2.2.2.6 BAMBI overexpression (adenoviral and lentiviral constructs)

HLE cells were plated in 6-wells plates (300000 cells/well) and let to attach before the infection with 5, 10 or 50 MOI of h-Ad-BAMBI (chapter 2.1.3.3) in fresh medium overnight. Ad-CMV-GFP was used to check the efficiency of the infection by monitoring the green fluorescent cells under the microscope. The over-expression efficiency was studied with an immunoblot analysis and with qRT-PCR. In order to detect any effect on TGF- β Smad1/Smad2/Smad3/Smad4 canonical signalling and P38 non-canonical signalling, an immunoblot analysis for (phosphorylated) Smad1/5/8, Smad2, Smad3 and P38 were performed.

In case of the lentiviral constructs for BAMBI over-expression (c-Flag-Bambi and c-Flag-pLV control), HLE cells (300000 cells/well) were cultured overnight in a 6-wells plate before infecting with 250 μ l of produced virus (chapter 2.2.2.6). The cells were let to recover for 24h before the selection with Puromycin started. As explained above, over-expression efficiency was studied by immunoblot and qRT-PCR. The effects on TGF- β canonical and non-canonical signalling were assessed by immunoblot analyses for (phosphorylated) Smad1/5/8, Smad2, Smad3 and p38.

2.2.2.7 Wound assay

The cells with stable BAMBI overexpression (hereafter named HLE-BAMBI) and downregulation (hereafter named H3B shBambi), the controls with empty plasmids (hereafter named HLE-Mock and H3B shMock) and the parental cells (HLE and Hep3B) were seeded in 6-wells plates (500000 cells/well) and let to attach before changing the medium to starvation overnight. On the next day, using a (white) 10 μ l pipette, straight scratches were done simulating a wound and the wells were washed before taking pictures at the microscope at time point 0 (before starting the treatment). The plate was marked with a perpendicular line to the wounds in order to find easily the same positions for the pictures along the different time points of the experiment.

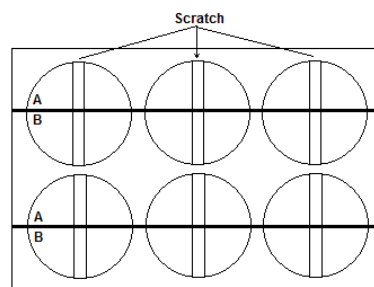


Figure 2.3 Disposition of the wounds in the plate. The wounds were done perpendicular to the mark line along the plate. While taking the pictures, the same position is easily assessed when making it above the line and naming it A, or below the line and naming it B.

Starvation medium with and without 5 ng/ml TGF- β 1 was added to the wells and the experiment continued until the closure of the wound (when possible) changing the medium every 48 h. The pictures were taken at 6, 12, 24, 48, 72 h (or longer when applicable) and the area of the wound was calculated with ImageJ. In order to translate this area to percentage of wound closure the formula used was:

$$\text{Migration (\%M)} = 100 * [(t_{0h} - t_h) / t_{0h}]$$

Where t_{0h} and t_h are gap areas measured at scratch time and the next time point (t_h), respectively

Normalization of the results were done in reference to the parental cells lines and/or to the non-treated cells.

2.2.2.8 Counting assay

Simple counting assays were performed to see the effect of BAMB1 over-expression and downregulation on proliferation and viability. 25000 cells/well were seeded and let to grow overnight in 12 wells plates before changing the medium to starvation. The cells were then either treated or not with 5 ng/ml of TGF- β 1 in starvation medium for 24, 48, 72 and 96 h (each condition in triplicates). Time point 0, before adding the treatment, and all the other time points (with and without treatment) were counted in a Neubauer chamber determining the viability of the cells using Trypan blue solution. The results were normalized to the non-treated controls and to the parental cell lines.

2.2.2.9 Caspase 3 assay

The effects of Bambi overexpression and downregulation on apoptosis were analysed using a Caspase 3 assay. Cells were let to attach at 100000 cell/well concentration for 4 h before changing the medium to starvation and let them grow overnight. The cells were then either treated with 5 ng/ml TGF- β 1 or not (as controls) for 24, and 48 h (triplicates for each condition were used). At the end of the treatment, supernatants with detached cells were collected, the cells were washed with HBSS, the used HBSS was combined with the supernatants and centrifuged at 2000 rpm for 5 min. Cells were disrupted on ice with 80 μ l/well of lysis buffer and assembled with the respective collected cells from the supernatant of the same sample. The samples were centrifuged at 13000 rpm for 5 min at 4°C and the supernatants were transferred to new tubes and let on ice for immediate assay or stored at -80°C. For a plate reading set up, 70 μ l of assay buffer were transferred to a 96 wells plate flat bottom white and mixed with 20 μ l of each sample (by triplicates). Then 10 μ l of caspase3 substrate (fluorimetric) were added to each well and mixed carefully by pipetting up and down. As blank controls a mix of 90 μ l assay buffer and 10 μ l caspase3 substrate were used. The plate was incubated covered by aluminium foil at 37°C for 1 h before measuring the fluorescence (excitation 400 nm; emission 505 nm) in a microplate reader. After extracting the blank from the values, the obtained results were normalized first to the concentration of the protein (also measured in triplicates for each condition; described in chapter 2.2.5.2) of the same sample, and afterwards, treated samples were normalized to untreated controls and parental cell lines.

2.2.2.10 Migration assay

A transwell assay was performed to analyse the migratory capacity of Bambi over-expressing and downregulating cells. Cells were cultured in starvation conditions overnight before being washed with HBSS, detached with 1xTrypsin-EDTA and spun down at 1200 rpm for 5 min. Single cell suspensions with 200000 cells/ml were prepared using starvation medium. Transparent PET transwell cell culture inserts with 8 μm pore size were transferred to 24 wells companion plates (Figure 2.4, A), which were filled with either 600 μl of starvation medium, starvation medium with 5 ng/ml TGF- β 1 or complete DMEM medium (as positive control). Bubbles at the bottom of the inserts were removed by careful tapping before transferring 100 μl cell suspension to the transwell inserts (Figure 2.4, B). Cell migration was allowed for 24 h (Figure 2.4, C). Each test was performed in triplicates. After incubation, the medium in the inserts was removed and they were carefully washed in HBSS before fixed in 90% ethanol for 30 min at 4°C. The cells were then washed again with HBSS and stained with 0.1% crystal violet for 15 min at RT (Figure 2.4, D). After double washed with ddH₂O, the non-migrant cells were removed from the upper face of the transwell membranes with cotton swabs and let dry for 5 min. The stained cells were subsequently photographed under light microscopy taking 5 fields at 10x magnification per transwell and counted.

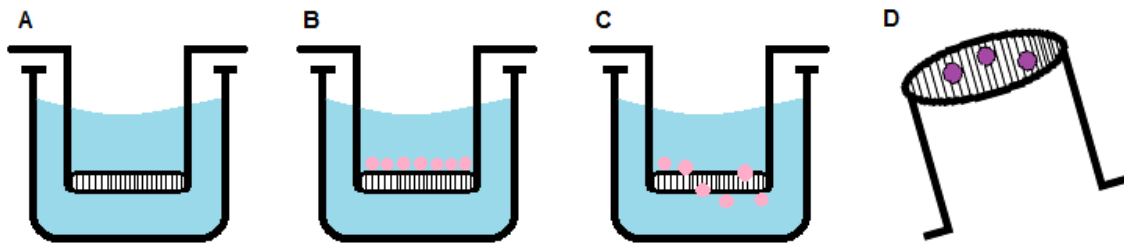


Figure 2.4 Illustration of the cell migration assay protocol.

The formulas used to calculate the migrated cells and the percentage of migrated cells were:

$$\text{Migrated cells} = (\text{Average cells} / 0.0254) * 0.3$$

$$\% \text{ Migration} = (\text{Migrated cells} / \text{Seeded cells}) * 100$$

Average cells = average of purple cells counted in 5 fields; 0.0254 = area of the microscope viewing field; 0.3 = entire area of the Transwell insert

The obtained results were normalized to non-treated controls and parental cell lines.

2.2.2.11 Invasion assay

A coated transwell assay was performed to analyse invasive capacity of the Bambi over-expressing and downregulating cells. Same procedure as described in chapter 2.2.2.13 for migration assay was used after treating the inserts with Matrigel (BD Matrigel Matrix Basement Membrane; BD Biosciences, San Jose, CA). The matrigel was thaw at 4°C and diluted to 1 mg/ml concentration in serum free-cold DMEM. 100 µl of the diluted matrigel was added into upper compartment of each insert and incubated for at least 1h at 37°C before carefully washing with HBSS and adding the cells suspension. After these steps, same procedures and calculations were performed as described for the migration assay in chapter 2.2.2.13. The results were normalized to non-treated controls and parental cell lines.

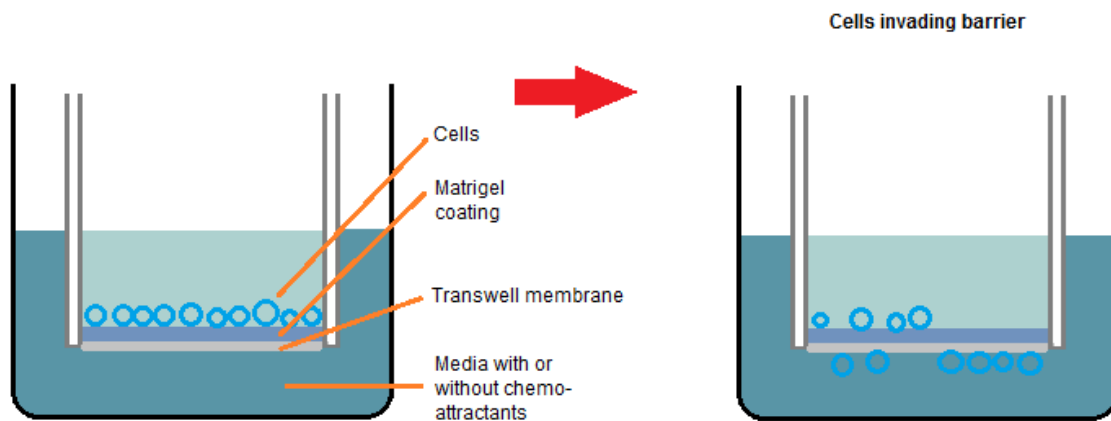


Figure 2.5 Illustration of the cell invasion assay protocol.

2.2.3 Patient and mouse samples

Human HCC tissue samples and corresponding non-tumour liver tissue were kindly provided by different collaboration partners in Germany and China:

Prof. Chun Fang Gao and Dr. Xing Gu (Department of Laboratory Medicine, Eastern Hepatobiliary Hospital, Second Military Medical University, Shanghai, China) provided the specimens enrolled in this study that were collected from September 2007 to December 2008 in Shanghai Eastern Hepatobiliary Surgery Hospital (EHBH, Shanghai, China). All patients signed informed consents and the experiments were conducted in accordance with the official recommendations of the Chinese Community Guidelines.

Prof. Dr. Stefan Wölfel's (IPMB, Heidelberg University, Germany) group provided liver tissue samples obtained from 6 HCC patients (undergoing surgery) collected from 2011–2014. The study has been approved by the ethics committee of the Medical Faculty Heidelberg of Heidelberg University (Ethikkommission I Heidelberg: Studienzeichen: S-202/2012) and described elsewhere [221].

Dr. Isabel Fabregat (Bellvitge Biomedical Research Institute (IDIBELL) and University of Barcelona, Barcelona, Spain) provided the DEN mice model samples used in the Fluidigm qRT-PCR analysis [164]. 15 days old mice received intraperitoneal injections of DEN (5 mg/kg) diluted in saline buffer; the control animals were injected

intraperitoneally with saline buffer only [216]. At 6, 9 and 12 months the mice were sacrificed and total RNA was isolated from their removed frozen liver tissues (as explained in chapter 2.2.4.1). Three to four animals per condition and two different tissue pieces per animal were processed for RNA extraction.

Wild type mice were obtained from Charles River or Jackson Laboratory and MDR2-KO (*Mdr2*^{-/-}) mice were kindly provided by F. Lammert, University Medical Center Saarland. Animals were maintained in a specific pathogen-free environment in the Animal Facility of the Medical faculty Mannheim (Heidelberg University) and the experiments were performed with age-matched mice. Genotyping was done as described elsewhere [217], and liver samples were obtained at 6, 9 and 12 months as described previously [218]. These particular samples were used for BAMBI expression assessment by qRT-PCR. The additional MDR2-KO (*Mdr2*^{-/-}) and control C57BL/6 wild-type mice RNA samples were kindly provided by P. Angel and J. Hess (Heidelberg). The mice were sacrificed at the age of 3, 6, 9, and 15 months and liver and blood samples were obtained according to standard operating procedures. These RNA samples were used for gene expression analysis by Fluidigm approach [164].

Double transgenic TGF- α /c-Myc mice samples were provided by Dr. Albrecht Piiper (Medizinische Klinik 1, Klinikum der Johann Wolfgang Goethe-Universität, Frankfurt am Main, Germany). Mice were generated by crossing c-Myc mice with TGF- α mice as described in [219]. In male TGF- α /c-Myc mice, hepatocarcinogenesis was induced by the addition of ZnCl₂ to the drinking water. Tumour development in the liver was detected by Gd-EOB-DTPA-enhanced magnetic resonance imaging [220]. Tumour and normal liver tissue were dissected and frozen at -80°C until use.

2.2.4 mRNA isolation and expression analysis

2.2.4.1 RNA isolation from tissue and cells using TRIzol reagent

20-50 mg of frozen mice liver samples were homogenized with a scalpel in 1 ml TRIzol[®] reagent on a petri dish and kept on ice for 15 min before removing the cell debris by centrifugation (10 min, 4°C, 12000xg). The room temperature adjusted supernatants were vigorously mixed with 200 μ l chloroform for 15 s, incubated at room temperature for 2 min and spun down (15 min, 12000xg, 4°C) to reach the separation. The top aqueous phase, containing the RNA, was transferred to a fresh tube and mixed with 500 μ l of isopropanol. After 10 min of incubation, the precipitated RNA was collected by centrifugation (10 min, 12000xg, 4°C). The pellets were washed twice with 75% ethanol (centrifugation at 10000xg and 4°C for 5 min), dried at RT and resuspended in 40-100 μ l RNase free water (5 min at 65°C on the ThermoBlot).

In the case of the cell cultures, 1ml of TRIzol[®] reagent was added to each well or petri dish with growing cells (washed previously with HBSS) and scratched on ice before collecting in fresh tubes. The following steps are the same explained above for RNA extraction from the tissue.

The RNA was stored at -80°C until further processing.

2.2.4.2 Tissue homogenization using Precellys Evolution Tissue Homogenizer

All the sterile material and work were prepared on dry ice. 600 µl of InviTrap® Spin Universal RNA Mini Kit lysis buffer (Stratec Molecular) were put in 2 ml homogenizer tubes with ceramic mix beads (1.4 and 2.8 mm) at RT. After cooling all the material on dry ice, small piece from the mouse liver was cut (always on dry ice) and transferred into the homogenizer tube. Once all the samples were prepared, we homogenized them at 5000 rpm for 10 s (only one cycle) and centrifuged at 10000 rpm for 5 min to break the formed foam. All content from the tubes were transferred into fresh ones. Any clumps were broken by an additional centrifugation at 10000 rpm for 5 min and the supernatant transferred to new tubes. RNA extraction from the samples followed the InviTrap® Spin Universal RNA Mini Kit protocol explained in the chapter 2.2.4.3.

2.2.4.3 RNA isolation using InviTrap® Spin Universal RNA Mini Kit

2 ml receiver tubes containing the tissue lysates were centrifuged for 2 min at maximum speed and 500 µl of the supernatant were transferred carefully to fresh 2 ml receiver tubes. Next, 330 µl of 96% ethanol were added to each sample, mixed thoroughly by pipetting up and down, completely transferred to the RTA Spin Filter Sets and incubated for 1 min at room temperature. After the incubation, the tubes were centrifuged for 2 min at 11000xg (and RT) and the flow-through was discarded. 600 µl of Wash Buffer R1 was added onto the RTA spin filter following a 1 min centrifugation at 11000xg and discarding the flow-through. Then 600 µl of Washing Buffer R2 were added onto the RTA spin filter and centrifuged for 1 min at 11000xg after 1 min of incubation. This step was repeated always discarding the flow-through before centrifuging the samples at maximum speed for 4 min in order to dry the RTA spin filter membrane. After the drying step, the RTA filters were transferred into RNase-free elution tubes and 30 µl of Elution Buffer R were pipetted directly onto the membranes. Once the incubation for 2 min at RT was over, the samples were centrifuged for 1 min at 11000xg and placed directly on ice.

The RNA was stored at -80°C until further processing.

2.2.4.4 Preparation of whole cell and nuclear RNA

1x10⁶ cells per dish were seeded in 10 Ø cm dishes until they reached 80-90% of confluence before they were washed with HBSS, detached with 1xTrypsin-EDTA, spun down (at 1200 rpm for 5 min) and resuspended in HBSS. The cells suspension was split in two parts, and the mRNA was extracted from the first part of collected cells using the TRIzol protocol (explained in chapter 2.2.4.1). The rest of the cells were washed with cold HBSS and centrifuged at 1500 rpm for 1 min before resuspended the pellets in 400 µl ice cold Buffer A and incubated for 10 min on ice. After, 25 µl of NP-40 10% were added to the mixtures and they were vortexed for 10 s. The suspensions were centrifuged at 9000 rpm for 1 min and the supernatants discarded. The resulted nuclear pellets were vortexed again with 500 µl of buffer A and 20 µl of NP-40 10% for 10 s, and centrifuged at 9000 rpm for 1 min. The resulted nuclear pellets were used for RNA extraction using the TRIzol protocol (chapter 2.2.4.1).

The RNA was stored at -80°C until further processing.

2.2.4.5 RNA gel electrophoresis

For the determination of RNA concentration and purity, 2 μ l of each RNA sample was loaded into a NanoQuant plate and analysed in a microplate reader using the Elution Buffer R or RNase-free water as blanks (depending on the RNA isolation protocol used for the extraction). In order to test the RNA integrity, a formaldehyde denaturation and electrophoresis of RNA samples were performed. Briefly, not more than 20 μ g of RNA per sample was transferred into a fresh tube and the volume was brought to 6 μ l with RNase-free water. Then 2 μ l of 10X MOPS Buffer, 2 μ l of 37% formaldehyde and 9 μ l of deionized formamide were added to each sample, mixed thoroughly and heated up for 10 min at 70°C. Samples were chilled on ice at least for 1 min before loading. For a 1% gel, 1 g of agarose was dissolved in 72 ml of RNase-free water and cooled down to 60°C in hot water bath before placing it in the fume hood. Immediately, 10 ml of 10X MOPS buffer and 5.5 ml of 37% formaldehyde, both prewarmed, were added to the agarose gel. While slowly swirling the solution, 1 μ l of GelRed per 10 ml was added to the gel and poured into the gel tray in the fume hood. At this point 2 μ l of formaldehyde loading buffer were added to each denatured RNA sample and loaded into the gel covered by 1X MOPS buffer inside the electrophoresis chamber. The separation was done at maximum of 5 V/cm (interelectrode distance) until the bromophenol blue crossed at least 80% of the way through the gel. GelRed stained RNA was visualized with a UV transilluminator system. Visible 28S and 18S ribosomal RNA (rRNA) bands, with the last one about half as intense as the 28S, indicated a good RNA integrity.

2.2.4.6 RNA analysis using Agilent RNA 6000 Nano kit

The Agilent RNA 6000 Nano kit was used together with the 2100 Bioanalyzer to assess the RNA integrity from the tissue samples and test the Precellys Evolution homogenizer. Briefly from the Agilent protocol, all reagents were let to equilibrate at RT for 30 min. 550 μ l of Agilent RNA 6000 Nano gel matrix (red) were placed into the top receptacle of a spin filter and centrifuged for 10 min at 4000 rpm. The 65 μ l aliquots of this gel were stored at 4°C and used within one month from preparation. To prepare the Gel-Dye mix, the components were let at RT for 30 min and protected from light during this time. The RNA 6000 Nano dye concentrate (blue) was vortexed for 10 s and spun down. 1 μ l of this dye concentrate was added to 65 μ l of filtered gel (described previously) and vortexed until proper mixing. The prepared mix was stored at 4°C in the dark prior use. The tube was spun down for 10 min at 14000 rpm and RT and used within one day. A new RNA Nano chip was placed on the station and 9 μ l of the gel-dye mix was pipetted at the bottom of the marked well. After setting the timer to 30 s, the chip priming station was closed and then released after 30 s. Then, 5 μ l of the RNA 6000 Nano marker (green) was pipetted into the marked well with the ladder symbol and each of the 12 sample wells in the chip. Before loading the samples on the chip, aliquots from the RNA stocks were taken and heated for 2 min at 70°C to minimize secondary structure. The chip was placed in the adapter of the IKA vortex mixer and vortexed for 60 s at 2400 rpm before being placed into the 2100 Bioanalyzer. Once the run is finished, the RNA Integrity Number (RIN), implemented with 2100 expert software version B.02.02 (check this) was displayed. To determine the RIN, the instrument software uses an algorithm that takes into account the entire electrophoretic trace of the RNA and it scales from 0 to 10. The software also estimates RNA concentration by comparing peak areas of a ladder with

RNA fragments of known concentration and peak areas of the unknown samples. Only the samples with a RIN between 7 and 10 and no DNA contamination were considered for further analysis.

2.2.4.7 Reverse transcription

Reverse transcription (RT) of RNA to cDNA was performed using the single components protocol. Briefly, in RNase-free tubes 500 ng of RNA were mixed with 0.5 μ l of Oligo(dT)18 primer, 0.5 μ l of Random hexamer primer and RNase-free water to 5.75 μ l. The resulted mix was heated up at 65°C for 5 min and then let at 25°C for 5 min. During this time the mix of reverse transcriptase was prepared putting together 2 μ l of 5X Reaction buffer, 1 μ l of 10 mM dNTPs and 0.25 μ l RevertAid H Minus Reverse Transcriptase (200 U/ μ L) for each sample. 3.25 μ l of the mix was added to each cDNA reaction tube and incubated at 42°C for 1 h. After that time the reaction was stopped by incubating the tubes at 70°C for 5 min. The resulted cDNAs were diluted 1:5 with RNase-free water and stored at -20°C or kept on ice for further use.

2.2.4.8 SYBR® Green real time PCR analysis

Expression levels of different TGF- β related genes were examined using SYBR® Green real time PCR.

Aqueous 1 ng/ μ l cDNA solutions were used for the detection of mRNA levels of various genes. A SYBR® Green master mix of an adequate volume for all samples (Table 2.5) was prepared and 18 μ l thereof was transferred to a suitable real time PCR plate. After the addition of 2 μ l cDNA or negative control (RNase-free water), the Real time PCR plate was sealed with a clear adhesive foil and briefly centrifuged at 1500 rpm.

| SYBR Green Master mix | |
|-------------------------------|--|
| Components | Volume for one 20μl reaction |
| Forward primer (5-10 μ M) | 1 μ l |
| Reverse primer (5-10 μ M) | 1 μ l |
| 2x SYBR® Green Master Mix | 10 μ l |
| ddH ₂ O | 6 μ l |

Table 2.4 Composition of SYBR Green Master mix for real time PCR

The used pairs of primers for specific cDNA detection are listed in Table 2.2 (page 6). Using the Stratagene MX 3005 P system, the PCR conditions were as follow: 10 min at 95°C (activation of DNA polymerase), 40 cycles of 30 s at 95°C (denaturation) and 1 min at 60°C (annealing and elongation). To exclude possible unwished signals of primer

dimers or unspecific primer binding, a dissociation curve between 60°C and 95°C was included at the end of each experiment. Each sample was analysed in triplicates and evaluated as described below (2.2.4.9).

2.2.4.9 Evaluation of real time PCR results

The fluorescence signal of DNA intercalated SYBR Green was detected after each elongation step. The threshold for collection of Ct values was set within the linear rise of the curve. Each sample was measured in triplicates and the data was analysed according to the $\Delta\Delta Ct$ method [225]:

$$\frac{(Ct_{GOI} - Ct_{ref})_{treated}}{(Ct_{GOI} - Ct_{ref})_{untreated}} = \Delta\Delta Ct$$

$$\text{Changes in expression} = 2^{-\Delta\Delta Ct}$$

GOI = gene of interest; ref = reference gene

18S rRNA and HPRT1 were identified as suitable reference genes by comparing the Ct values in all the cell lines used: the mean Ct values (of 2-3 experiments) were calculated for each cell line and varied between 19 and 20 with a standard error below 0.2 in all cases. PPIA was the reference gene used in qRT-PCR experiments with mice samples.

2.2.5 SDS-PAGE gel electrophoresis and immunoblots analysis

2.2.5.1 Protein lysates of cultured cells

HCC cell lines were allowed to attach to 6 wells plates before replacing growth medium with starvation medium. The next day, cells were either treated or not with 5 ng/ml TGF- β 1 for 0, 1, 6, or 16 h before collecting the cells. For basal levels of protein comparison each treatment had its own control without TGF- β 1, stopped at the same time point. At the end of an experiment, cells were washed with HBSS and disrupted in ice-cold RIPA or 8M Urea lysis buffer containing phosphatase and protease inhibitors. Cells were stored at -20°C until further processing and for a better cell disruption. Cell lysates were scrapped, transferred to fresh tubes and spun down to remove cell debris (10 min, 13000 rpm, 4°C). After determination of protein concentration (chapter 2.2.5.2), proteins were separated by an SDS-PAGE gel electrophoresis and immobilized on a membrane for immunodetection.

2.2.5.2 Determination of protein concentration

Protein concentrations were determined using a BC Protein assay, which is based on the Lowry method. The principle of this assay is the reaction of aminoacids with an alkaline copper tartrate and Folin reagent, which results in a reduction of Folin to a blue product. Prior to the protein addition, a mix of solution A (20 μ l/well) and solution S (0.4

µl/well) was calculated and prepared for all the samples and the BSA (bovine serum albumin) standard curve. 2 µl of protein samples and of BSA standard curve with known concentrations (0-10 mg/ml) were transferred to a 96 wells plate with the mix of solution A and solution S already pipetted in the wells (20 µl/well). 200 µl of solution B (Folin reagent) was added and after 10-15 min of incubation on a shaker, the absorbance was detected at 690nm using a microplate reader. The BSA standard curve and each sample were measured in triplicates and the unknown protein concentration were calculated using the BSA standard curve by linear regression.

2.2.5.3 Samples preparation for immunoblot

For denaturation of disulphide bonds, the mixtures of 10-20 µg of protein lysates and the amount of Urea loading buffer up to 20 µl final volume per sample were incubated at 95°C for 10 min and stored on ice for at least 1 min. After spinning down, the samples were loaded to an SDS-PAGE gel for protein separation.

2.2.5.4 Preparation of SDS-polyacrylamide gels and gel electrophoresis

Protein separation by size was achieved performing an SDS-PAGE (sodium dodecyl sulphate-polyacrylamide gel electrophoresis). 1.5 mm thick Bis-acrylamide (10%) gels were poured in gel casting systems from Bio-Rad: the separating gel (Table 2.6) was freshly prepared and immediately casted between two glass plates, leaving enough space for the stacking gel. This separating phase was covered with 70% ethanol to ensure a sharp and linear edge. The gel was allowed to polymerize for 30 min before the ethanol was removed. The left space was filled up with a freshly prepared stacking gel (Table 2.6) and a comb with 10 or 15 slots was inserted. After the polymerization for 30 min, the gels were installed in the electrophoresis module. The space between the two gels and the running chamber itself were filled with 1x Lämmli buffer (page 8). The comb was carefully removed and the wells were washed before loading a protein marker of known sizes and the samples in to the gel wells. Protein alignment in the collection phase was allowed at 80V for 15 min. Once the running front reached the separating gel, the voltage was increased to 120V.

| Separating gel, 10% | | Stacking gel | |
|-----------------------|---------|--------------------|---------|
| Acrylamide 30% | 3.33 ml | Acrylamide 30% | 0.67 ml |
| 1.5M Tris-HCl, pH 8.8 | 2.5 ml | 1M Tris-HCl pH 6.8 | 0.5 ml |
| ddH ₂ O | 3.96 ml | ddH ₂ O | 2.7 ml |
| 10% SDS | 100 µl | 10% SDS | 40 µl |
| 10% APS | 100 µl | 10% APS | 40 µl |
| TEMED | 4 µl | TEMED | 4 µl |

Table 2.5 Composition of separating and stacking gels for SDS-PAGE gel electrophoresis. Shown quantities display the amount for one gel.

In order to reduce the time of the procedure and the gel variation due to handling, the NuPAGE® Novex® system was used for protein separation. In this system, pre-casted gels NuPAGE® Novex® 4-12% Bis-Tris Gels 1.5 mm thick and 10, 12 or 15 wells were used and the electrophoresis chamber was filled up with 1x NuPAGE® MOPS SDS Running Buffer. The preparation of the samples was the same as explained above for the Bio-Rad system and the electrophoresis was conducted at 150V without the protein alignment step.

2.2.5.5 Western blot transfer

Immunoblot (Western blot) analysis was used to immobilize proteins on a nitrocellulose membrane (0.2 µm pore size, Whatmann, Maidstone, England). A sandwich was prepared, with the gel and the membrane in the middle surrounded by chromatography papers (3MM Chr, Whatmann, Maidstone, England), and blotting pads on both sides. To build this sandwich, the different layers were soaked in 1x Wet transfer buffer with methanol (page 8) and bubbles between the layers were carefully removed to ensure accurate protein transference. The transfer was performed in a blotting module filled with 1x Wet transfer buffer with methanol, with the membrane closer to the anode and the gel closer to the cathode. For protein transfer, 300-400 mA per membrane was applied over a time period of 3h.

In the case of NuPAGE® Novex® system, same steps were performed as explained for Bio-Rad system but using the provided NuPAGE® Novex® transfer device. The same layers sandwich was prepared using 1x NuPAGE® Novex® transfer buffer with methanol (page 8) and the bubbles were carefully removed. In this system 300 mA for 3 h were applied per membrane.

2.2.5.6 Immunodetection of proteins

Membrane bound proteins were temporarily stained with Ponceau S Red solution to ensure loading, satisfying blot quality and to identify possible transfer and/or handling errors. The membrane was washed in TBST (page 8) and blocked with 5% non-fat dried milk or 5% BSA (depending on the antibody) in TBST for 1h at RT to avoid unspecific binding and, therefore, to reduce the background. After washing with TBST, the membranes were incubated with a protein specific (first/primary) antibody overnight at 4°C and then washed again (3 x 5min) with TBST to remove unbound antibodies. The membranes were then incubated with a species specific (secondary) antibody conjugated to a horseradish peroxidase (HRP). Antibodies are listed in the Table 2.3 (page 9). After 1 h at room temperature incubation, the membranes were washed three times in TBST. All washing and incubation steps were conducted under agitation on a shaker. The HRP activity was detected by wetting the membranes in ECL, SuperSignal™ West Dura Extended Duration Substrate or Western Lightning® Plus-ECL Substrate and capturing the resulting chemiluminescence using a luminescent image analyser.

For further analysis with the same membranes, the antibodies associated to the membrane were detached. For this, the membranes were washed in TBST and incubated in Stripping buffer (62.5 mM Tris, 2% SDS, pH 6.7) for 30 min at 65°C with agitation. After washing them in TBST, the membranes could be used again.

2.2.6 Bacterial transformation and plasmids purification

2.2.6.1 Bacterial transformation using One Shot® TOP10 Competent Cells

In order to prepare the plasmids received from Prof. Peter ten Dijke, the One Shot® TOP10 Competent Cells kit was used to transform the competent cells with the plasmids. For this, the plasmids and 50 µl vials of One Shot® cells for each transformation were thaw on ice and 5 µl of each plasmid was pipetted into the vials of competent cells. The cells were incubated for 30 min on ice, then 30 s in 42°C water bath and placed on ice again. 250 µl of pre-warmed S.O.C. medium was added to each vial and incubated at 37°C for 1 h at 225 rpm in a shaking incubator. 100 µl from each transformation vial were spread on pre-warmed (at 37°C) separate LB agar plates with ampicillin. The plates were inverted and incubated at 37°C overnight or until the appearance of colonies. Then the colonies were taken with a tip (only one per glass of medium), placed in 50 ml of LB medium with ampicillin and incubated for 24 h at 300 rpm in a shaking incubator. Once the incubation was finished, the plasmids were extracted and purified with a HiSpeed® Plasmid Purification Midi kit (chapter 2.2.6.2).

2.2.6.2 Plasmids purification using HiSpeed® Plasmid Purification Midi kit

The HiSpeed® Plasmid purification Midi kit was used to purify the plasmids from the transformed competent cells (chapter 2.2.6.1). This protocol is based on a modified alkaline lysis procedure, followed by binding of plasmid DNA to a resin under appropriate low-salt and pH conditions. Briefly, the cells were harvested by centrifugation at 6000xg for 15 min (4°C) and the supernatants were completely discarded. The resulted pellets were resuspended in 6 ml of Buffer P1 by vortexing until no cell clumps were remaining.

After adding 6 ml of Buffer P2, the falcons were mixed by inverting 4-6 times and incubated at RT for 5 min. 6 ml of chilled buffer P3 were added to the lysates and mixed again by inverting the tubes before pouring them into the barrels of QIAfilter Cartridges and incubating at RT for 10 min. HiSpeed Midi columns were equilibrated by adding 4 ml of QBT and allowing the columns to empty by gravity flow before the cell lysates were filtered into the columns by attaching a plunger into each QIAfilter cartridge. Once the lysate completely entered the resin by gravity flow, the columns were washed with 20 ml of Buffer QC and then the DNA was eluted with 5 ml of Buffer QF. The DNA was precipitated by adding 3.5 ml of isopropanol (at RT) and incubated for 5 min. During the incubation, the QIAprecipitator Midi modules were attached to the outlet nozzles and the eluate/isopropanol mixtures were filtered through them using constant pressure. The DNA inside the precipitator modules was washed attaching the modules to syringes with 2 ml of 70% ethanol and then dried by attaching to empty syringes and pressing air through them twice. The precipitator modules were attached to syringes with 1 ml of Buffer TE and the DNA was eluted into collection tubes. 2 μ l of each DNA sample was loaded into a NanoQuant plate and analysed in a microplate reader using the TE Buffer as a blank.

The plasmids were stored at -20°C until further processing.

2.2.7 Immunohistochemistry of paraffin embedded samples

The paraffin embedded liver samples from HCC patients were cut in the microtome station the day before to perform the immunohistochemistry (IHC) protocol. The slides were cut 2 μ m thickness and dried in the incubator at 37°C overnight.

On the next day IHC protocol was used to locate specific proteins in the tissue. Briefly, the slides were deparaffinised in two xylene washes (5 min each) and rehydrated in two washes of 100% ethanol and one 96% ethanol for 5 min each wash. After finishing the rehydration steps, the slides were left for 5 min in 1x PBS for before the unmasking antigen step. For this, the slides were brought to a sub-boiling temperature in 1mM EDTA (pH 8.0) buffer for 10 min. In order to achieve that, the slides were microwaved for 10 s and let 50 s outside ten times in a row and left at RT for 30 min before washing the slides in 1x PBS (2 x 10min). A DAKO peroxidase blocking reagent was poured carefully covering the whole tissue on each slide and let to act for 10 min. The slides then were washed twice with 1x PBS (10 min each wash) before covering the tissues with a protein specific (first) antibody and incubating overnight at 4°C in a humidified atmosphere. As a negative control only PBS were used on the tissues during this step. Finished the incubation, the slides were washed three times with 1x PBS for 10 min and incubated with a species specific (secondary) antibody conjugated to a horseradish peroxidase (HRP) at room temperature for 45 min. The slides then were washed with 1x PBS (3 x 5 min) and covered by freshly prepared DAB (3,3'-Diaminobenzidine) solution. To prepare the DAB, one DAB pill was dissolved in 15 ml of DAB buffer (0.05M Tris, pH 7.6) in a falcon covered with aluminium and filtered to a new covered tube before adding 12 μ l of peroxide (H₂O₂). Once the slides were covered with DAB solution, the appearance of brown colour in the tissues was monitored under the microscope and the reaction was stopped by submerging the slides in ddH₂O water. The slides were stained in Eosin Y-solution (0.5% aqueous) for one minute and washed under running tap water for 15 min.

Once the excess of Eosin Y-solution was washed out, the slides were dehydrated again in one 96% ethanol and two 100% ethanol washes (5 min each) and let in xylene until covering the slides. To ensure a longer storage of the slides DAKO Fluorescent Mounting Medium was used in the cover step. Antibodies used in these experiments are listed in the Table 2.4 (page 11).

2.2.8 Statistical analysis

2.2.8.1 Statistical analysis of experimental work

Cell line data are presented as the mean \pm standard deviation (SD) of a representative result from three independent experiments or standard error (SE) of at least three independent experiments, if not stated otherwise. In some cases, statistically significant differences were identified by Student's *t*-test or One-way ANOVA. Correlation analysis was performed by calculating the Pearson correlation coefficient *r*. For all tests, significant levels are identified as * $p < 0.05$, ** $p < 0.01$, *** $p < 0.001$ and **** $p < 0.0001$.

2.2.8.2 Analysis of publicly available HCC data

Publicly available databases (iCOD, omics.tmd.ac.jp/icod_pub_eng/; Oncomine, <https://www.oncomine.org/>; GEO, <http://www.ncbi.nlm.nih.gov/gds>; Arrayexpress, <http://www.ebi.ac.uk/arrayexpress/>; and PubMed, <http://www.ncbi.nlm.nih.gov/pubmed>), as well as data generated within the SFB/TRR77 on Liver Cancer (GSE50579 [183]) and those collected from our own collaborative projects, were used in order to analyse expression of TGF- β signalling regulator (TSR) candidates. Furthermore, TSRs expression was analysed in 18 HCC cell lines (<http://medicalgenomics.org/cellminerhcc>) [188].

35 TSRs were pre-selected using the following criteria: significance below 0.05 (p -value < 0.05) and significant difference in expression in at least 3 cohorts when compared to normal liver or surrounding tissue samples (Scheme 2.1). After screening the available information about their interaction with TGF- β pathway and/or HCC, the list was reduced to 16 candidates from which only five (BAMBI, TWSG1, DPT, CHRDL and NEDDL4) did not present information on function and molecular mechanisms, hence I focused my interest on these candidates. Next, Bioconductor (R) 2.13 (3.0.1) and GraphPad Prism6 tools were used to retrieve and analyse the expression data from 6 HCC sample cohorts (Table 2.7) comprising a total number of 803 HCC patients, presented from different etiologies. Each candidate was analysed in the mentioned cohorts using the single patient expression data in order to see the intra and inter-cohort expression distribution of the pre-selected candidates in the patients. Their expression values were matched to normal liver samples and/or to each patient's surrounding tissues (Scheme 2.1). Additionally, I calculated the tendency in mean expression to show the intra and inter-variation of TSRs candidates' expression values in the cohorts. Only patients with $\text{Log}_2(\text{Fold Change}) > 0.5$ and < -0.5 were considered as significantly regulated. The meta-analyses results revealed significant regulation of 3 from the target genes identified above (BAMBI, Twisted and Dermatopontin), from which I decided to focus my investigation on BAMBI (further disclosed in chapter 3.1.1).

For human HCC patient samples, X-tile software [187] was used to identify different populations of patients based on their Bambi expression levels (low, medium or high) and the Pearson correlation coefficient r was performed to identify possible associations with clinical-pathological characteristics. In some cases, statistically significant differences were identified by Student's t -test, One-way ANOVA or Mann-Whitney test. In order to calculate the p -value for Pearson correlations (r), the function TDIST was used:

$$\text{TDIST} = ((r * \text{Sqrt}(N-2)/\text{Sqrt}(1-(r^2))), N, 2)$$

Where r = Pearson correlation coefficient; N = number of observations; Sqrt = square root

For all tests, significant levels are identified as * $p < 0.05$, ** $p < 0.01$, *** $p < 0.001$, and **** $p < 0.0001$.

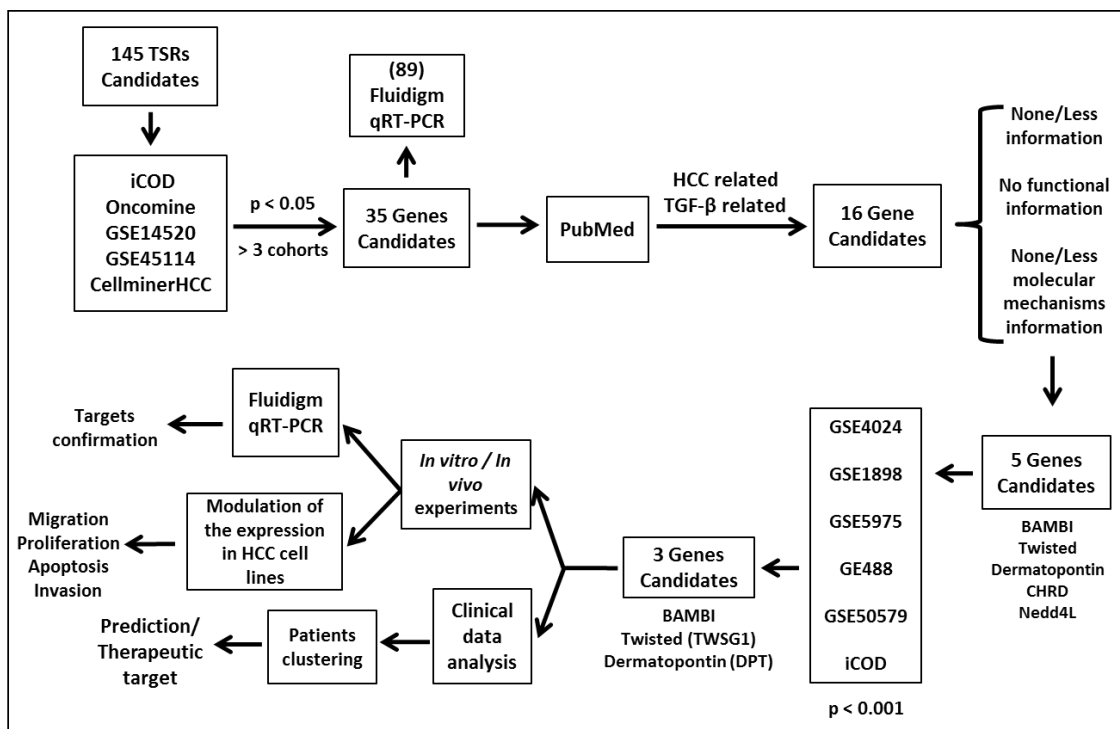


Figure 2.6: Schematic overview of the screening. The flow chart illustrates the steps of the screening in order to have a general view about their expression and significance. Only candidates present in more than 3 cohorts and with a p -value < 0.05 were selected for further screening. PubMed available information about our candidates were screened to discriminate the candidates and select only those potentially related to the TGF- β pathway and/or HCC, with a current lack of knowledge about functional implication in HCC. Then each candidate was analyzed in further details in 6 cohorts of patients. The selected candidates were analyzed in a Fluidigm qRT-PCR platform with genetic (TGF- α /c-Myc, MDR2-KO) and chemical (DEN) mouse models of liver cancer to experimentally investigate the potential TSR targets, with special impact for the preselected candidates. *In vitro* and *in vivo* experiments were carried out with selected candidates to explore molecular mechanisms of their implication in hepatic-carcinogenesis.

| | | N°HCC patients | Etiologies | Normal Liver | Surrounding tissue |
|--|------------------|----------------|---|--------------|--------------------|
| Roessler S, Cancer Res., 2010 [180] | GE488 (GSE14520) | 247 | HBV | | 247 |
| Wang XW, Clin Cancer Res., 2007 [181] | GSE5975 | 236 | Ep_CAM +/-; HBV+; Cirrhosis +/- | | 236 |
| Thorgeirsson SS, Nature Genetics, 2004 [182] | GSE1898 | 91 | HBV+; HCV+; co-infection; HBV/Alcohol; HCV/Alcohol, Hemochromatosis | 18 | |
| Neumann O, Hepatology, 2012 [183] | GSE50579 | 40 | HBV+; HCV+; co-infection; Alcohol; Cryptogenic; Hemochromatosis; Others | 7 | |
| Lee JS, Nat Med 2006 [185] | GSE4024 | 49 | HBV+; HCV+; co-infection; ALD; ALD + infection; Other; Unknown | 19 | |
| Shimokawa K, BMC Genomics, 2010 [184] | iCOD | 140 | HBV+; HCV+; co-infection; Alcohol; HCV+Alcohol, Diabetes; Cirrhosis; Unknown | NA | |
| Thorgeirsson SS, Nature Genetics, 2004 [182] Lee JS, Nat Med, 2006 [185] | GSE4024/ GSE1898 | 142 | HBV+; HCV+; co-infection; Alcohol; Cryptogenic; Hemochromatosis; NASH; Adenoma; Autoimmune; Unknown; Others | 10 | |

Table 2.6 Publicly available HCC's microarray data cohorts used in the meta-analysis of the TSRs expression.

3 RESULTS

3.1 BAMBI expression meta-analysis in publicly available datasets from HCC patient cohorts and mice models

3.1.1 BAMBI is significantly upregulated in more than 70% of HCC- patients from different cohorts and aetiologies

As explained in chapter 2.2.8.2, BAMBI was significantly (p -value < 0.05) upregulated in the mean in three out of the initial four patient cohorts (iCOD, Oncomine, and GSE14520). Single patient data analysis showed BAMBI upregulation in all six HCC cohorts investigated when compared to normal liver or surrounding tissue samples and revealed a major upregulation distribution within the different cohorts when represented in a dot plot (Figure 3.1, A). Interestingly, the GSE5975 data cohort presented significant ($***p = 7.05e^{-7}$) mean BAMBI overexpression in the epithelial cell adhesion molecule (EpCAM) positive subpopulation (Figure 3.1, B), but not in EpCAM-negative patients ($p = 0.95$). Therefore, the EpCam-negative population was excluded from this study. As can be observed in Figure 3.1 B, 62% ($n=412$) of 661 patients presented a significant BAMBI modulation, taken as acceptable change the $\text{Log}_2(\text{Fold change}) > 0.5$ or < -0.5 once referred to normal liver and/or surrounding tissue. After further analysis, BAMBI upregulation was detected in 77.67% ($n=320$) of the patients with relevant BAMBI modulation (Figure 3.1, C).

As explained in chapter 1.3, despite all the studies performed on different types of cancers, BAMBI's function and the mechanisms that BAMBI uses to drive its effects in HCC have not been fully discovered. BAMBI downregulation was found to be related to fibrosis progression [159] but was also found upregulated in many different cancers including HCC [144]. These meta-analysis findings confirm BAMBI upregulation in HCC patients and suggest a role in hepatic-carcinogenesis, most probably related to the modulation of TGF- β signalling and the Wnt/ β -catenin pathway (see chapter 1.3), which needs to be confirmed by further studies.

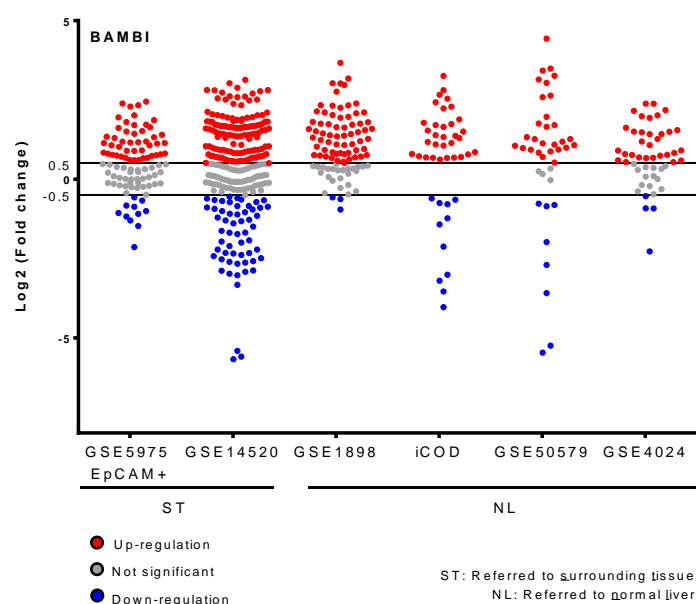


Figure 3.1: BAMBI is upregulated in publicly available HCC cohorts. Dot plot representing the variations between intra- and inter-cohort expression of BAMBI, demonstrating the upregulation tendency.

| BAMBI | N° patients | Significant patients | Adj. <i>p</i> - Value | Mean Log ₂ (Fold change) |
|----------------|-------------|----------------------|-----------------------|-------------------------------------|
| GSE5975 EpCAM+ | 94 | 58 | 7.05E-7 | 0.51 |
| GSE14520 | 247 | 183 | <0.0001 | 1.26 |
| GSE1898 | 91 | 67 | 2.03E-17 | 1.09 |
| iCOD | 140 | 43 | NA | 1.64 |
| GSE50579 | 40 | 36 | 0.001 | 0.71 |
| GSE4024 | 49 | 25 | 0.02 | 0.99 |
| TOTAL | 661 | 412 | | |
| | % | 62.33 | | |

Table 3.1: BAMBI expression in publicly available HCC cohorts. Patients with significant changes [Log₂(Fold change) >0.5 or <-0.5] in BAMBI expression, when referred to their respective controls, among the cohorts.

| BAMBI | Significant patients | N°patients Up-reg. | N°patients Down-reg. |
|----------------|----------------------|--------------------|----------------------|
| GSE5975 EpCAM+ | 58 | 47 | 11 |
| GSE14520 | 183 | 126 | 57 |
| GSE1898 | 67 | 64 | 3 |
| iCOD | 43 | 32 | 11 |
| GSE50579 | 36 | 28 | 8 |
| GSE4024 | 25 | 23 | 2 |
| TOTAL | 412 | 320 | 92 |
| | % | 77.67 | 2.33 |

Table 3.2: BAMBI expression in HCC-significant patients. Percentage of significant patients that show BAMBI upregulation within the HCC cohorts. NA = not announced.

3.1.2 BAMBI expression in chemical-induced liver carcinogenesis (DEN) and genetic (MDR2-KO) mice models

The candidates selected after the first steps of the screening (see chapter 2.2.8.2, Scheme 2.1) were analysed in a microfluidic Fluidigm's BioMark HD high-throughput quantitative chip platform [164] with transgenic (TGF- α /c-Myc, MDR2-KO) and chemical (DEN) mouse models of liver disease to experimentally investigate the potential TSR targets with a special impact on the preselected candidate (BAMBI).

The Fluidigm data analysis did not show any significant changes for BAMBI expression in the TGF- α /c-Myc transgenic model (data not shown), while the MDR2-KO mice presented significant BAMBI upregulation in early and intermediate stages of chronic liver disease (CLD), 3 (***p* = 0.0007) and 6 (**p* = 0.04) months (Figure 3.2, A). Generally, MDR2-KO mice develop cancer after one year. On the other hand, late-stage MDR2-KO

samples (15 months) showed a tendency towards upregulation; however, it was not statistically significant (Figure 3.2).

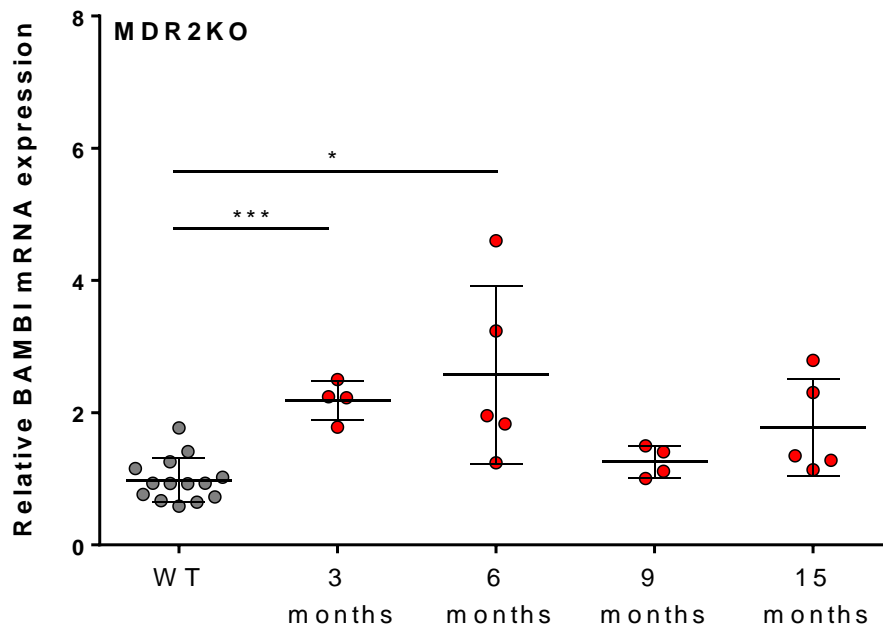
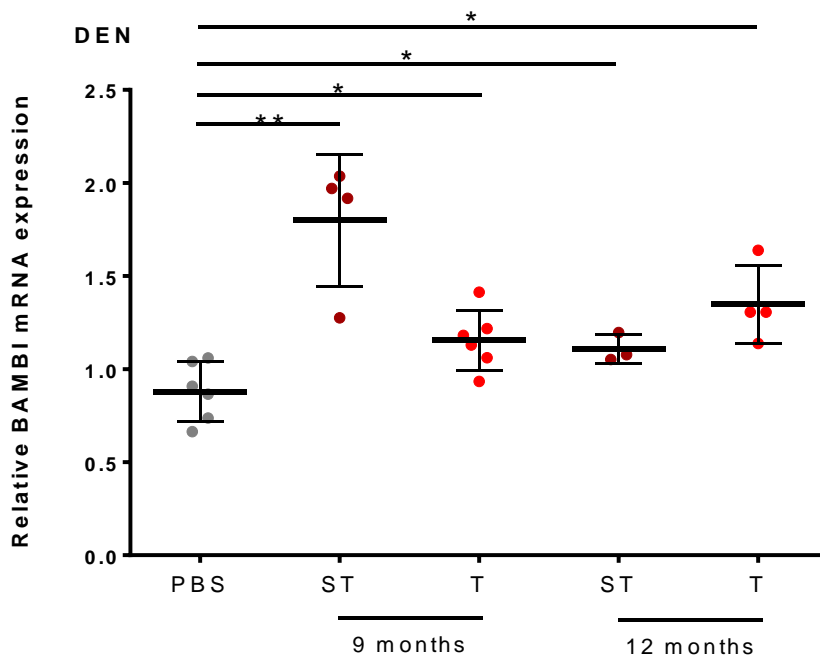


Figure 3.2: Fluidigm qRT-PCR assessed BAMBI expression levels in MDR2-KO murine model. In MDR2-KO samples at 3, 6, 9 and 15 months of age, BAMBI expression was determined and compared to the respective wild type (WT) controls. A close analysis of the WT samples did not show any significant variation in BAMBI expression; therefore, they were all used together as a reference, thus increasing the number of control samples (data not shown). * $p < 0.05$; ** $p < 0.01$; *** $p < 0.001$. Adapted and modified according to [164].

In addition, BAMBI was found upregulated in tumour and surrounding tissue samples of DEN-treated mice when compared to untreated controls after 9 (* $p = 0.02$) and 12 (* $p = 0.01$) months (Figure 3.3, A). Interestingly, tumour samples after 9 months of treatment presented lower levels of BAMBI compared to their matched surrounding tissue samples, whereas at 12 months, the levels were comparable (Figure 3.3, B). These results suggest a possible influence of the tumour stroma.

The Fluidigm qRT-PCR MDR2-KO results were confirmed in our own MDR2-KO model by qRT-PCR. BAMBI expression was found to be increased in the early stages, 3 (** $p = 0.007$) and 6 (** $p = 8.36E-09$) months, but not significant after 12 months ($p = 0.08$), even though an upregulation tendency could be observed (Figure 3.4). This result indicates a possible role of BAMBI in early stages of the disease and HCC progression.

A)



B)

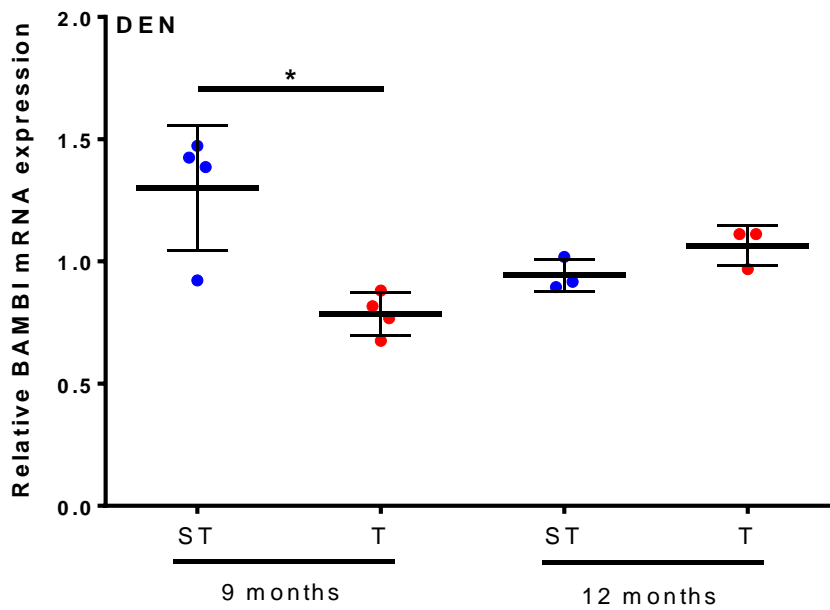


Figure 3.3: Fluidigm qRT-PCR assessed BAMBI expression levels in DEN murine model. In DEN-induced tumour samples, BAMBI expression was determined and compared to the respective PBS-treated controls (A) or matched surrounding tissues of the same animals (B). A close analysis of the PBS samples did not show any significant variation in BAMBI expression; therefore, they were all used together as a reference, thus increasing the number of control samples (data not shown). * $p < 0.05$; ** $p < 0.01$. Adapted and modified according to [164].

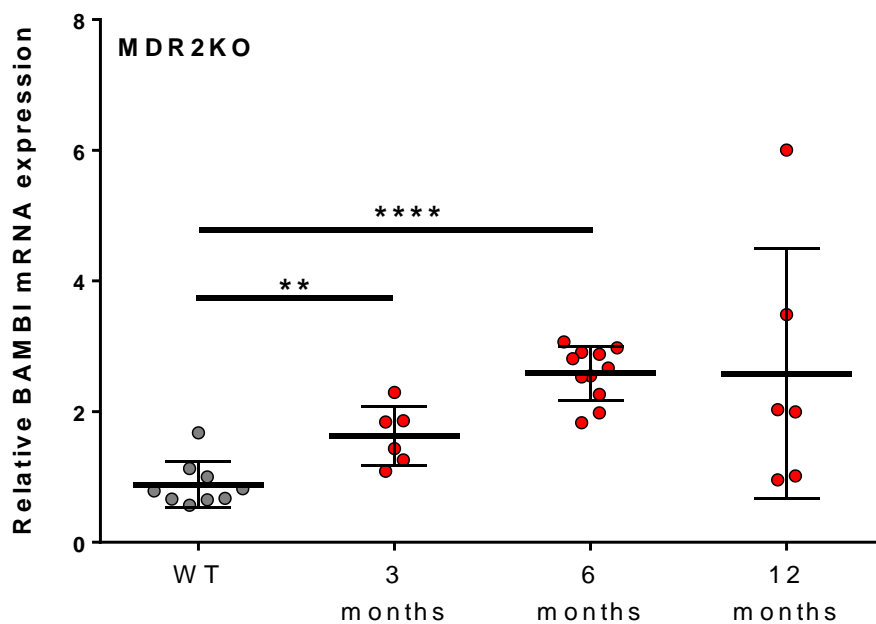


Figure 3.4: qRT-PCR assessed BAMBI expression levels in the MDR2-KO model. The expression in MDR2-KO samples was determined and compared to all the respective wild-type controls (Balb/c mice) together since there was no significant variation in BAMBI expression among the wild-type samples (data not shown). ** $p < 0.01$; **** $p < 0.0001$. PPIA expression was used as a reference.

3.1.3 Correlation with clinical-pathological data

During TSR meta-analysis, the integrated Clinical Omics Database (iCOD) [184] proved to be a highly useful tool that combined the expression data from Japanese HCC patients and their clinical-pathological information. Despite some missing information, this database is an outstanding example of how publicly available patient data should be presented to the scientific and clinical communities. In the iCOD HCC cohort ($n=140$), BAMBI was found upregulated (shown in Figure 3.1) and its expression significantly correlated ($p = 0.03$) with portal vein/hepatic vein invasion, suggesting a possible effect of BAMBI enhancing the invasion of tumour cells during HCC progression.

Furthermore, the X-tile [187] free software tool was used to group the patients in the GSE14520 cohort [180] ($n=247$) depending on their BAMBI expression. The aim was to analyse whether BAMBI could be implicated in the survival and other clinical-pathological data of the patients. As seen in Figure 3.5, the patients were separated into three groups by the software's algorithm according to their status (dead or alive), time of survival (months) and BAMBI expression level (low, middle, or high). Unfortunately, BAMBI did not show any significant correlation with the survival of the patients. Interestingly, this result mimics the BAMBI expression profile in the 12 months old MDR2-KO mice (presented in the chapter 3.1.2). Regardless the lack of significance in the correlation with survival, there were two positive correlations, with (1) age – there was an increment in patients < 50 years old in the group with high BAMBI levels; and (2) BCLC staging, where a higher percentage of advanced stage C was found in the group with higher levels of BAMBI expression (Table 3.3).

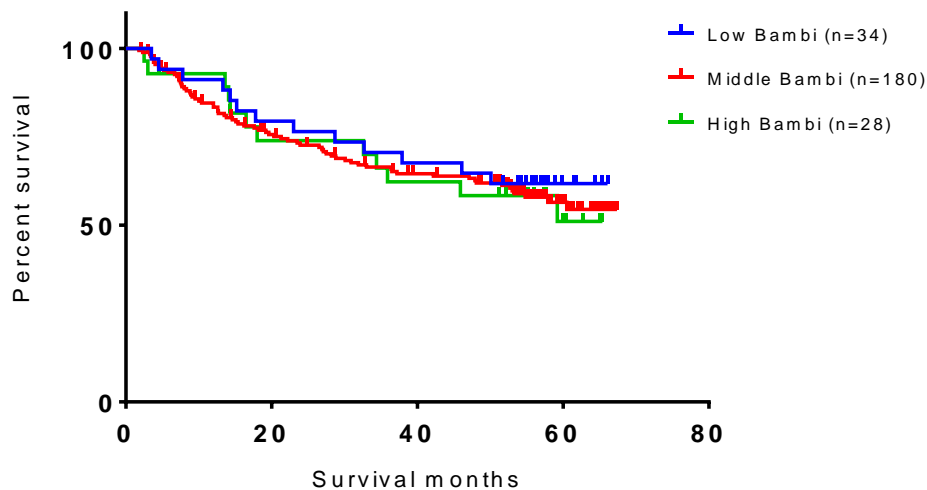


Figure 3.5: Kaplan-Meier survival analysis of patients in the GSE14520 cohort. The patients were separated into three groups according to their BAMB I expression levels (low, middle, or high) by the X-tile software.

| Clinico-pathological factors | Middle Bambi (n=180, %) | High Bambi (n=28, %) | P - value ^a |
|------------------------------|-------------------------|----------------------|------------------------|
| Age(years) | | | 0.03 |
| <50 | 74(41.11) | 18(64.29) | |
| ≥50 | 106(58.89) | 10(35.71) | |
| Gender | | | 0.36 |
| Male | 159(88.33) | 23(82.14) | |
| Female | 21(11.67) | 5(17.86) | |
| T stage | | | 0.12 |
| T1-T2 | 133(73.89) | 17(60.71) | |
| T3-T4 | 33(18.33) | 9(32.14) | |
| Multinodular | | | 0.43 |
| Yes | 32(17.78) | 3(10.71) | |
| No | 148(82.22) | 25(89.29) | |
| Cirrhosis | | | 0.27 |
| Yes | 166(92.22) | 24(85.71) | |
| No | 14(7.78) | 4(14.29) | |
| Main tumor size | | | 0.55 |
| <5 | 79(43.89) | 14(50) | |
| ≥5 | 101(56.11) | 14(50) | |
| Recurrence | | | 0.22 |
| 0 | 82(45.56) | 9(32.14) | |
| 1 | 98(54.44) | 19(67.86) | |
| HBV viral status | | | 1 |
| CC | 114(66.33) | 19(67.86) | |
| AVR-CC | 46(25.56) | 7(25) | |
| BCLC Staging | | A vs C | 0.04 |
| A | 119(66.11) | 15(53.57) | |
| B | 17(9.45) | 2(7.14) | |
| C | 17(9.45) | 7(25) | |
| Survival | | | 0.84 |
| 0 | 109(60.56) | 16(57.14) | |
| 1 | 71(39.44) | 12(42.86) | |

Table 3.3: Correlation of BAMB I expression levels with clinical-pathological characteristics in the GSE14520 cohort. ^aFishers' exact test.

In summary, the results presented in chapter 3.1 demonstrate that BAMBI is over-expressed in publicly available HCC patient cohorts and mice models. Overall, 77.67% of the patients presented BAMBI upregulation, which was correlated with age and the display of more advanced BCLC stage cases in a 247-patients cohort (GSE14520). A closer look at HCC mice models suggests that BAMBI may play a role in the early stage of the disease, with a possible influence from the stroma.

3.2 Expression analysis of BAMBI in HCC cell lines

A comparative analysis of endogenous BAMBI expression levels was performed to investigate the impact of BAMBI up- or downregulation in further experiments. Moreover, we wanted to confirm the results of the Cell Miner HCC database [188] where BAMBI appeared highly expressed in early TGF- β signature cells (Hep3B, HUH6 and HUH7, among others) compared to the transformed normal liver epithelial cell line, THLE-3 (Figure 3.6; see chapter 1.1.5 for further information about TGF- β gene signatures).

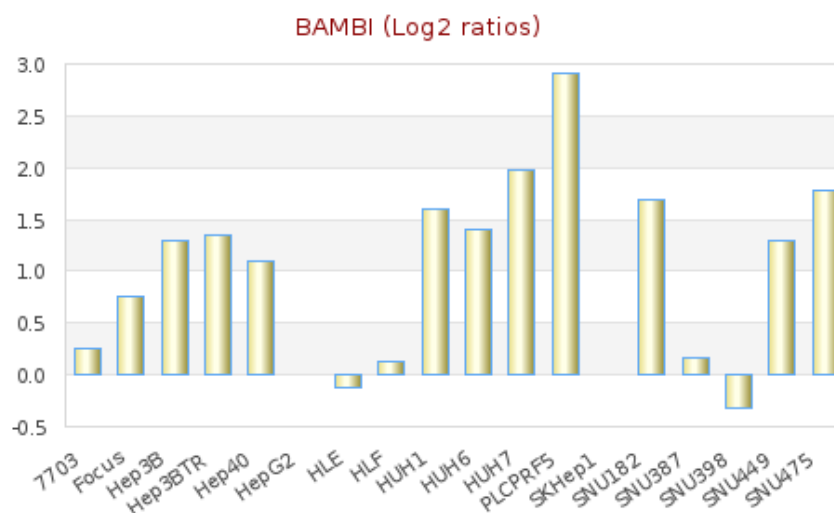


Figure 3.6: BAMBI expression in HCC cell lines from Cell Miner HCC database [188]. Image taken from the website <http://medicalgenomics.org/cellminerhcc>

3.2.1 BAMBI is expressed differently in HCC cell lines with early (epithelial phenotype) versus late (mesenchymal phenotype) TGF- β signature

BAMBI qRT-PCR analysis revealed a variation in relative mRNA levels in different HCC cell lines compared to a normal human hepatocyte RNA pool (Figure 3.7). High expression levels occurred in Hep3B, HUH7 and HepG2 cells (12.6, 20.3 and 9.3 fold difference, respectively), which present an early TGF- β gene signature and an epithelial phenotype [62]; while FLC4, HLE and HLF (with late TGF- β signature and mesenchymal phenotype) showed a lower level of expression comparable to the human hepatocyte pool (0.09, -0.01 and 0.08 fold difference, respectively).

This finding provides strong confirmation for the BAMBI expression pattern in HCC cell lines found in the Cell Miner HCC database and is comparable when a human

hepatocyte RNA pool is used as control. Furthermore, this result allowed selecting the Hep3B and HLE HCC cell lines for BAMBI modulation in further experiments.

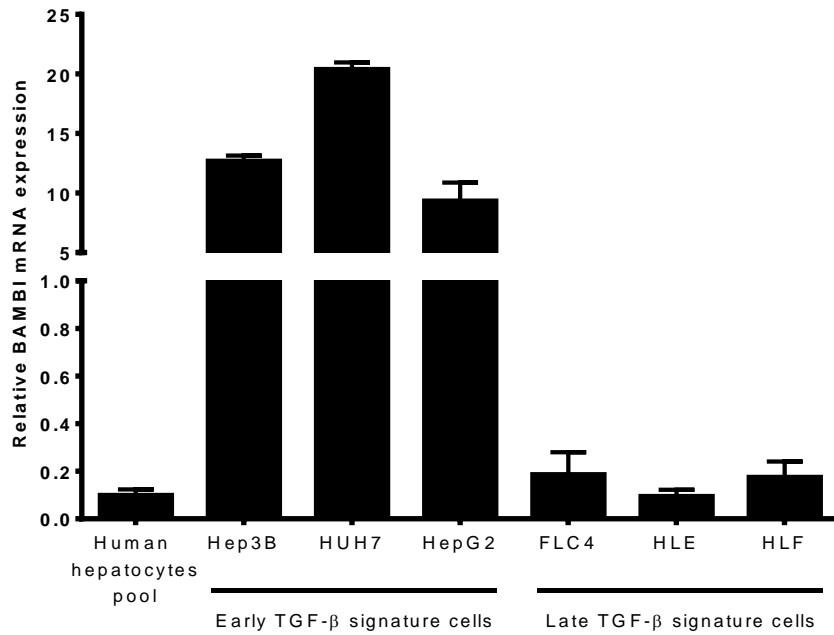


Figure 3.7: BAMBI mRNA levels correlate with early TGF- β gene signature cell lines. Relative BAMBI expression levels were detected using SYBR® Green real time PCR. The expression of 18S rRNA was used as a reference gene and a normal human hepatocyte RNA pool was used as a control reference for the cell lines. The result is pictured as a representative mean \pm SD of two independent experiments

3.2.2 BAMBI antibody evaluation and protein expression in HCC cell lines

3.2.2.1 BAMBI antibody evaluation

In order to assess the specificity of the HPA010866 BAMBI rabbit polyclonal antibody, in situ hybridization (ISH) [189, 221] of HCC paraffin-embedded serial sections was performed by Dr. Shahrouz Ghafoory, while I conducted the IHC staining in parallel. Figure 3.8 shows the co-localisation of the specific RNA BAMBI probe with the antibody staining in the IHC, confirming the specificity of the HPA010866 antibody.

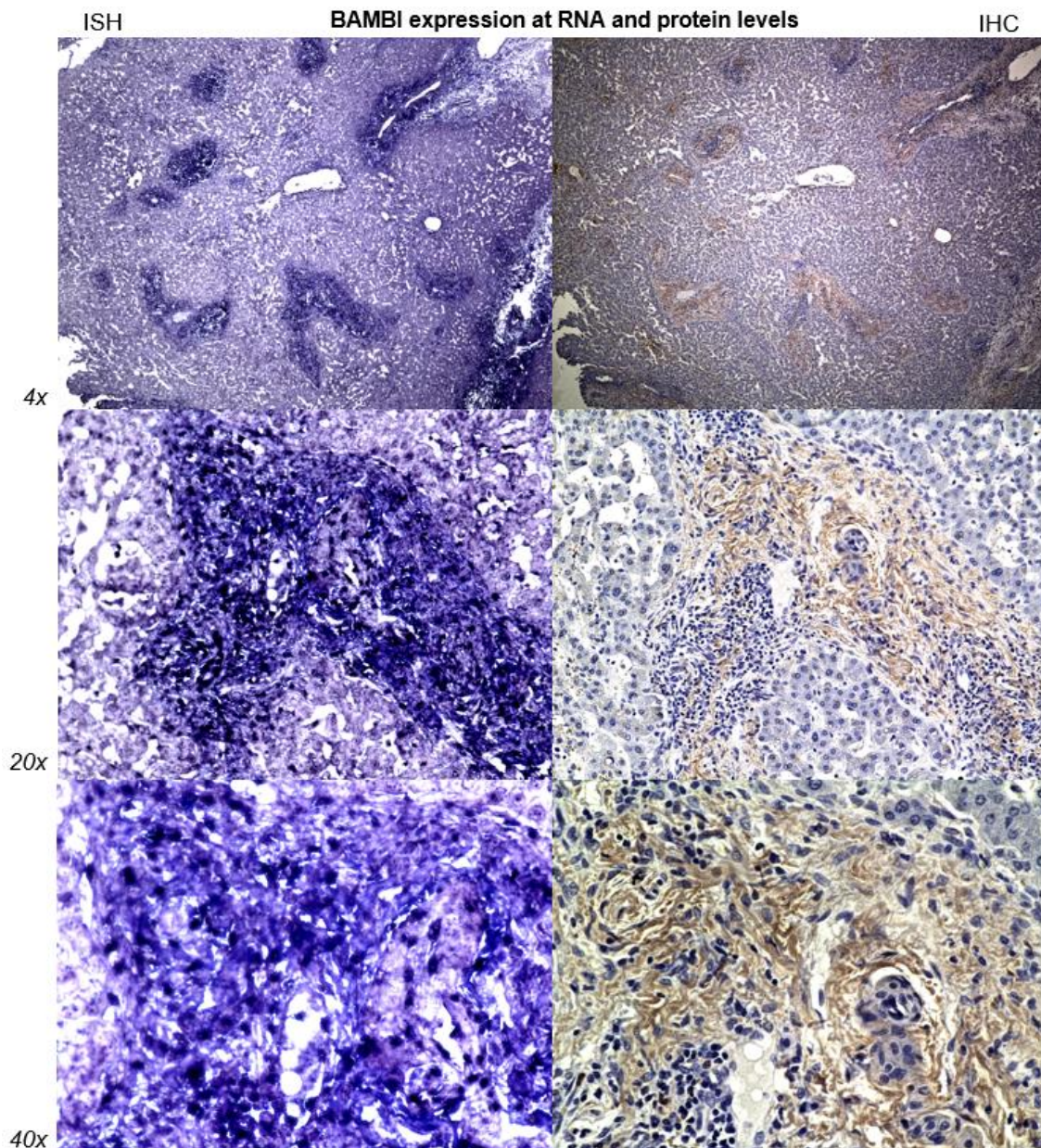


Figure 3.8: ISH and IHC images of HCC patient serial sections at different levels of magnification. (Left panels) The digoxigenin-labelled RNA showing the presence of BAMBI RNA in the tissue. (Right panels) IHC displaying the location of the BAMBI protein in the liver tissue. ISH performed by Dr. Shahrouz Ghafoory. IHC performed by Tatjana Dediulia (myself). Images taken by Dr. Shahrouz Ghafoory.

3.2.2.2 BAMBI mRNA accumulation in the nucleus of HLE cells

During ISH analysis, the concern was raised that in some patients, the BAMBI RNA probe seemed to be trapped inside the nucleus of the cells. The analysis of nuclear and total BAMBI mRNA by qRT-PCR in HLE cells infected with Ad-h-BAMBI (adenovirus) and mBAMBI c-Flag pLV-puro (lentivirus) revealed higher amounts of RNA in the nucleus (Figure 3.9, A and B), raising the hypothesis that the RNA was trapped inside the nucleus and not translating into protein in the HLE cells. The amount of RNA in the nucleus was 3.5 fold higher in the cells infected with a lentiviral overexpression construct (cFlag-pLV-mBAMBI) compared to nucleus RNA levels in the same cells (Figure 3.9, B). However, the overexpression still was extremely high when compared to untreated or mock infected cells (Figure 3.9, A). The same case occurred in nuclear RNA levels.

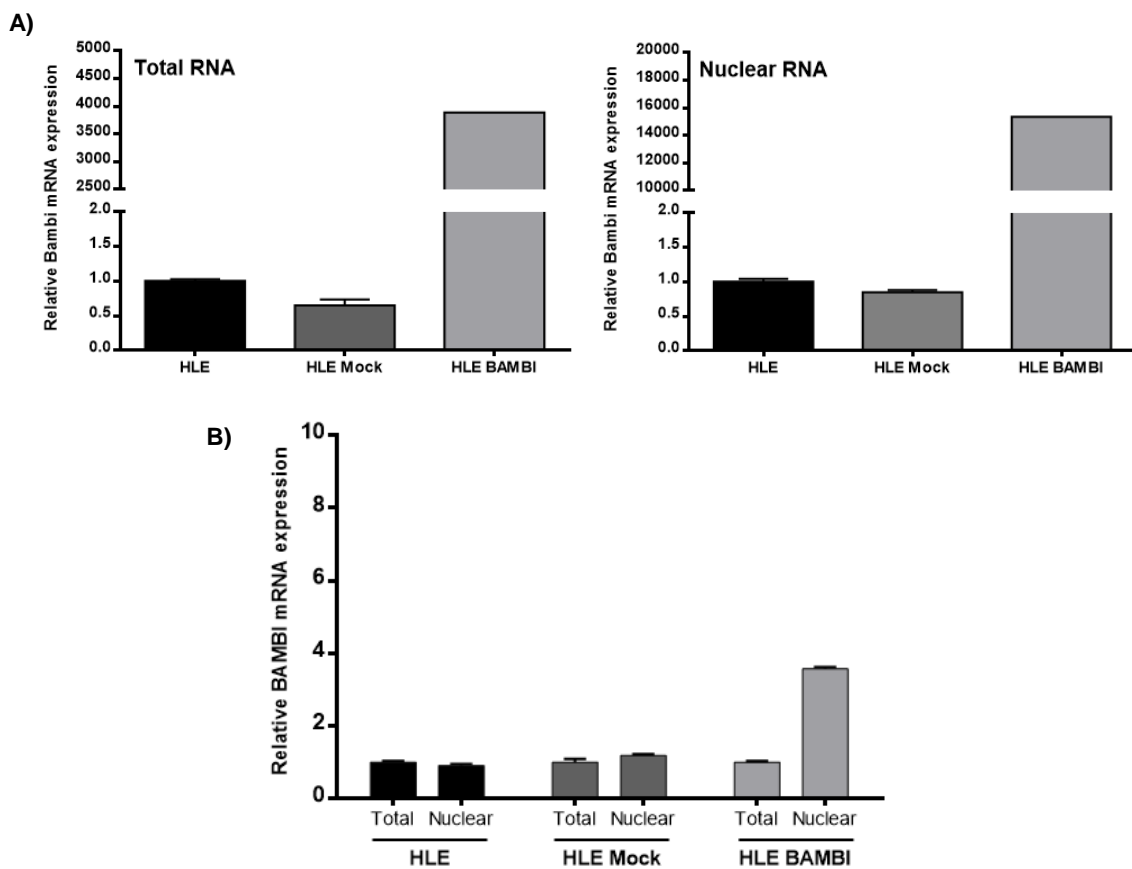


Figure 3.9: HLE cells infected with lentiviral constructs showed BAMBI mRNA accumulation in the nucleus. A) and B) Stable infected HLE cells with cFlag-pLV empty vector and cFlag-pLV-mBAMBI lentivirus were analysed by qRT-PCR after the extraction of total and nuclear RNA, with HPRT1 expression as a reference.

On the other hand, Ad-hBAMBI-infected cells presented a 28 fold increment in nucleus RNA compared to untreated cells or cells infected with Ad-GFP control (Figure 3.10, A), but just as in the lentivirus-infected cells, the total RNA was extremely high in cells overexpressing BAMBI (Figure 3.10 A and B). The conclusion is that in both cases, the protein should be translating into high amounts despite the accumulation of BAMBI mRNA in the nucleus.

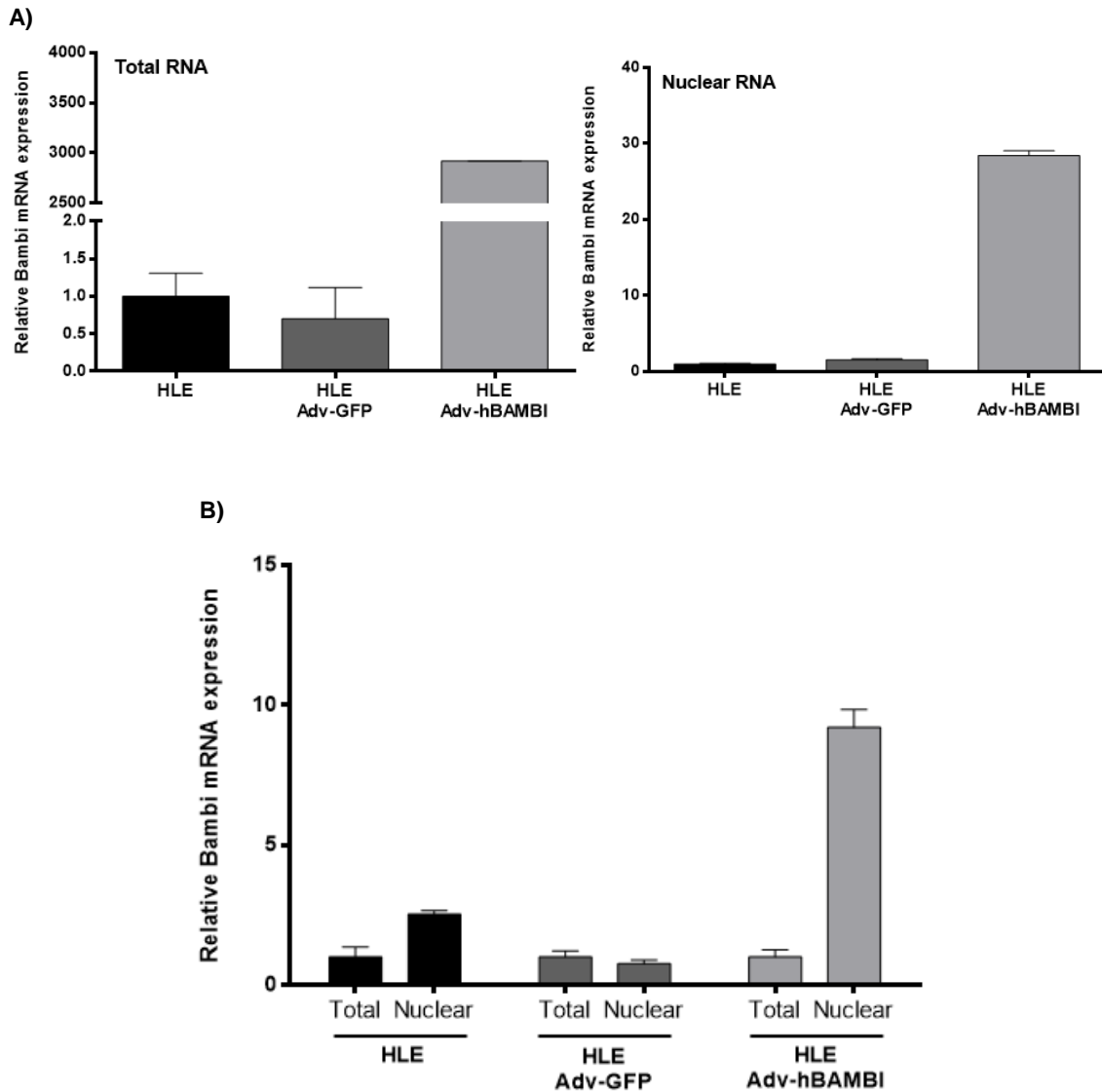


Figure 3.10: HLE cells infected with adenoviral constructs showed BAMBI mRNA accumulation in the nucleus. A) and B) Adenovirus-infected HLE cells with Adv-GFP control and Adv-hBAMBI were analysed by qRT-PCR after the extraction of total and nuclear RNA, with HPRT1 expression as a reference.

3.2.2.3 Confirmation of ectopic BAMBI protein expression and effects in HLE cells

In order to confirm the functionality and production of the BAMBI protein in infected HLE cells, an immunoblot study of canonical and non-canonical TGF- β signalling components (explained in chapters 1.2.2 and 1.2.3) was performed. The use of immunoblot analysis allowed assessing the effect of BAMBI on HLE cell lines and confirming the production of functional BAMBI protein (Figure 3.11).

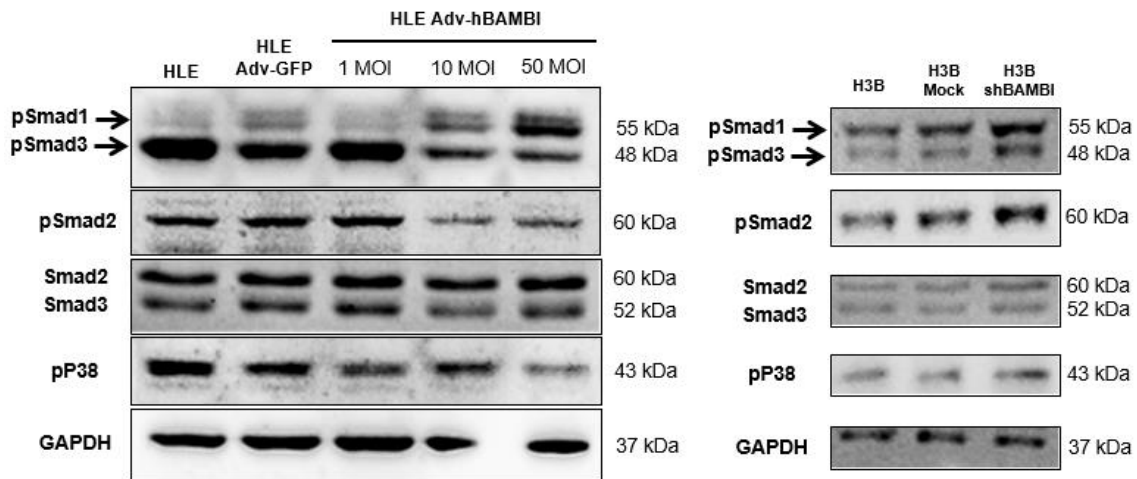


Figure 3.11: BAMBI modulation in HLE and H3B cells affected SMAD2, SMAD3 and P38 phosphorylation. Expression of canonical (pSMAD1, pSMAD2 and pSMAD3) and non-canonical (pP38) TGF- β signalling components in HLE and H3B (Hep3B) cells upon BAMBI overexpression in the case of adenovirus infection (Adv-hBAMBI) using different MOI, and BAMBI downregulation using the shRNA 8752 construct. Evaluated by means of an immunoblot using GAPDH as loading control. The results show one representative of two independent experiments.

SMAD3 phosphorylation was reduced upon BAMBI overexpression and seemed to reach the maximum reduction at 10 MOI infection (Figure 3.11, left). The same result was achieved during pSMAD2 analysis, while P38 phosphorylation was affected at higher MOI (50MOI). As explained in chapter 1.3, BAMBI is a negative regulator of TGF- β signalling and this result confirms the blocking effect of BAMBI on canonical and non-canonical TGF- β signalling components. The pSMAD1 increment in adenovirus-infected cells was not seen in further experiments with lentiviral-infected cells (refer to chapter 3.3.3), indicating that this effect may be virus- rather than BAMBI-related. Therefore, the lentiviral constructs were selected for their use in further experiments. On the other hand, Hep3B cells (H3B) with stable BAMBI downregulation presented higher SMAD1, SMAD2 and SMAD3 phosphorylation, but no clear effect was seen on the non-canonical P38 component (Figure 3.11, right).

In conclusion, studies on BAMBI expression show higher levels of this regulator in epithelial phenotype cells (Hep3B, HepG3 and HUH7) correlating with early TGF- β signature. Moreover, BAMBI overexpression decreases SMAD2, SMAD3 and P38 phosphorylation, confirming its effect on both canonical and non-canonical TGF- β signalling components. Despite the increment in SMAD2 and SMAD3 phosphorylation, no effect on P38 was found upon BAMBI downregulation in Hep3B cells.

3.3 Selection between TGF- β - and BMP-signalling pathways

Being a negative regulator of TGF- β - and BMP-mediated signalling (chapter 1.3), BAMBI turned out to be a highly challenging candidate since so many molecular pathways and components might be involved. Consequently, several experiments were conducted in order to discriminate the most promising pathway between TGF- β and BMP for further analysis upon BAMBI modulation.

3.3.1 BAMBI expression upon cytokine treatment in Hep3B and HLE cells

As explained in chapters 1.1.3 and 1.2.5, altered cytokine expression contributes to HCC progression. The overexpression of TGF- β 1, which has been associated with hepatocellular cancer, is usually correlated with tumour progression, metastasis, angiogenesis and poor prognosis [121 – 124]. Given that BAMBI is a TGF- β signalling regulator that might be induced by the stroma in HCC, a small panel of cytokines was investigated in order to see which one was able to enhance BAMBI expression in Hep3B and HLE cells.

qRT-PCR analysis identified different kinds of BAMBI induction by BMP6, BMP9 and TGF- β 1 cytokines following 6 hours and 16 hours of treatment in both cell lines (Figures 3.12 and 3.13). Hep3B cells showed comparable inductions at 6 hours and 16 hours of treatment by these three cytokines, but BMP6 and BMP9 produced higher levels of BAMBI (12 fold) than the 6 fold induction by TGF- β 1 (Figure 3.12, A and B). On the other hand, BAMBI was only induced in HLE cells by BMP6 and BMP9 after 6 hours of treatment and only by TGF- β 1 after 16 hours (Figure 3.13, A and B).

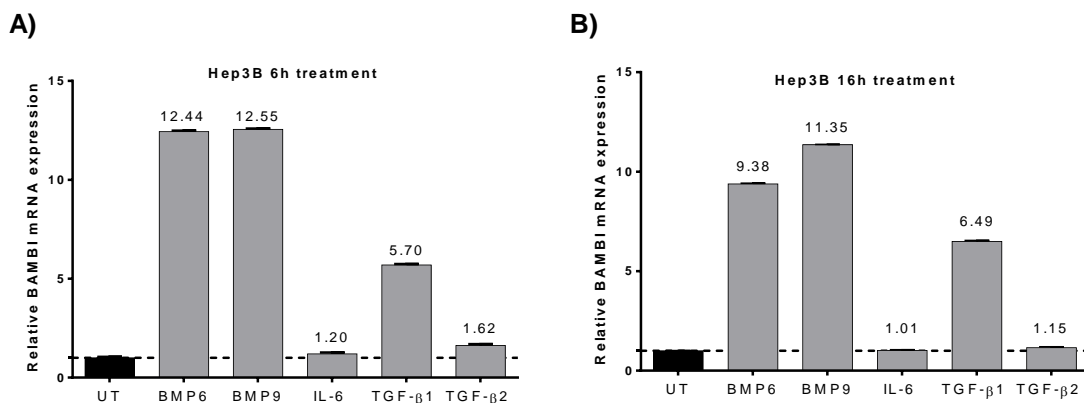


Figure 3.12: BMP6, BMP9 and TGF- β 1 induced BAMBI expression in Hep3B cells. Hep3B cells were treated with BMP6 (25ng/ml), BMP9 (5ng/ml), IL-6 (6ng/ml), TGF- β 1 (5ng/ml), TGF- β 2 (5ng/ml), or left untreated (UT) for 6 hours (A) and 16 hours (B). Relative BAMBI expression levels were evaluated using real time PCR with HPRT1 as a reference gene. The results show the mean \pm SD of one representative of two independent experiments.

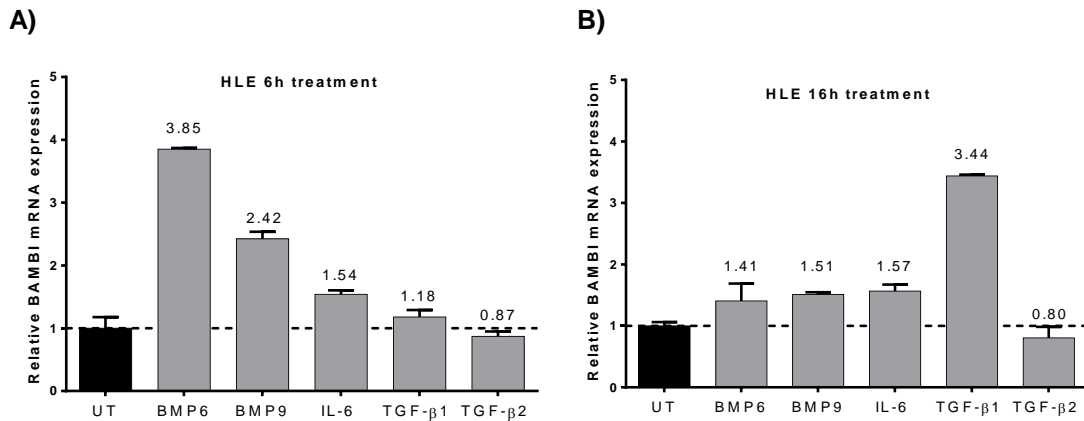


Figure 3.13: BMP6, BMP9 and TGF- β 1 induced BAMBI expression in a different patron in HLE cells. HLE cells were treated with BMP6 (25ng/ml), BMP9 (5ng/ml), IL-6 (6ng/ml), TGF- β 1 (5ng/ml), TGF- β 2 (5ng/ml), or left untreated (UT) for 6 hours (A) and 16 hours (B). Relative BAMBI expression levels were evaluated using real time PCR with HPRT1 as a reference gene. The results show the mean \pm SD of one representative of two independent experiments.

3.3.2 Correlation of BAMBI expression with TGF- β - and BMP-target genes in HCC patients cohorts

Due to the differences in cytokine effects on Hep3B and HLE cells, correlation analyses between BAMBI and the typical downstream genes affected by TGF- β (PAI1 and CTGF) and BMP-mediated (HAMP and ID1) signalling were performed in HCC patient cohorts with BAMBI upregulation (shown in Figure 3.1; chapter 3.1.1).

As presented in Figure 3.14 and Table 3.4, significant correlations were found with TGF- β signalling downstream genes SERPINE1 (PAI1) and CTGF in the GSE5975 (EpCAM+) and GSE14520 cohorts. On the other hand, Heparin-binding EGF-like motif (HAMP) and ID1 did not show any significant correlations with BAMBI expression in any cohort (Table 3.4), establishing that TGF- β mediated signalling is the one used by BAMBI to drive its effects in HCC.

| BMP-mediated signalling downstream genes | | <i>r</i> | <i>p</i> - value | TGF- β -mediated signalling downstream genes | | <i>r</i> | <i>p</i> - value |
|--|------|----------|------------------|--|----------|----------|------------------|
| GSE5975 (EpCAM ⁺) | HAMP | -0.018 | 0.86 | GSE5975 (EpCAM ⁺) | SERPINE1 | 0.226 | *0.03 |
| | ID1 | 0.102 | 0.33 | | CTGF | 0.280 | **0.006 |
| GSE14520 | HAMP | -0.044 | 0.49 | GSE14520 | SERPINE1 | 0.267 | ***<0.0001 |
| | ID1 | 0.043 | 0.50 | | CTGF | 0.225 | ***0.0004 |

Table 3.4: BMP and TGF- β -mediated signalling downstream genes correlations with BAMBI expression in the GSE5975 and GSE14520 cohorts. Correlation analyses were performed by calculating the Pearson coefficient *r* between BAMBI expression and HAMP, ID1, SERPINE1 and CTGF expression. **p*<0.05; ***p*<0.01; ****p*<0.001; *****p*<0.0001. The *p*-values were calculated using the function TDIST.

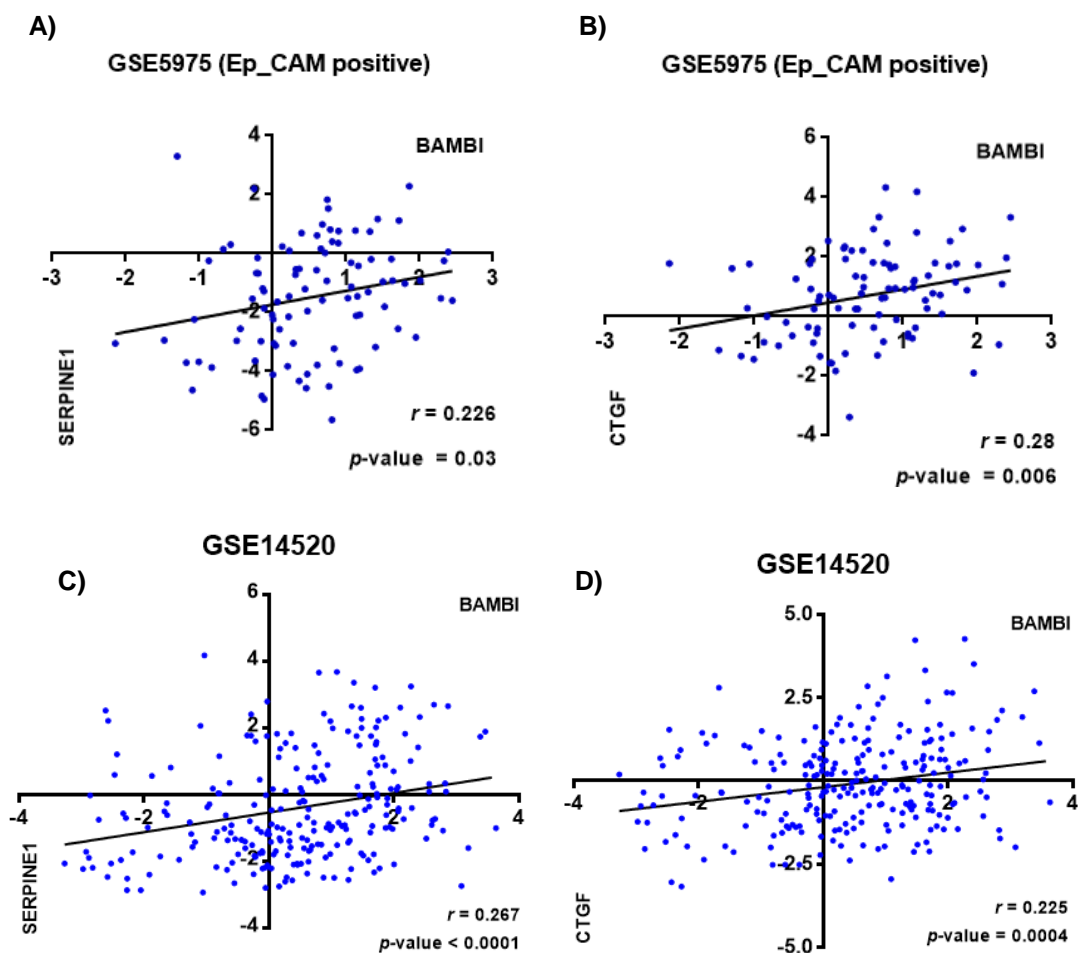


Figure 3.14: BAMBI expression significantly correlates with TGF- β -mediated signalling downstream genes. Correlation analyses were performed by calculating the Pearson coefficient r between BAMBI expression and (A and C) SERPINE1 (PAI1) and (B and D) CTGF expression in the GSE5975 and GSE14520 publicly available HCC cohorts. The p-values for the Pearson correlations were calculated using the function TDIST: $\text{TDIST} = ((r * \text{Sqrt}(N-2)) / \text{Sqrt}(1-(r^2)))$, N , 2); where r = Pearson correlation coefficient; N = number of observations; Sqrt = square root.

3.3.3 Effects of BAMBI modulation on SMAD3 activity in Hep3B and HLE cells

SMAD3 activation produces the formation of a transcription factor complex, which regulates gene expression by binding to a CAGA element (chapter 1.2.2). To analyse whether BAMBI blocks or enhances Smad3 signalling, a CAGA-reporter luciferase assay with or without TGF- β stimulation for 16 hours was performed in stable-infected H3B and HLE cell lines and their respective controls (parental and mock-infected cells).

The produced stable HLE cells with BAMBI upregulation (called HLE BMABI hereafter) decreased Smad3 phosphorylation levels compared to the mock control (HLE Mock) and parental (HLE) cells upon 16 hours of TGF- β 1 treatment (Figure 3.15, B), corroborating the negative regulation of the TGF- β signalling pathway by BAMBI. The result was confirmed by an immunoblot analysis of canonical and non-canonical TGF- β signalling

components upon 1 hour of TGF- β 1 stimulation, where a reduction of pSMAD3, pSMAD2 and pP38 signals was observed (Figure 3.15, C and D).

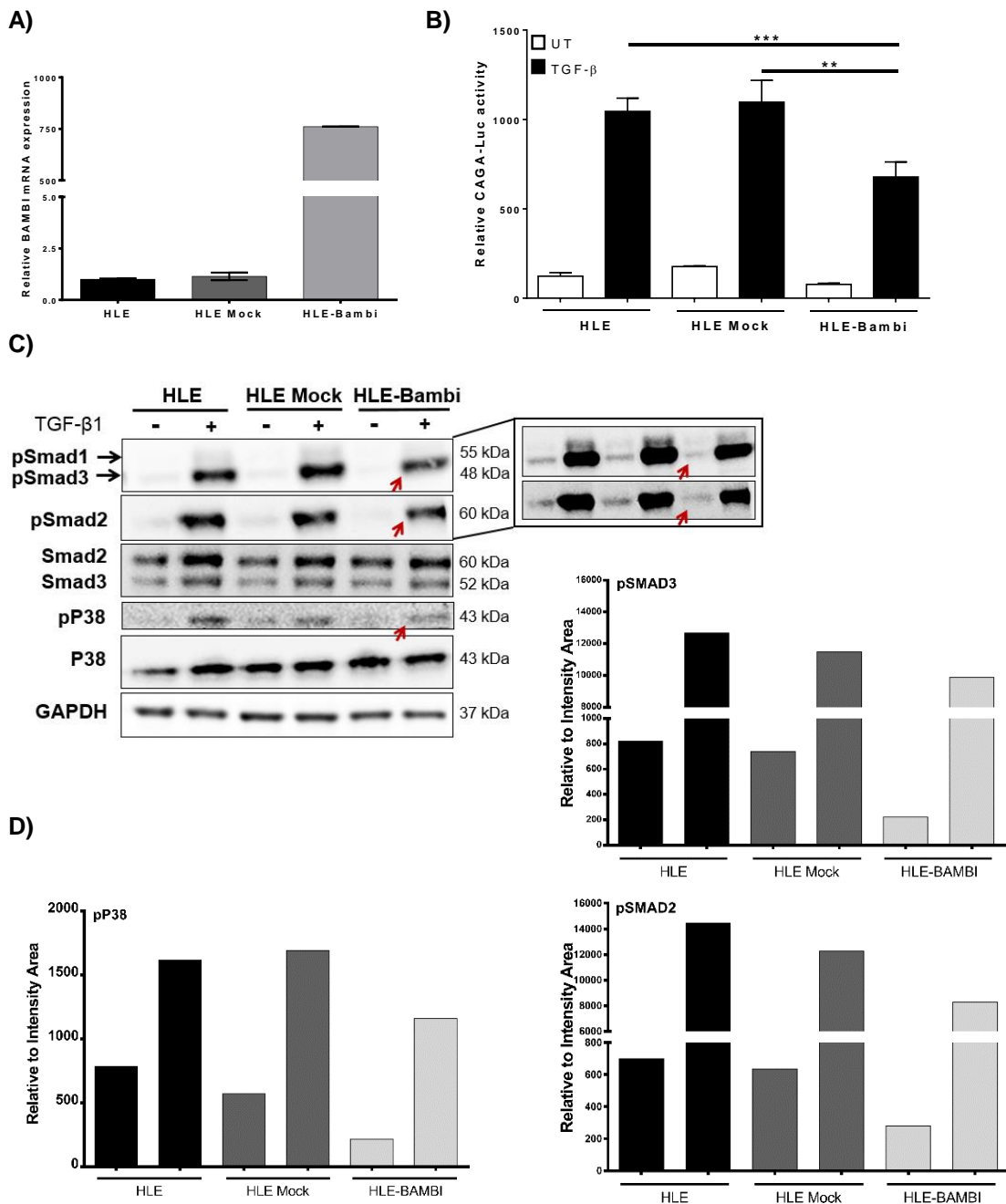


Figure 3.15 : TGF- β -mediated Smad3 activation is reduced by BAMBI overexpression in HLE cells.

A) HLE cells were infected with an empty vector (Mock) and BAMBI lentivirus and selected with puromycin. BAMBI overexpression was confirmed by qRT-PCR using HPRT1 as a reference gene. The result is shown as the mean \pm SD of one representative experiment. B) Stable cell lines were infected with an adenovirus encoding a luciferase gene under the control of the CAGA response element. Smad3/Smad4 activity was detected 16 hours after treatment with or without 5 ng/ml TGF- β 1. The result is presented as the mean \pm SD representative of three independent experiments. C) Immunoblot analysis of phosphorylated Smad1, Smad3 and P38, as well as their total proteins upon 1 hour of TGF- β 1 treatment was performed using GAPDH as loading control. D) WB bands quantification: relative area calculated from the intensity bands with ImageJ software. ** $p < 0.01$; *** $p < 0.001$.

On the other hand, Hep3B with stable BAMBI downregulation cells (by shRNA 8752 lentiviral construct), called H3B shBambi hereafter, showed the opposite effect to the one seen for BAMBI upregulation. Smad3/Smad4 activity was enhanced upon BAMBI downregulation (Figure 3.16, B). An immunoblot analysis confirmed the induction of Smad3 phosphorylation upon 1 hour of TGF- β 1 treatment, although no effect on P38 was found so far in these cells (Figure 3.16, C and D).

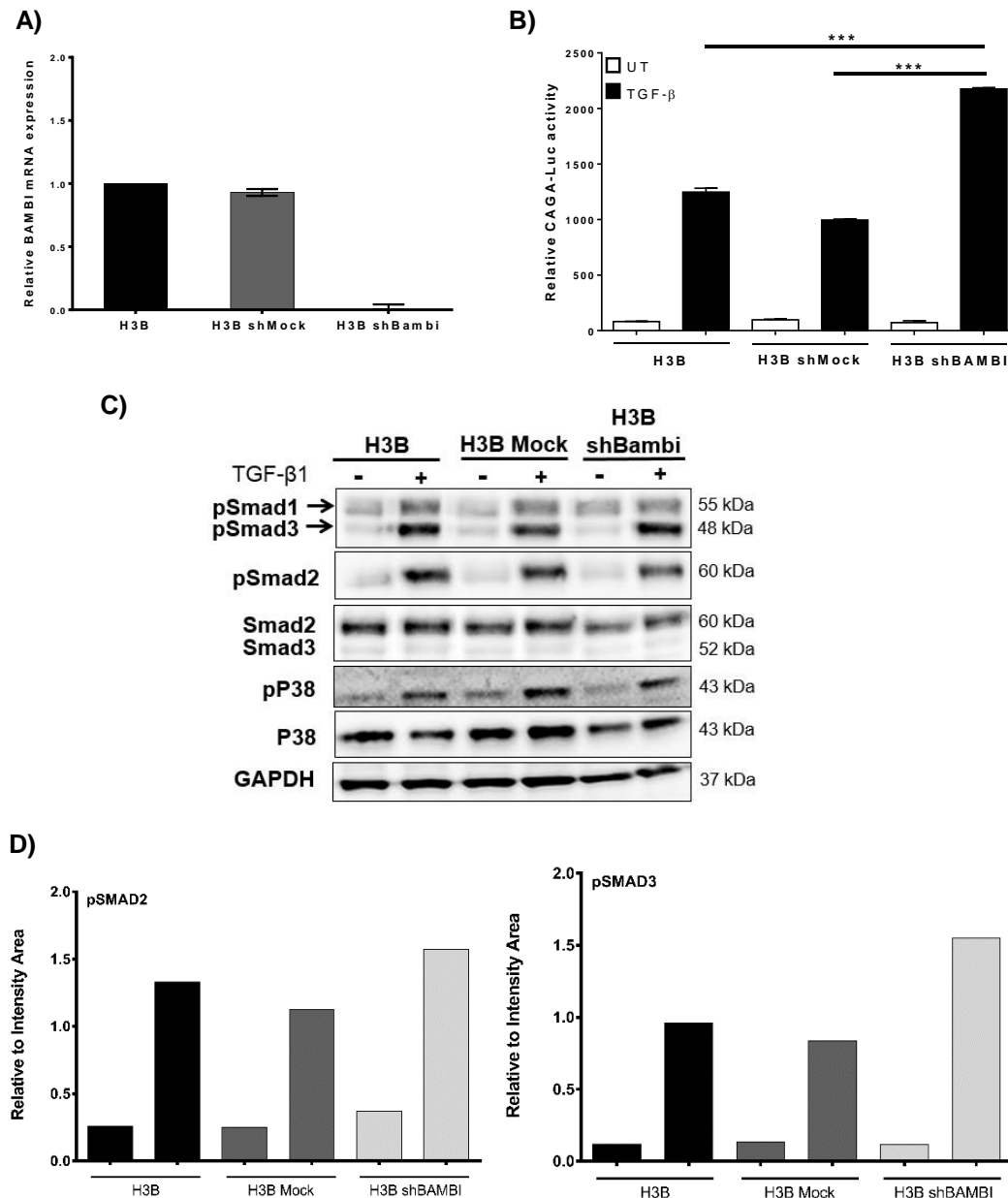


Figure 3.16: TGF- β -mediated Smad3 activation is enhanced by BAMBI downregulation in Hep3B cells. A) Hep3B cells were infected with an empty vector (Mock) and shRNA-BAMBI (8752) lentivirus and after selection with puromycin, cell cloning using a serial dilution protocol was performed in order to enhance knockdown efficiency. BAMBI downregulation was confirmed by qRT-PCR using HPRT1 as a reference gene. The result shows the mean \pm SD of one representative of three independent experiments. B) Stable cell lines were infected with an adenovirus encoding a CAGA-Luc response element. Smad3/Smad4 activity was detected 16 hours after treatment with or without 5 ng/ml TGF- β 1. The result is presented as the mean \pm SD representative of three independent experiments. C) Immunoblot analysis of phosphorylated Smad1, Smad3 and P38, as well as their total proteins upon 1 hour of TGF- β 1 treatment was performed using

GAPDH as loading control. D) WB bands quantification: relative area calculated from the intensity bands with ImageJ software and referred to GAPDH bands intensity. *** $p < 0.001$.

In summary, even though BAMBI expression can be induced by TGF- β 1, BMP6 and BMP9 cytokines, the correlation with downstream genes only showed a positive result for TGF- β -mediated signalling genes (SERPINE1/PAI1 and CTGF) in HCC patient cohorts. Further analysis confirmed the induction of Smad3/Smad4 activity by BAMBI downregulation in Hep3B cells and the decrement of the activation upon BAMBI upregulation in HLE cells. Moreover, the non-canonical TGF- β signalling component P38 seemed to be affected by upregulation. Altogether, these results demonstrate BAMBI's effect on TGF- β signalling components in HCC cell lines.

3.4 BAMBI protein expression in paraffin-embedded HCC patient tissues

3.4.1 BAMBI is up-regulated in 50% of HCC tissue samples

Using the HPA010866 BAMBI rabbit polyclonal antibody (Prestige Antibodies; Sigma-Aldrich, St. Louis, Missouri, USA), I performed IHC stainings for eight HCC patients with paired surrounding tissues from our collaborative project with Prof. Chun Fang Gao and Dr. Xing Gu, and for six patients of Prof. Dr. Stefan Wöfl. Six of the eight patients from the China cohort and one of the six patients from the Heidelberg cohort were positively stained for BAMBI. The surrounding tissues presented BAMBI around the vessels and in the fibrotic tissues (data not shown), while the hepatocytes and the major cells population were negative for BAMBI (Figure 3.17, left images). The presence of BAMBI in the surrounding tissue was expected because we cannot assume it to be normal or non-sick. On the other hand, the tumour samples from the patients showed positive BAMBI staining in the tumour cells and the stroma (Figure 3.17, right images). Taking all samples together, 50% of the patients had BAMBI upregulation, which confirms the results obtained during the meta-analysis of BAMBI expression (chapter 3.1).

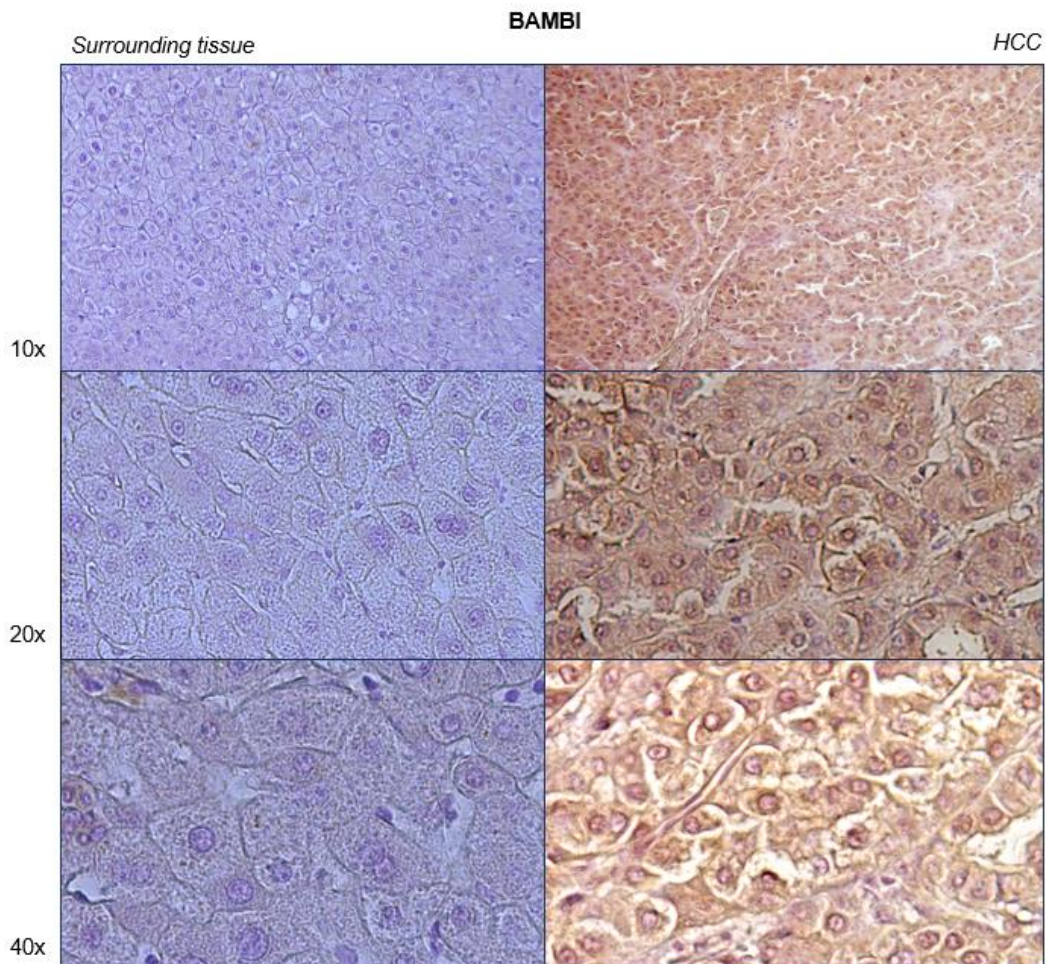


Figure 3.17: Immunohistochemical staining of BAMBI in tumour and surrounding HCC tissues. HCC patients' slides and their paired surrounding tissues, stained according to the IHC protocol, showed the presence of the BAMBI protein located in the nucleus and cytoplasm of tumour cells

3.4.2 BAMBI is upregulated in 76% of the samples in an HCC Tissue Microarray (TMA)

In order to confirm the meta-analysis results for BAMBI obtained in the HCC cohorts (chapter 3.1.1), I stained a tissue microarray (TMA) with the samples of 75 HCC patients from different aetiologies and 15 CCA (cholangiocarcinoma).

Of the 75 HCC patients, 8% showed BAMBI downregulation (n=6), 16% showed no change (n=12) and 76% showed upregulation (n=57) (Figure 3.18). The upregulated samples were classified into three groups according to their staining intensity (1+, 2+ and 3+; Figure 3.19), with 29.8% (n=17) showing lower intensity (1+), 47.4% (n=27) intensity 2+ and 22.8% (n=13) higher intensity (3+).

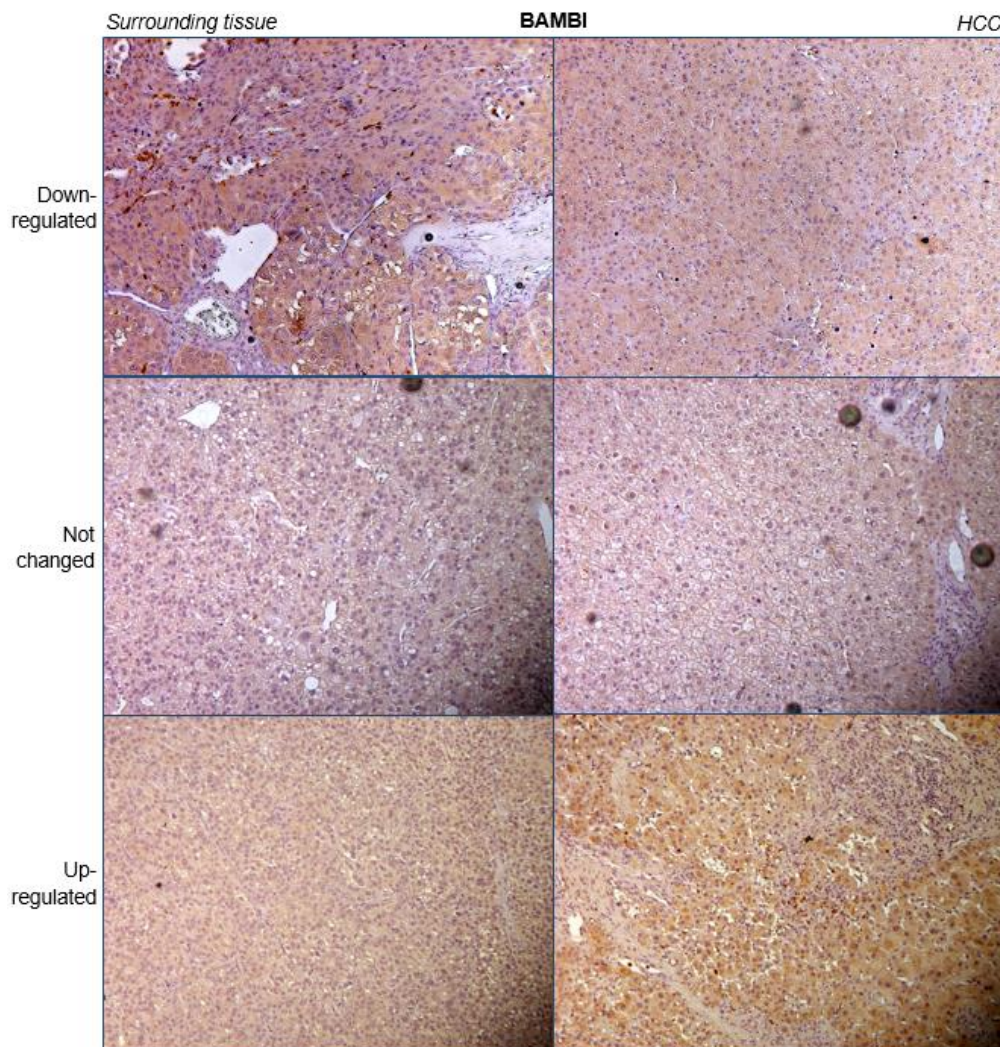


Figure 3.18: Immunohistochemical staining of BAMBI in the HCC tissue microarray (TMA). HCC tumour tissues were classified into three groups according to their staining intensity compared to their surrounding tissues: downregulated, not changed and upregulated (magnification 10x). The images show one representative patient from each group.

Interestingly, some patients presented BAMBI-positive infiltrated structures that resembled inflammatory cells (Figure 3.19, white arrows); the quantity of these bodies was directly proportional to the BAMBI intensity in the samples.

After correlation screening between BAMBI and inflammatory markers in the HCC patient cohorts, the list of possible markers (Table 3.5) was reduced to CD14, IL4, IL15 and MMP9, with CD14 (** $p = 0.0017$) monocyte activation marker being the most promising one (Table 3.6). On the other hand, IL15 and MMP9 are commonly related to bad prognosis and invasion, respectively. In fact, Zhou *et al.* [157] found that MMP9 activity and expression were enhanced by BAMBI overexpression in human osteosarcoma cells.

Further, Table 3.7 presents the correlation between the expression of BAMBI and the patients' clinical-pathological data in the TMA. There was a significant correlation between BAMBI expression and the hepatitis B antigen and antibody (HBeAg and HBeAb) as well as a significant increment of stage 3 cirrhosis in the low level BAMBI group (compared to the medium-intensity group). Moreover, the percentage of TNM stage III patients appeared increased in the medium BAMBI expression group. Furthermore, positive and significant correlations were found between BAMBI and prothrombin time (PT; $r = 0.31$; ** $p = 0.008$) and activated partial thromboplastin time (APTT; $r = 0.29$; * $p = 0.015$) among the blood parameters.

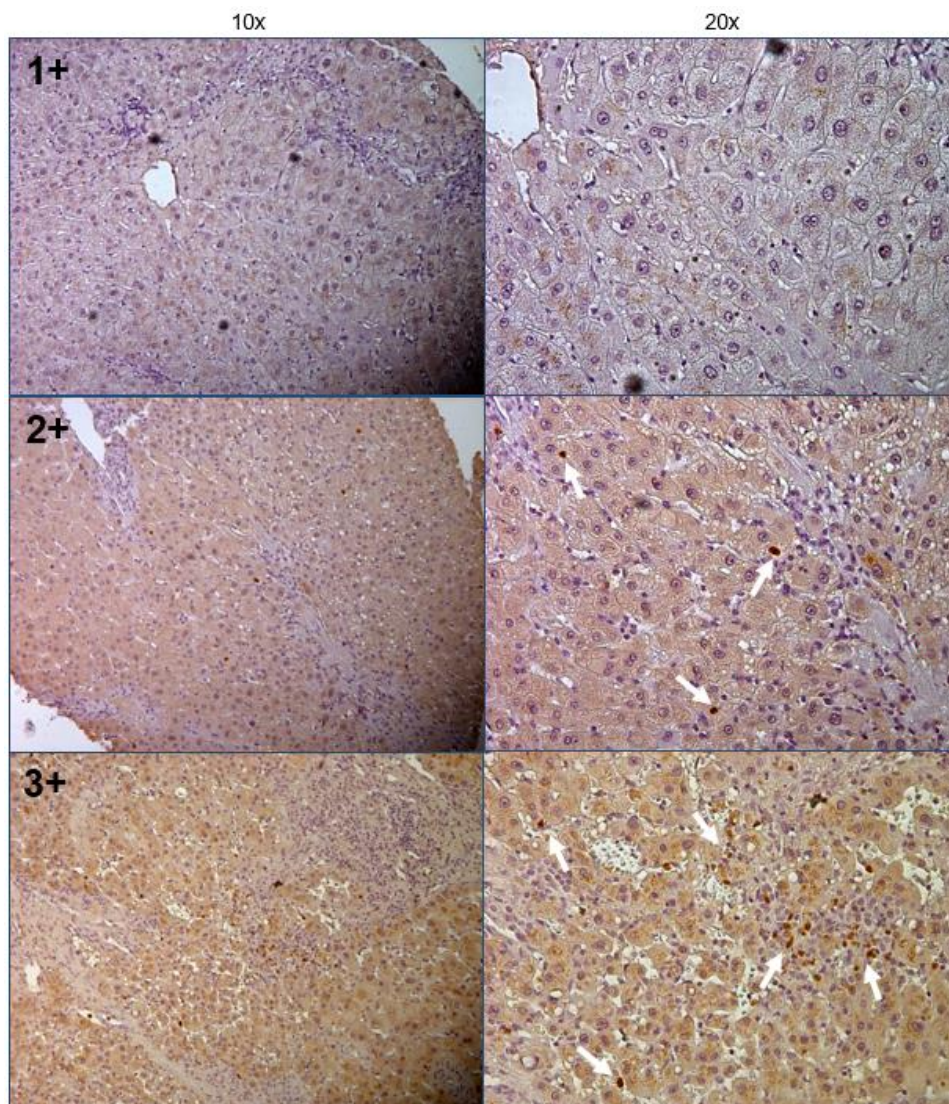


Figure 3.19: HCC sample classification by BAMBI staining intensity in TMA. BAMBI-upregulated tumour HCC samples were classified into three groups according to their staining intensity: 1+, 2+ and 3+. The images show 10x and 20x magnifications from three HCC patients. White arrows indicate the presence of infiltrated cells

| List of markers | | |
|---------------------|--------|-------|
| PPARG | CD3 | ICAM1 |
| PPARD | CD4 | VCAM1 |
| PPARA | CD8 | CXCL9 |
| PPARBP | CD11c | ISG15 |
| PPARGC1A | CD14 | ISG56 |
| PPARGC1B | CD20 | MMP2 |
| TNF | CD68 | MMP9 |
| IL1B | CD274 | CCL5 |
| IL2 | IFNA1 | OAS1 |
| IL4 | IFNG | OAS2 |
| IL6 | EMR1 | OAS3 |
| IL8 | S100A4 | TLR5 |
| IL10 | LY6E | TLR6 |
| IL15 | LY6D | TLR7 |
| PD1/PD-L1 | LY6K | TLR8 |
| IP-10 | LY6H | TLR9 |
| MIP1 α,β | STAT6 | TLR10 |

Table 3.5 List of inflammatory markers used for correlation with BAMBI expression.

| | GSE1898 (n=91) | | GSE5975 Ep_CAM ⁺ (n=94) | | GSE14520 (n=247) | |
|------|-------------------|------------------|---------------------------------------|------------------|---------------------|----------------------|
| | <i>r</i> | <i>p</i> - value | <i>r</i> | <i>p</i> - value | <i>r</i> | <i>p</i> - value |
| CD14 | -0.3240 | 0.0017** | -0.2068 | 0.04275* | -0.2653 | <0.0001*** |
| MMP9 | 0.1565 | 0.0186* | 0.2272 | 0.0277* | 0.1749 | 0.0059** |
| IL4 | -0.2391 | 0.0225* | -0.1270 | NS | -0.1369 | 0.0315* |
| IL15 | -0.2771 | 0.0078** | -0.2954 | 0.0039** | -0.0984 | NS |

Table 3.6: Positive correlations with BAMBI expression in the GSE1898, GSE5975 and GSE14520 cohorts. Correlation analyses were performed by calculating the Pearson coefficient *r* between the expressions of BAMBI and the list of markers from Table 3.3. The *p*-values were calculated using the function TDIST. **p*<0.05; ***p*<0.01; ****p*<0.001.

| Clinical-pathological factors | Middle Bambi (n=27, %) | Low Bambi (n=15, %) | P-value ^a | Clinical-pathological factors | Middle Bambi (n=27, %) | High Bambi (n=14, %) | P-value ^a |
|-------------------------------|---------------------------|------------------------|----------------------|-------------------------------|---------------------------|-------------------------|----------------------|
| Age(years) | | | 0.74 | Age(years) | | | 0.75 |
| <50 | 17(62.96) | 8(53.33) | | <50 | 17(62.96) | 8(57.14) | |
| ≥50 | 10(37.04) | 7(46.67) | | ≥50 | 10(37.04) | 6(42.86) | |
| Ascites | | | 0.54 | Ascites | | | 1 |
| Yes | 3(11.11) | 0(0) | | Yes | 3(11.11) | 1(7.14) | |
| No | 24(88.89) | 15(100) | | No | 24(88.89) | 13(92.86) | |
| TNM stage | | | 0.75 | TNM stage | | | 0.03* |
| I+II | 16(59.26) | 10(66.67) | | I+II | 16(59.26) | 13(92.86) | |
| III+IV | 11(40.74) | 5(33.33) | | III+IV | 11(40.74) | 1(7.14) | |
| Metastasis | | | 1 | Metastasis | | | 1 |
| Yes | 1(3.70) | 0(0) | | Yes | 1(3.70) | 0(0) | |
| No | 26(96.30) | 15(100) | | No | 26(96.30) | 14(100) | |
| Portal vein hypertension | | | 0.53 | Portal vein hypertension | | | 1 |
| Yes | 2(7.41) | 0(0) | | Yes | 2(7.41) | 1(7.14) | |
| No | 25(92.59) | 15(100) | | No | 25(92.59) | 13(92.86) | |
| Main tumor size | | | 0.75 | Main tumor size | | | 1 |
| <5 | 11(40.74) | 5(33.33) | | <5 | 11(40.74) | 6(42.86) | |
| >5 | 16(59.26) | 10(66.67) | | >5 | 16(59.26) | 8(57.14) | |
| Vascular invasion | | | 0.75 | Vascular invasion | | | 1 |
| 0 | 16(59.26) | 8(53.33) | | 0 | 16(59.26) | 8(57.14) | |
| 1 | 11(40.74) | 7(46.67) | | 1 | 11(40.74) | 6(42.86) | |
| Portal vein thrombosis | | | 0.45 | Portal vein thrombosis | | | 0.23 |
| 0 | 20(74.07) | 13(86.67) | | 0 | 20(74.07) | 13(92.86) | |
| 1 | 7(25.93) | 2(13.33) | | 1 | 7(25.93) | 1(7.14) | |
| Capsule property | | | 0.72 | Capsule property | | | 0.72 |
| 0 | 7(25.93) | 5(33.33) | | 0 | 7(25.93) | 3(21.43) | |
| 1 | 17(62.96) | 8(53.33) | | 1 | 17(62.96) | 11(78.57) | |
| 2 | 3(11.11) | 2(13.33) | | 2 | 3(11.11) | 0(0) | |
| Lymph node invasion | | | 1 | Lymph node invasion | | | 1 |
| 0 | 26(96.30) | 14(93.33) | | 0 | 26(96.30) | 14(100) | |
| 1 | 1(3.70) | 1(6.67) | | 1 | 1(3.70) | 0(0) | |
| Invasion to adjacent organs | | | 0.69 | Invasion to adjacent organs | | | 1 |
| 0 | 23(85.19) | 12(80) | | 0 | 23(85.19) | 12(85.71) | |
| 1 | 4(14.81) | 3(20) | | 1 | 4(14.81) | 2(14.29) | |
| Cirrhosis stage | | 0 vs 3 | 0.03* | Cirrhosis stage | | | 0.72 |
| 0 | 15(55.56) | 4(26.67) | | 0 | 15(55.56) | 6(42.86) | |
| 1 | 9(33.33) | 5(33.33) | | 1 | 9(33.33) | 5(35.71) | |
| 2 | 1(3.70) | 2(13.33) | | 2 | 1(3.70) | 1(7.14) | |
| 3 | 1(3.70) | 4(26.67) | | 3 | 1(3.70) | 2(14.29) | |
| HBsAg | | | 1 | HBsAg | | | 1 |
| 0 | 1(3.70) | 0(0) | | 0 | 1(3.70) | 0(0) | |
| 1 | 23(85.19) | 12(80) | | 1 | 23(85.19) | 11(78.57) | |
| HBsAb | | | 1 | HBsAb | | | 1 |
| 0 | 23(85.19) | 12(80) | | 0 | 23(85.19) | 11(78.57) | |
| 1 | 1(3.70) | 0(0) | | 1 | 1(3.70) | 0(0) | |
| HBeAg | | | 0.01* | HBeAg | | | 0.03* |
| 0 | 7(25.93) | 9(60) | | 0 | 7(25.93) | 8(57.14) | |
| 1 | 17(62.96) | 3(20) | | 1 | 17(62.96) | 3(21.43) | |
| HBeAb | | | 0.03* | HBeAb | | | 0.09 |
| 0 | 0(0) | 3(20) | | 0 | 0(0) | 2(14.29) | |
| 1 | 24(88.89) | 9(60) | | 1 | 24(88.89) | 9(64.29) | |
| HBcAb | | | 1 | HBcAb | | | 0.31 |
| 0 | 0(0) | 0(0) | | 0 | 0(0) | 1(7.14) | |
| 1 | 24(88.89) | 12(80) | | 1 | 24(88.89) | 10(71.43) | |

Table 3.7: Correlation of BAMB I expression level with clinical-pathological characteristics in the tissue microarray (TMA). ^a Fishers' exact test

3.4.3 Presence and/or absence of BAMBI impacts on pSMAD2 staining

Since BAMBI's effect on TGF- β signalling had been confirmed in previous experiments, serial sections staining was performed with the same patients used for the BAMBI IHC assays using pSMAD2 and BAMBI antibodies in order to confirm BAMBI modulation on TGF- β -mediated signalling in vivo.

As can be observed in Figure 3.20, pSMAD2 was absent in the staining when the patients were positive for BAMBI (lower panel), while the negative BAMBI slides showed positive staining for pSMAD2 (upper panel). This result demonstrates the blocking effect of BAMBI on TGF- β canonical signalling in vivo.

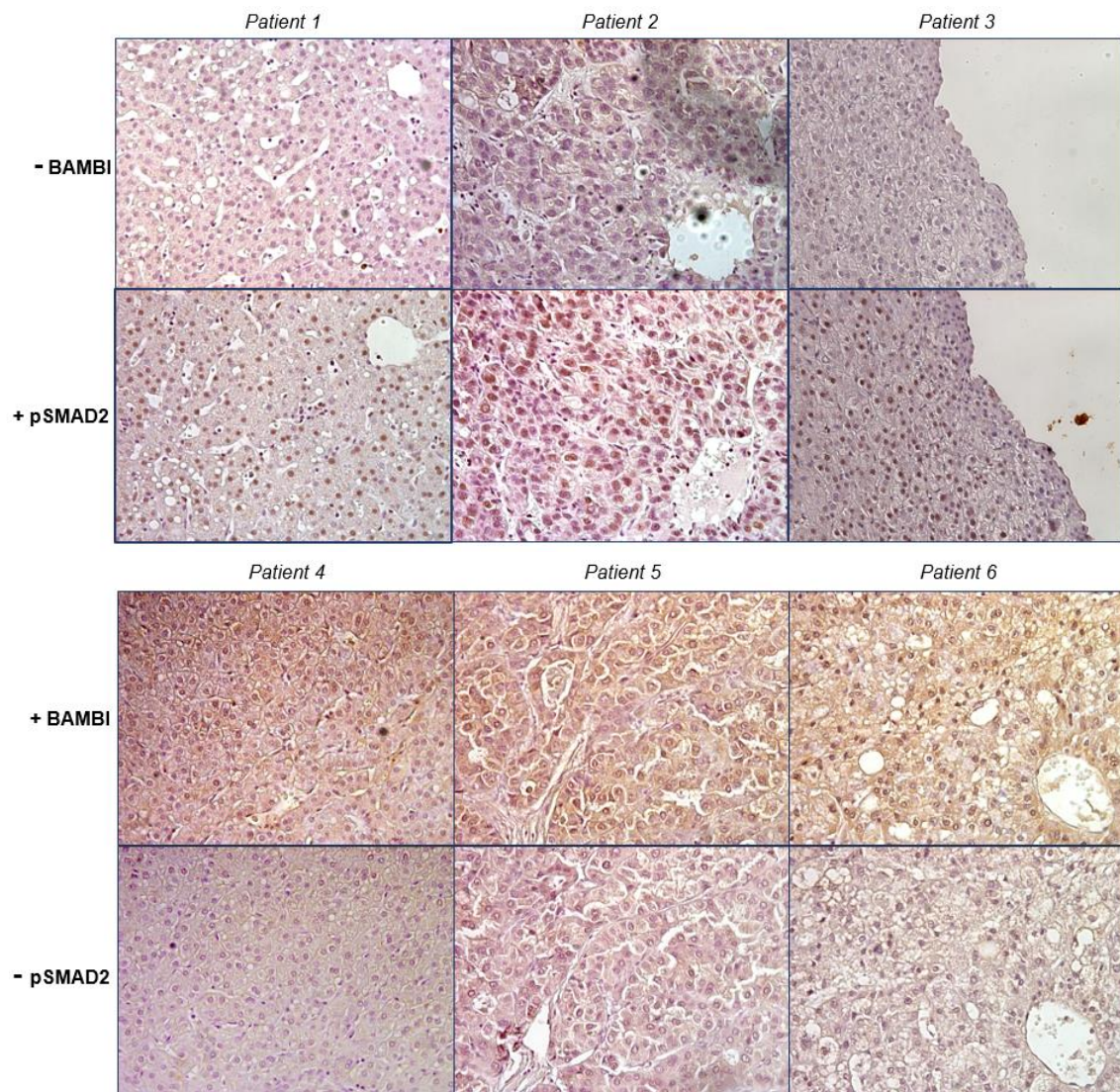


Figure 3.20: BAMBI blocks SMAD2 phosphorylation in HCC patients. Serial sections of paraffin-embedded HCC patient samples, positive or negative for BAMBI (chapter 3.4.1), were stained with BAMBI and pSMAD2 antibodies (upper panel). The comparative analysis of the same segments of tissues showed the presence of pSMAD2 positive cells in BAMBI negative cells. pSMAD2 staining was absent in BAMBI positive cells (lower panel)

3.5 BAMBI effects on proliferation and apoptosis in HLE and Hep3B cells

TGF- β is known to induce cell growth arrest and apoptosis in different cell types, e.g., hepatocytes and epithelial cells [190-192], and to have tumour suppressing effects in several cancers. However, TGF- β can also exert pro-tumorigenic functions in various tumours, including HCC (chapter 1.2.5). As explained in chapter 1.3.1, BAMBI's function together with the mechanisms it uses to drive the effects have not been fully discovered in HCC. It is known and has been proven in previous experiments of this thesis, that BAMBI negatively affects TGF- β -mediated signalling; therefore, modulations in the TGF- β tumour suppressor and/or tumour promotor effects are expected.

In this study, Hep3B cells with stable BAMBI downregulation (H3B shBAMBI) and HLE cells with stable upregulation (HLE-BAMBI) were analysed with respect to the functionality of TGF- β signalling, with a special focus on the proliferative, migratory and apoptotic effects of TGF- β .

3.5.1 Proliferation changes following BAMBI up- or downregulation

Cell death and growth arrest are known to be induced by TGF- β in early-signature HCC cell lines [193-195], while in late TGF- β -signature cells, the effects could be even pro-proliferative and/or anti-apoptotic [196-198]. Therefore, the proliferative and apoptotic responses of H3B shBAMBI and HLE-BAMBI cells were evaluated.

During the counting assay, H3B shBAMBI cells presented a significantly lower number of cells 72 and 96 hours after seeding (Figure 3.21). The slow growth rate in H3B shBAMBI indicated that BAMBI downregulation affected proliferation in these cells. Moreover, the high number of dead cells observed in further wound assays hints at enhanced apoptosis and was therefore analysed further in a Caspase-3 assay (chapter 3.5.2).

In contrast, HLE-BAMBI cells showed a higher growth rate compared to parental and mock-infected HLE cells (Figure 3.22, A) These results indicate that BAMBI overexpression positively affected proliferation in HLE cells and possibly blocked the apoptotic effects of TGF- β signalling (which will be further discussed in chapter 3.5.2). In addition, we found a decrement in p21 expression and an increment in PCNA (proliferating cell nuclear antigen) in the HLE-BAMBI cell line. Both changes are characteristic of highly proliferative cells (Figure 3.22, B).

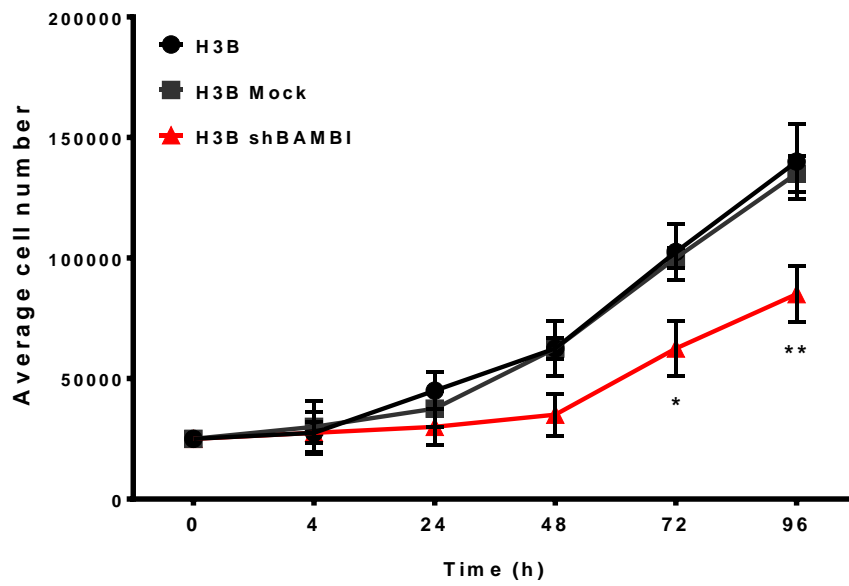
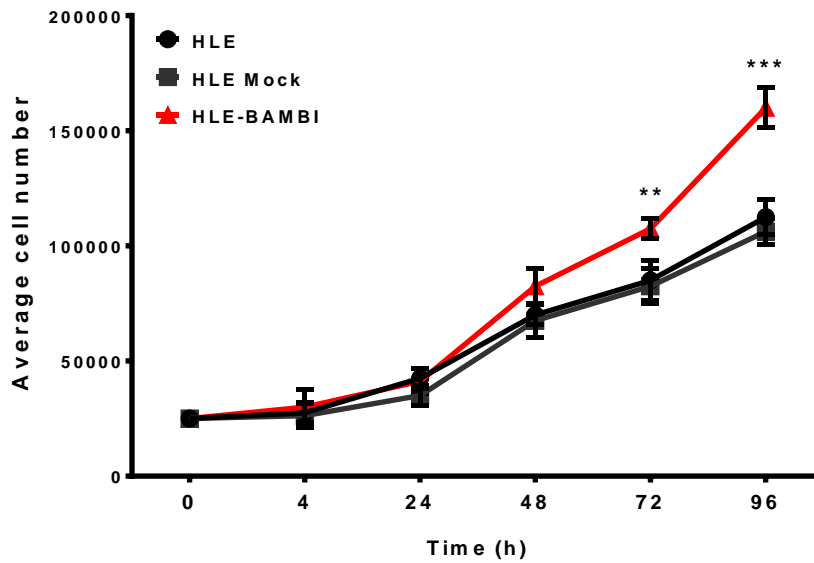


Figure 3.21: BAMBI downregulation decreased proliferation in Hep3B cells. H3B parental cells, H3B shMock and H3B shBAMBI were seeded as triplicates for each time point (24, 48, 72 and 96h). At each time point, the cells were detached with trypsin and counted in a Neubauer chamber. The result shows the mean \pm SD of one representative of three independent experiments. * $p < 0.05$; ** $p < 0.01$.

A)



B)

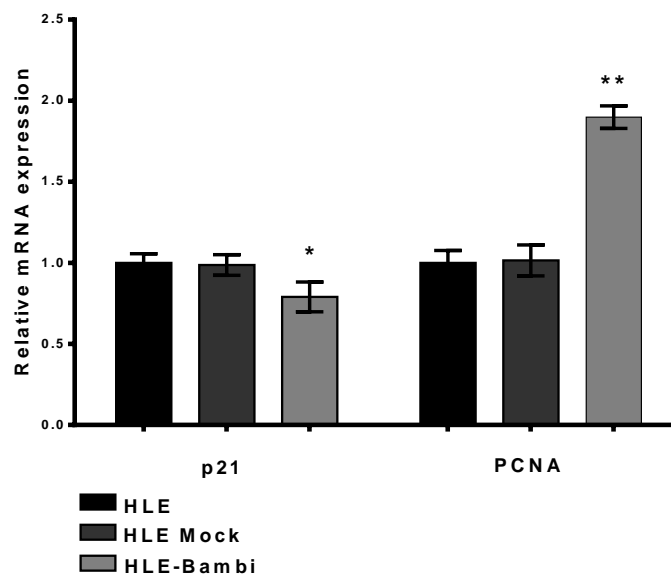


Figure 3.22: BAMBI upregulation increased proliferation in HLE cells. HLE parental cells, HLE mock and HLE-BAMBI were seeded as triplicates for each time point (24, 48, 72 and 96h). A) At each time point, the cells were detached with trypsin and counted under the microscope. The result shows the mean \pm SD of one representative of three independent experiments. B) Relative p21 and PCNA expression levels were evaluated using real time PCR with HPRT1 as a reference gene. The results show the mean \pm SE of two independent experiments. * $p < 0.05$; ** $p < 0.01$; *** $p < 0.001$.

3.5.2 BAMBI blocks the apoptotic effect of TGF- β signalling

Apoptosis is a form of programmed cell death that involves biochemical changes such as nuclear and DNA fragmentation, chromatin condensation and membrane blebbing. This process is essential for tissue remodelling, elimination of altered cells and developmental processes. Mechanistically, apoptosis is executed through the activation of caspases. Caspase-3 is a widely expressed dimeric peptidase that is the primary downstream mediator of apoptotic-associated proteolysis. During apoptosis, proCaspase-3, the inactive cytosolic homodimer, is activated by cleavage into p20 and p12 subunits; p20 is trimmed to yield the p17 subunit. Active Caspase-3, which contains two p17 and two p12, can cleave other caspases (e.g., Caspase 6, 7 and 9) and other relevant targets in order to activate them. Caspase activity can be detected using Caspase-specific peptides coupled with colorimetric or fluorimetric reporter systems in order to assess activity in the cell lysates. The previous results showed that there may be a possible effect of BAMBI modulation on apoptosis in Hep3B and HLE cells; therefore, a Caspase-3 assay was performed on both sets of cells.

As shown in Figure 3.23, H3B shBAMBI cells presented enhanced Caspase 3 activity with and without TGF- β 1 treatment after 24 and 48 hours, which translates into a higher rate of apoptosis following BAMBI downregulation. The immunoblot analysis of apoptotic (pBcl2 and Mcl1) and proliferation (c-Myc) markers confirmed the pBcl2 induction and c-Myc decrement, both of which are characteristic changes in the reduction of cell proliferation and the increase of apoptosis (Figure 3.23, lower panel). c-Myc is a multifunctional, nuclear phosphoprotein that plays a role in cell cycle progression, apoptosis and cellular transformation [199]. It is capable of driving cell proliferation (downregulating p21), but it also plays a very important role in regulating apoptosis by downregulating B-cell lymphoma 2 (Bcl2), a protein that blocks cell death and apoptosis [200]. Curiously, the myeloid leukaemia cell differentiation protein (Mcl-1), a member of the Bcl2 family that enhances cell survival by inhibiting apoptosis, did not show any changes on the protein level in these cells.

The opposite result was found in HLE-BAMBI cells when Caspase 3 activity was analysed. Apoptosis was reduced following BAMBI overexpression with and without TGF- β 1 treatment after 24 and 48 hours (Figure 3.24, upper graphs) as seen by the decrease in Cas3 activity. Moreover, higher levels of c-Myc and Mcl1 proteins were found in HLE-BAMBI cells compared to the parental and mock controls, while the phosphorylation of Bcl2 did not show any clear difference (Figure 3.24, immunoblot panel).

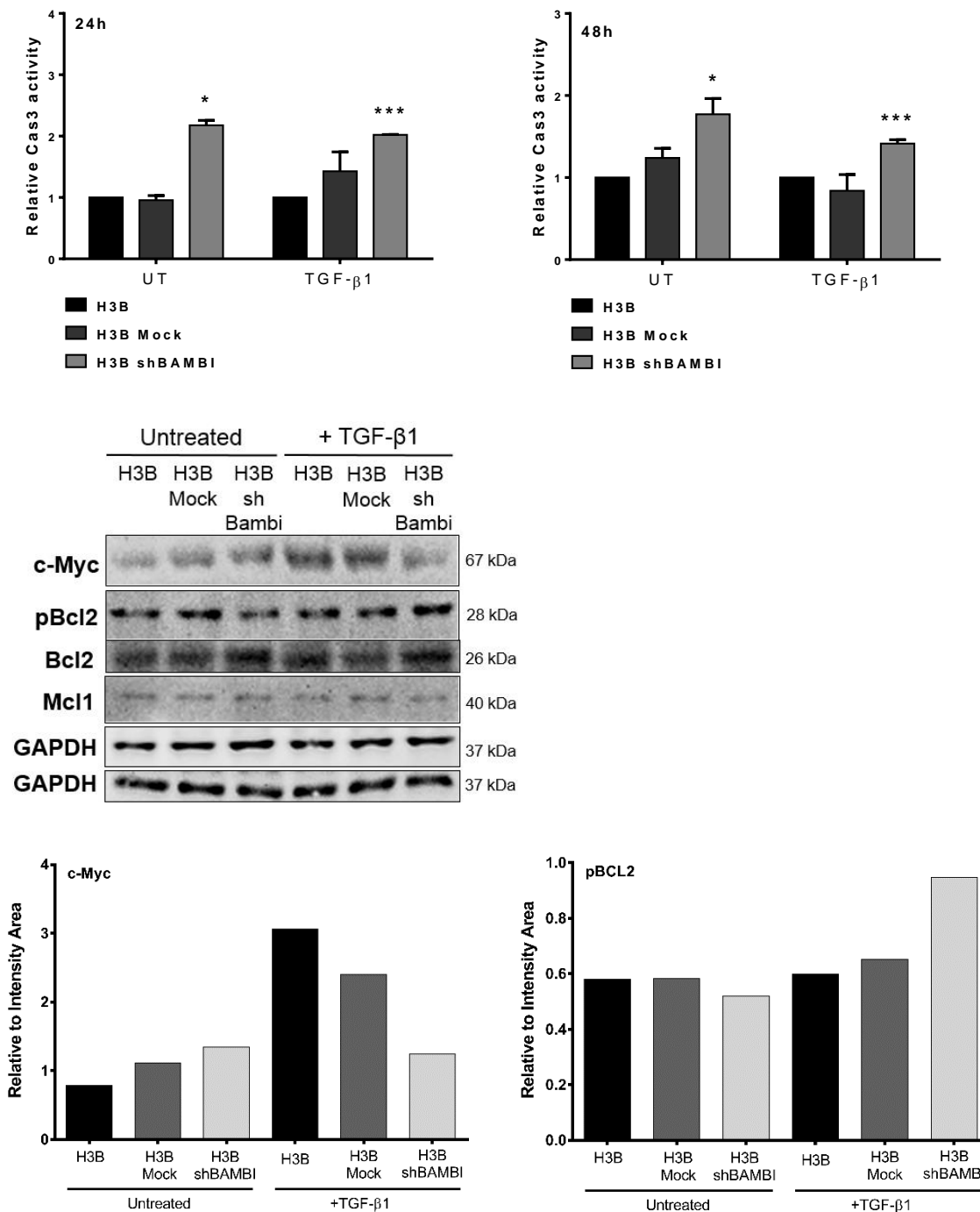


Figure 3.23: Apoptosis is increased upon BAMBI downregulation in Hep3B cells. Cells were seeded in triplicates for each condition (with or without 5 ng/ml TGF-β1 treatment). After 24 and 48 hours, the cells were detached and collected together with the supernatants. The samples followed the fluorimetric Cas3 protocol and the measured fluorescence was normalized to the protein concentration. The results represent the mean ± SE of three independent experiments. (Immunoblot) Immunoblot analysis of c-Myc, Mcl1 and phosphorylated Bcl2 ± 24h TGF-β1 treatment was performed in these cells using GAPDH as loading control. WB bands quantification: relative area calculated from the intensity bands with ImageJ software and referred to GAPDH bands intensity. *p<0.05; ***p<0.001.

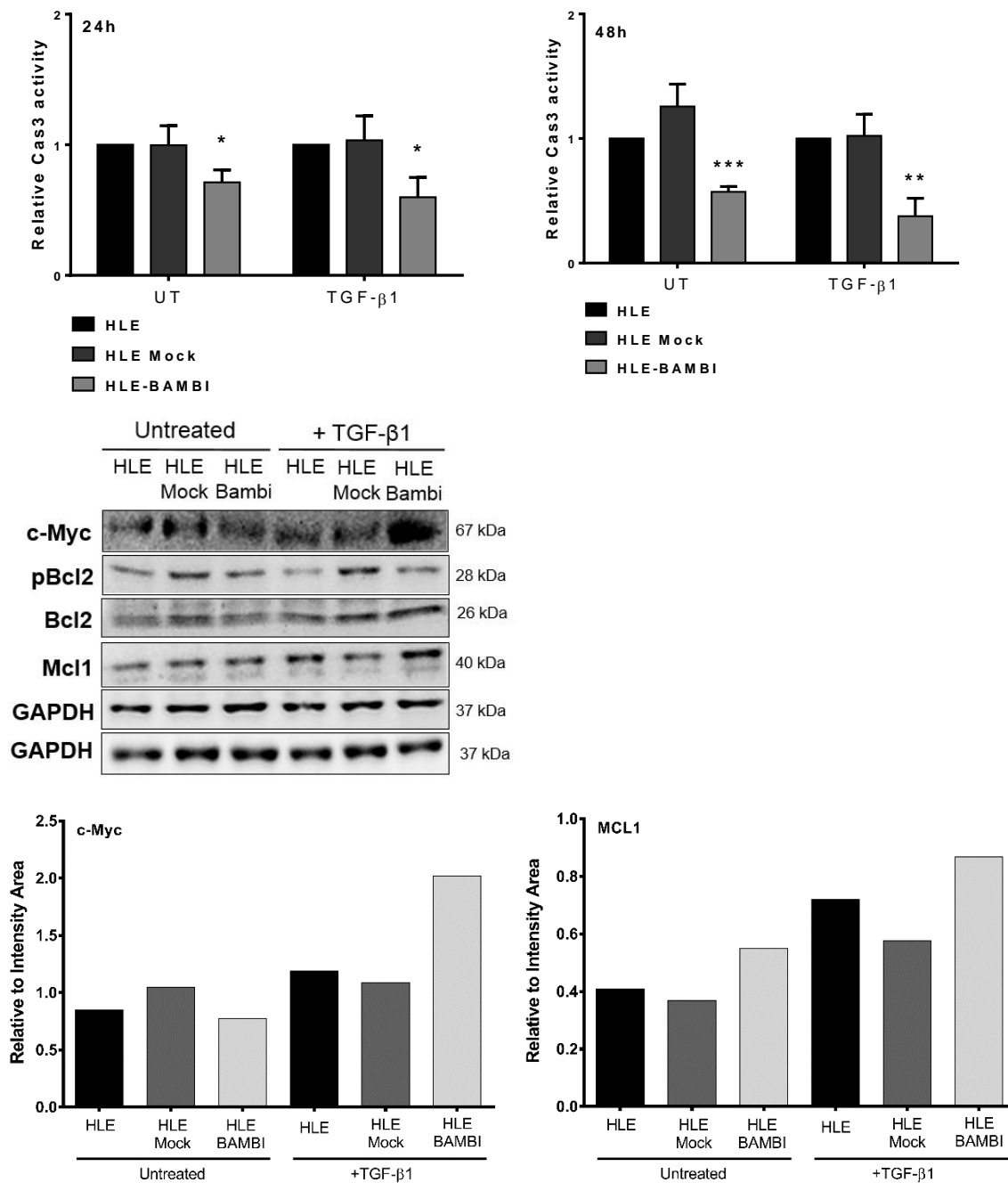


Figure 3.24: BAMB1 overexpression reduced apoptosis in HLE cells. Cells and samples followed the same steps as explained for H3B cells in the legend of Figure 3.22 (24h and 48h graphs). The results represent the mean \pm SE of three independent experiments. (Immunoblot) Immunoblot analysis of c-Myc, Mcl1 and phosphorylated Bcl2 \pm 24h TGF- β 1 treatment was performed in these cells using GAPDH as loading control. * $p < 0.05$; ** $p < 0.01$; *** $p < 0.001$.

In conclusion, the proliferation and apoptosis assays confirmed the effect of BAMB1 on both processes, shedding some light on its function in HCC. In early TGF- β signature cells (Hep3B), BAMB1 mainly blocks TGF- β -mediated apoptosis, allowing these cells to escape the tumour suppressor effects of TGF- β . In HLE cells (late TGF- β signature), BAMB1 is capable of enhancing proliferation and reducing apoptosis, allowing these cells to use the TGF- β tumour promotor effects to enhance their malignancy.

3.6 BAMBI effects on migration and invasion in HLE and Hep3B cells

Cancer metastasis requires that malignant cells acquire the ability to move and penetrate the surrounding tissues in order to spread the malignancy and form new tumours in different organs [201]. Invasion, intravasation and extravasation are the main processes of the metastatic cascade. Malignant cells can dissociate as a result of the loss of cell-cell adhesion and changes in cell-matrix interactions, and invade the stroma. The initialised angiogenesis within the tumour provides a route for migratory cells towards the circulatory system, enabling them to reach distant tissues [202]. The biochemical interactions between malignant and endothelial cells at the new metastasis point develop stronger adhesions, which allows them to penetrate the endothelium and basement membrane in order to produce a secondary tumour focus.

TGF- β plays a significant role in cancer by acting as a tumour promotor in later stages. In this context, it can promote proliferation and invasion, immune scape and metastasis of cancer cells (see chapter 1.2.5). Due to BAMBI's ability to modulate TGF- β signalling and its capacity to increase cell proliferation in HLE cells (chapter 3.5.1), it was of interest to study the migration and invasion capacity of these cells upon BAMBI overexpression.

3.6.1 HLE cells with BAMBI overexpression display enhanced migration

An in vitro wound healing migration assay was performed to characterise the cell line with stable BAMBI overexpression (HLE-BAMBI) with regard to migratory capacity. The cells migrated faster in HLE-BAMBI cells compared to parental and mock controls (Figure 3.25). All the wounds were closed after 72 hours but BAMBI overexpression meant a higher motility rate for the cells, even upon TGF- β 1 treatment, which indicates that BAMBI might be enhancing the tumour promotor effects of TGF- β 1 signalling and probably modulating the crosstalk with other pathways involved in cancer progression. Figure 3.26 translates the areas taken in the pictures from the wound assays into wound closure percentages. These results demonstrate that the HLE-BAMBI cell line presented high cell motility with and without TGF- β 1 treatment (left and right diagrams, respectively).

In order to confirm the wound assay result, an in vitro transwell migration assay was performed. Figure 3.27 (left) demonstrates that HLE cells with BAMBI overexpression showed higher cell motility than HLE parental cells and cells infected with mock control.

TGF- β is an important regulator of epithelial-mesenchymal transition (EMT), a process that allows cancer cells to gain migratory capacity. Usually, this step is accompanied by the induction of several matrix-regulating genes such as PAI1 [190, 191]. Previous results (chapter 3.3.2) revealed a significant and positive correlation between BAMBI and PAI1 in two HCC patient cohorts. The qRT-PCR analysis (Figure 3.27, right) showed that higher motility in HLE-BAMBI cells was accompanied by the overexpression of the EMT marker PAI1 compared to parental (HLE) and mock infected cells (HLE Mock).

When the wound migration assay was performed with H3B shBAMBI cells, an elevated number of dead cells could be observed in the supernatant throughout the whole experiment (Figure 3.29, A). As presented in Figure 3.28, H3B shBAMBI cells failed to

close the wound; the percentage of wound closure was even lower with TGF- β 1 treatment (Figure 3.29, B). Hep3B cells have a low migratory rate, which is decreased upon TGF- β 1 treatment, caused by its capacity to activate the apoptosis cascade (chapter 3.5.2). Since the activation of apoptosis was higher in H3B shBAMBI cells, the transwell migration assay did not show more than 0.6% migration for these cells (0.04% with TGF- β 1 treatment) compared to parental and mock controls in a transwell migration assay (data not shown).

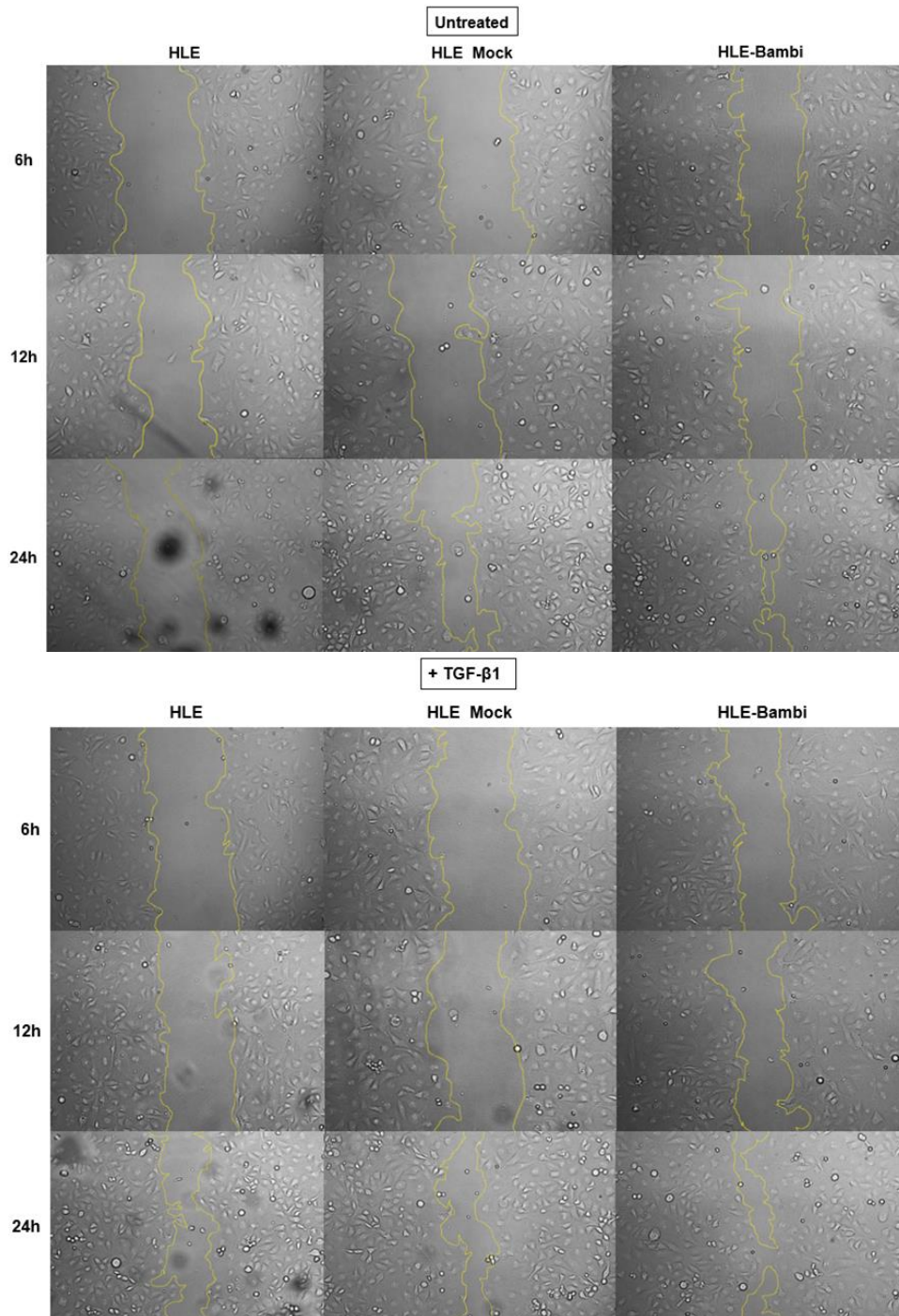


Figure 3.25: Wound closure increases upon BAMBI overexpression and TGF- β 1 treatment. The basal migration rate (up) and the migration rate upon TGF- β 1 treatment (down) of HLE-BAMBI cells as well as the parental and mock controls were evaluated using a wound assay. The images were taken at 0, 6, 12, 24, 48, and 72 hours after the wounds had been inflicted. The microscope images with 10x magnification show one representative of three independent experiments.

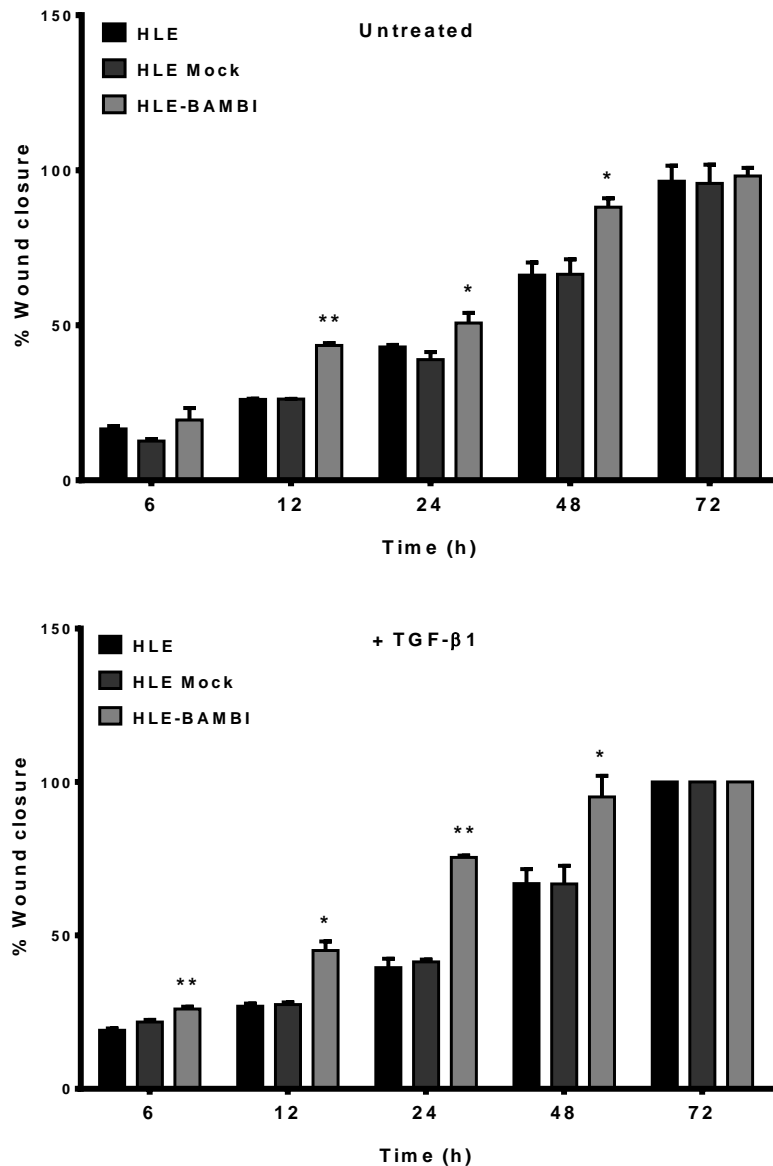


Figure 3.26: Migration capacity increases with BAMBI overexpression and TGF-β1 treatment. The basal migration rate (left) and the migration rate upon 5ng/ml TGF-β1 treatment (right), represented by the percentage of wound closure, of HLE-BAMBI cells and the parental and mock controls were evaluated. The wound areas at each time point were calculated with ImageJ and translated into the percentage of wound closure using the formula: $\text{Migration (\%M)} = 100 \cdot [(t_0h - t_h) / t_0h]$; where t_0h and t_h are gap areas measured at scratch time and at the next time point (t_h), respectively. The results represent the mean \pm SE of three independent experiments. * $p < 0.05$; ** $p < 0.01$.

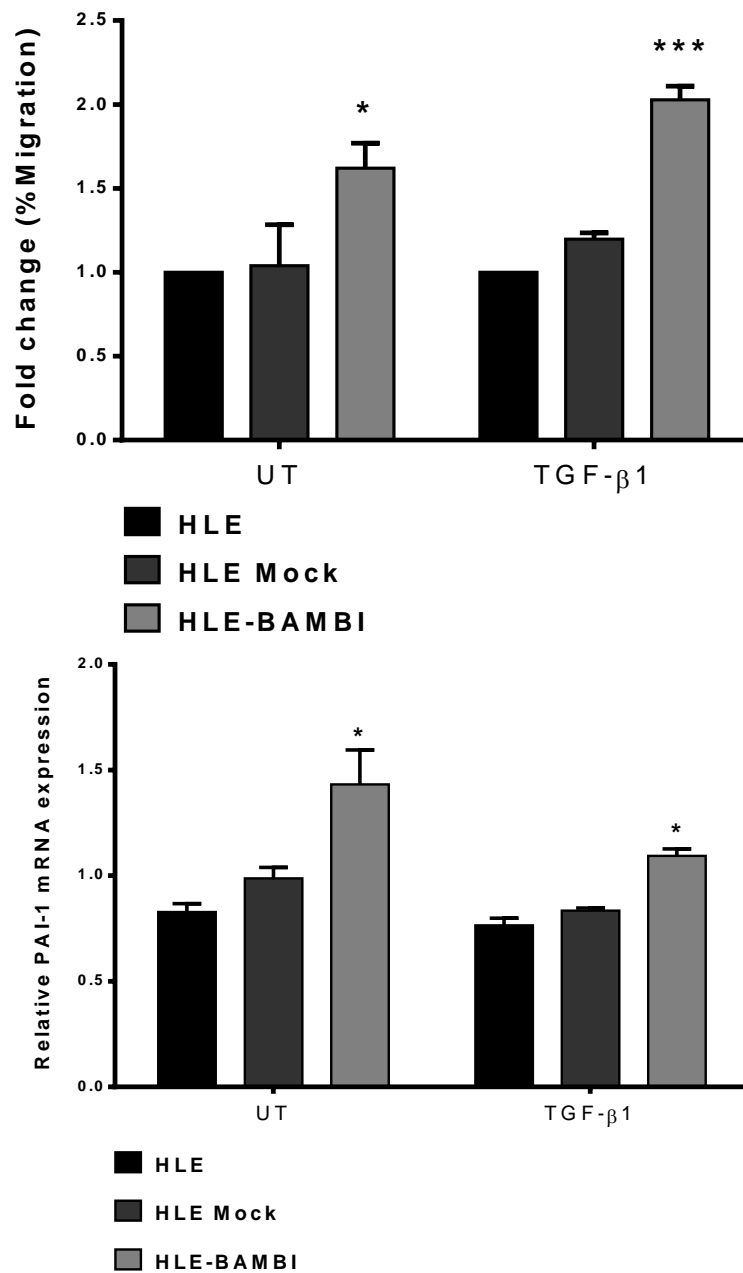


Figure 3.27: Migration capacity accompanies BAMBI overexpression and higher PAI1 levels. (Left) The migration rate of HLE, HLE Mock and HLE-BAMBI cells with and without TGF-β1 treatment was evaluated using a transwell assay. The graph shows the mean \pm SE of three independent experiments. (Right) Cells with and without TGF-β1 treatment were cultured in a starvation medium for 24 hours. qRT-PCR was performed to detect PAI1 expression using HPRT1 as a reference gene. The diagram represents the mean \pm SE of two independent experiments. * $p < 0.05$; ** $p < 0.01$; *** $p < 0.001$.

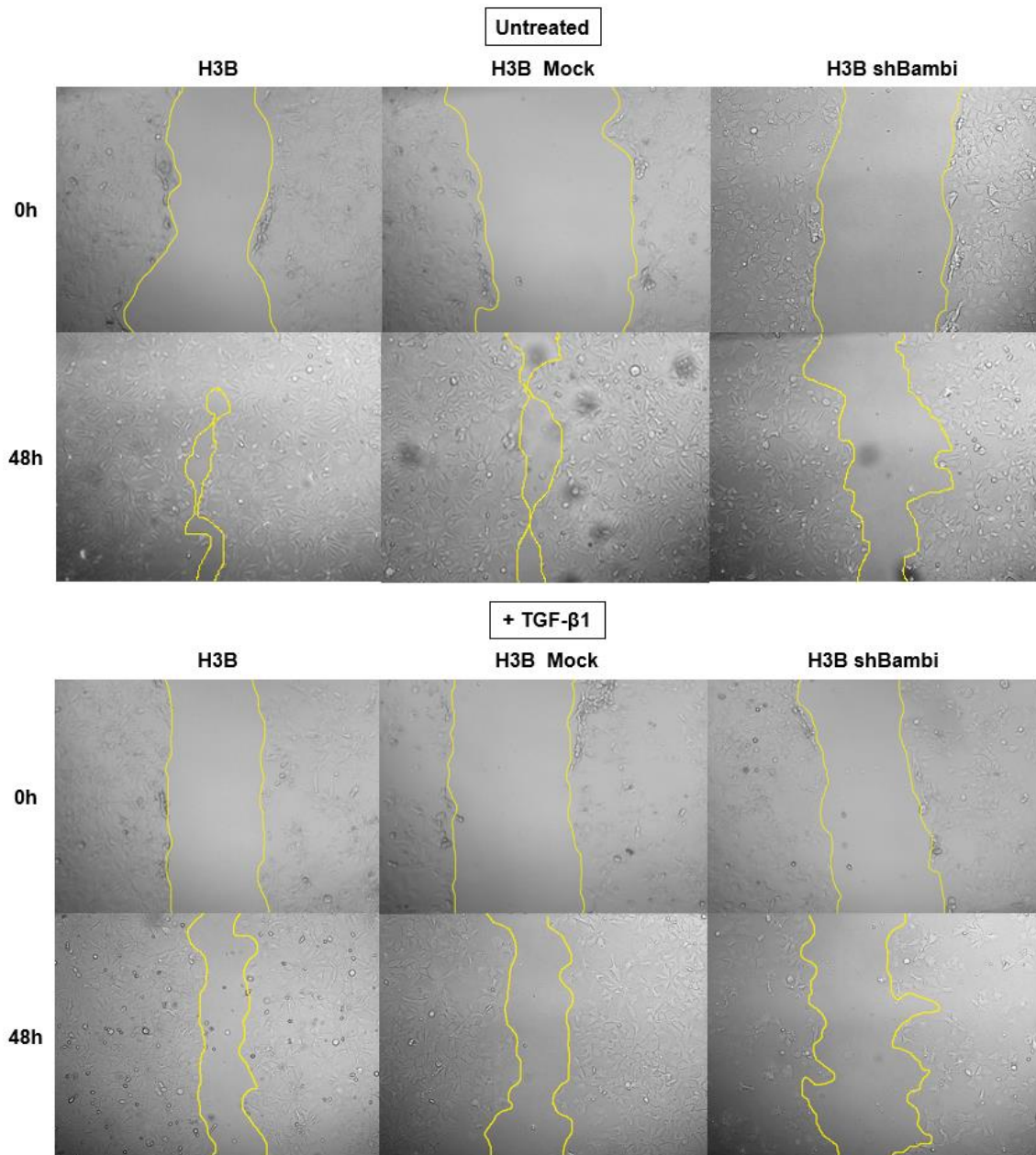
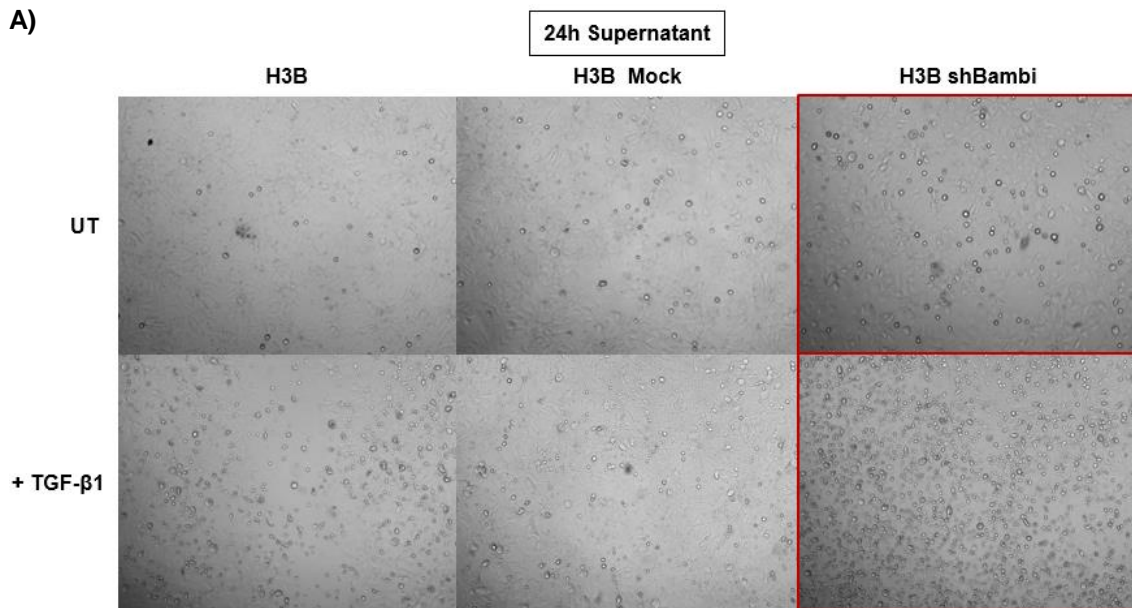


Figure 3.28: Migration decreases upon BAMBI downregulation and TGF- β 1 treatment. The basal migration rate (up) and the migration rate upon TGF- β 1 treatment (down) of H3B shBAMBI cells and the parental and mock controls were evaluated using a wound assay. The images were taken 0, 6, 12, 24, 48 and 72 hours after the wounds had been inflicted. The microscope images with 10x magnification show one representative of three independent experiments.



B)

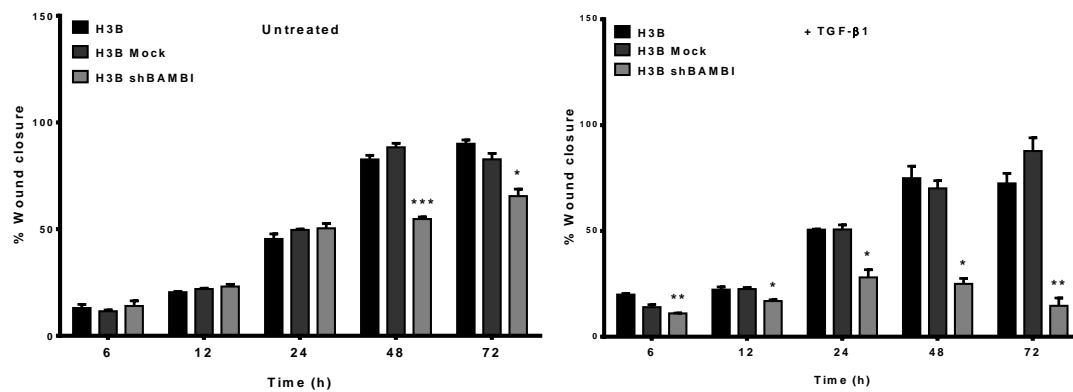


Figure 3.29: High apoptosis levels reduce the migration capacity of H3B shRNA cells. A) Images of the wound assay supernatant taken after 24 hours, showing one representative of three independent experiments. B) The migration rate of H3B, H3B Mock and H3B shBAMBI cells with and without TGF-β1 treatment was evaluated using a wound migration assay. The graph shows the mean \pm SE of three independent experiments. * $p < 0.05$; ** $p < 0.01$; *** $p < 0.001$.

3.6.2 Invasion increases upon BAMBI overexpression in HLE cells

In order to study the invasive capacity of the HLE-BAMBI cell line, a transwell Matrigel-coated assay was performed together with the qRT-PCR analysis of some angiogenesis and invasiveness (CTGF, VEGF and MMP9) markers described in HCC.

As presented in Figure 3.30, the invasive rate in HLE-BAMBI was higher compared to the parental and mock controls, although upon TGF-β1 treatment, the invasion was comparable to the one seen in the controls, suggesting possible crosstalk activation with other pathways involved in malignancy progression. These results corroborate once

again that BAMBI mainly blocks the tumour suppressor effects of TGF- β -mediated signalling.

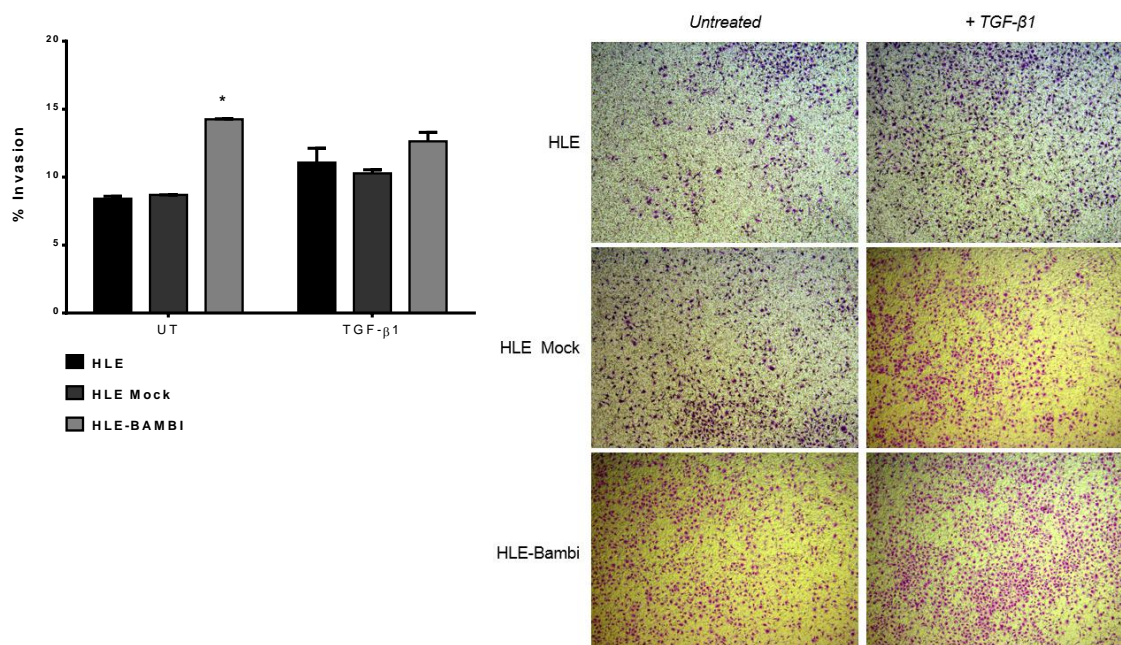


Figure 3.30: The invasive capacity of HLE cells increased upon BAMBI overexpression and TGF- β 1 treatment. The invasion rate of HLE, HLE Mock and HLE-BAMBI cells with and without TGF- β 1 treatment was evaluated using a transwell assay with Matrigel coating. (Left) The graph shows the mean \pm SE of three independent experiments. Significant differences between the mock cells and HLE-BAMBI are labelled as * $p < 0.05$, ** $p < 0.01$, *** $p < 0.001$ (Student's t-test). (Right) The microscope images with 5x magnification show one representative of three independent experiments.

In chapter 3.3.2, the correlation analysis in HCC patient cohorts showed a significant and positive correlation between CTGF and BAMBI expression. The connective tissue growth factor (CTGF) is a secreted matricellular protein that interacts with surface receptors, growth factors, cytokines and the extracellular matrix (ECM). It is known to modulate the activities of other growth factors, such as TGF- β and VEGF. The effects of CTGF are context- and cell-dependent and, even though its functions are complex, CTGF has been shown to play a role in fibrogenesis and tumorigenesis [203]. Regarding HCC, CTGF is produced in large amounts in invasive HCC cells, helping to develop highly stromal tumours. Mazzocca *et al.* [204], found that CTGF synthesis and release was inhibited upon TGF- β receptor inhibitor (LY2109761) treatment in HCC cells, which was translated into less tumour growth and lower intravasation and metastasis rates. In our study, I found that the CTGF protein level increased upon BAMBI overexpression and was even greater upon TGF- β 1 treatment (Figure 3.31, right).

Moreover, CTGF is capable of modulating VEGF activity [203]. The vascular endothelial growth factor (VEGF) is a well-known angiogenesis-enhancer cytokine that has been found overexpressed in many malignant tumours, such as ovarian cancer, gastric

cancer, colon cancer, breast cancer and hepatocellular carcinoma [205]. The resulting vascular growth, as a response to VEGF, is known to develop the disorganized angiogenesis seen in tumours (for more detailed information, see chapter 1.1.3). In the HLE-BAMBI cell line, the VEGF protein level was enhanced and more evident upon TGF- β 1 stimulation (Figure 3.31, right). In addition, the correlation analysis in the HCC patient cohorts showed a positive and significant correlation between BAMBI and VEGF expression (Figure 3.31, bottom). These results suggest that BAMBI may play a role in tumour-stroma crosstalk, facilitating angiogenesis and tumour progression.

Last but not least, several studies have demonstrated the central role of matrix metalloproteinase-9 (MMP-9) in tumour invasion and in the development of metastases, as well as its overexpression in HCC [206, 207]. Thieringer *et al.* [206] showed that high expression of MMP-9 was associated with time to recurrence (TTR) and overall survival (OS), postulating MMP9 over MMP2 as a key player in invasiveness and recurrence in hepatocellular carcinoma. In addition, BAMBI overexpression improved the activity of MMP9 in human osteosarcoma cells [157]. In my qRT-PCR analysis of HLE-BAMBI cells, MMP9 was found overexpressed, which supports the greater invasion rate (Figure 3.31, left). Furthermore, the correlation presented in chapter 3.4.2 showed a positive and significant correlation between BAMBI and MMP9 expression in three HCC patient cohorts.

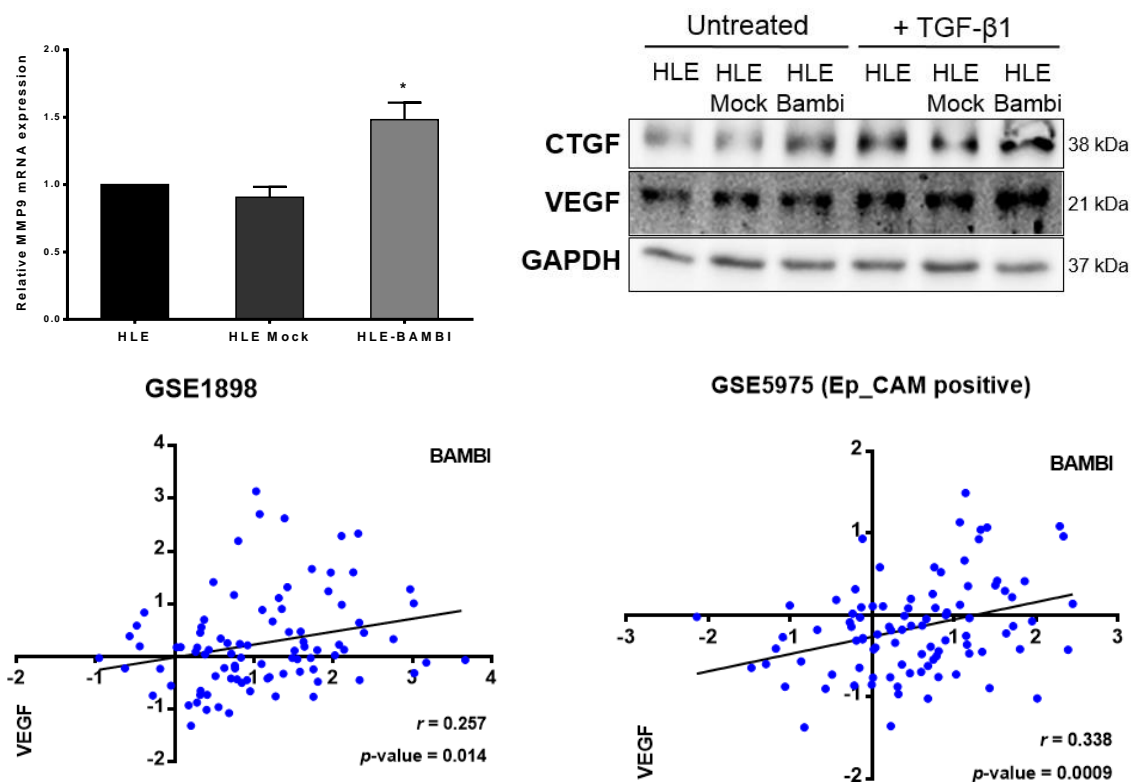


Figure 3.31: MMP9 overexpression and CTGF and VEGF induction accompany BAMBI overexpression and TGF- β 1 treatment. (Top left) Relative MMP9 expression levels were evaluated using real time PCR with HPRT1 as a reference gene. The result shows the mean \pm SE of three independent experiments. (Top right) Representative immunoblot of two independent experiments show the analysis of CTGF and VEGF with and without 24h TGF- β 1 treatment using GAPDH as loading control. (Down) Correlation analyses were performed by calculating the Pearson coefficient r between BAMBI expression and VEGF expression in the GSE5975 and GSE1898 publicly available HCC cohorts. The p-values for the Pearson correlations were calculated using the function TDIST. * $p < 0.05$.

In summary, the transwell Matrigel-coated assays confirmed the increment in the invasion rate upon BAMBI overexpression and TGF- β 1 treatment in HLE cells. In addition, the enhanced expression and protein level of MMP9, CTGF and VEGF proteins and their correlation with BAMBI expression in publicly available HCC patient cohorts suggest that BAMBI may play a role in tumour-stroma crosstalk and that there may be a possible effect from the tumour microenvironment promoting tumour progression.

3.7 Influence of BAMBI modulation on other signalling pathways

Hepatocellular carcinoma presents a large number of molecular alterations ranging from DNA mutations and chromosome copy number changes, which affect oncogenes and tumour suppressor genes, to the excess of cytokine signalling, which can activate molecular pathways without any molecular alteration per se. These kinds of changes modify molecular pathways in order to drive HCC (chapter 1.1.2). A great number of studies have focused on unravelling the consequences of these alterations and their influence on HCC progression and development. Some of the affected pathways associated with HCC are Wnt, JNK/p38 MAPK, AKT, MAPK/ERK and NF κ B. Taking together all the affected pathways and their links with BAMBI and/or TGF- β signalling, it was of interest to perform a study of some molecular components of these pathways on the protein level using Western blotting analysis.

Single modifications can affect all the different pathways since they are crosslinked and work in a tightly regulated network. The anti-apoptotic effects of BAMBI caused by the blockage of TGF- β tumour suppressor signalling trigger the activation and modulation of other pathways in crosstalk with TGF- β . Moreover, BAMBI has not only been related to TGF- β - and BMP-mediated signalling, but is also able to positively regulate Wnt/ β -catenin in order to promote cell proliferation [145, 149, 157] and enhance ERK1/2 phosphorylation, producing a switch to a pro-angiogenic TGF- β response [146]. On the other hand, Seki *et al.* [158] found that NfKBP50 is responsible for BAMBI transcriptional repression, resulting in enhanced TGF- β signalling in HSCs cells during fibrogenesis.

Wnt, regulates the expression of genes associated with proliferation, metabolism and ECM remodelling, such as c-Myc, c-Jun, cyclin D1 and matrix metalloproteinases (MMPs). The Hedgehog (Hh) signalling pathway is involved in embryonic tissue development and it has been reported that its enhanced activity increases proliferation and decreases apoptosis in HCC cells (chapter 1.1.2). MEK and ERK expression and phosphorylation are related to proliferation and HCC progression by inhibiting TGF- β -induced cytostasis while the EMT remains activated [208]. Thus, using an antibody that recognises the active form of β -catenin (dephosphorylated on Ser37 and/or Thr41), H3B shRNA presented a decreased protein level of β -catenin with and without TGF- β 1 treatment. The changes in the protein level of β -catenin were not affected by TGF- β 1 treatment in H3B cells, suggesting that the Wnt pathway is modulated by BAMBI, whereas TGF- β mainly acts as a tumour suppressor in these cells. On the other hand, HLE BAMBI showed a slightly increased β -catenin protein level in the untreated cells compared to the parental HLE cell line. However, TGF- β 1 was able to increase β -catenin in HLE cells and the increment was comparable to that seen in the untreated HLE BAMBI cell line. This result confirms the cell proliferation promotion by BAMBI in HLE cells

through modulation of the Wnt/ β -catenin pathway, as well as the switch of TGF- β to its tumour promotor function in late TGF- β signature cells (HLE).

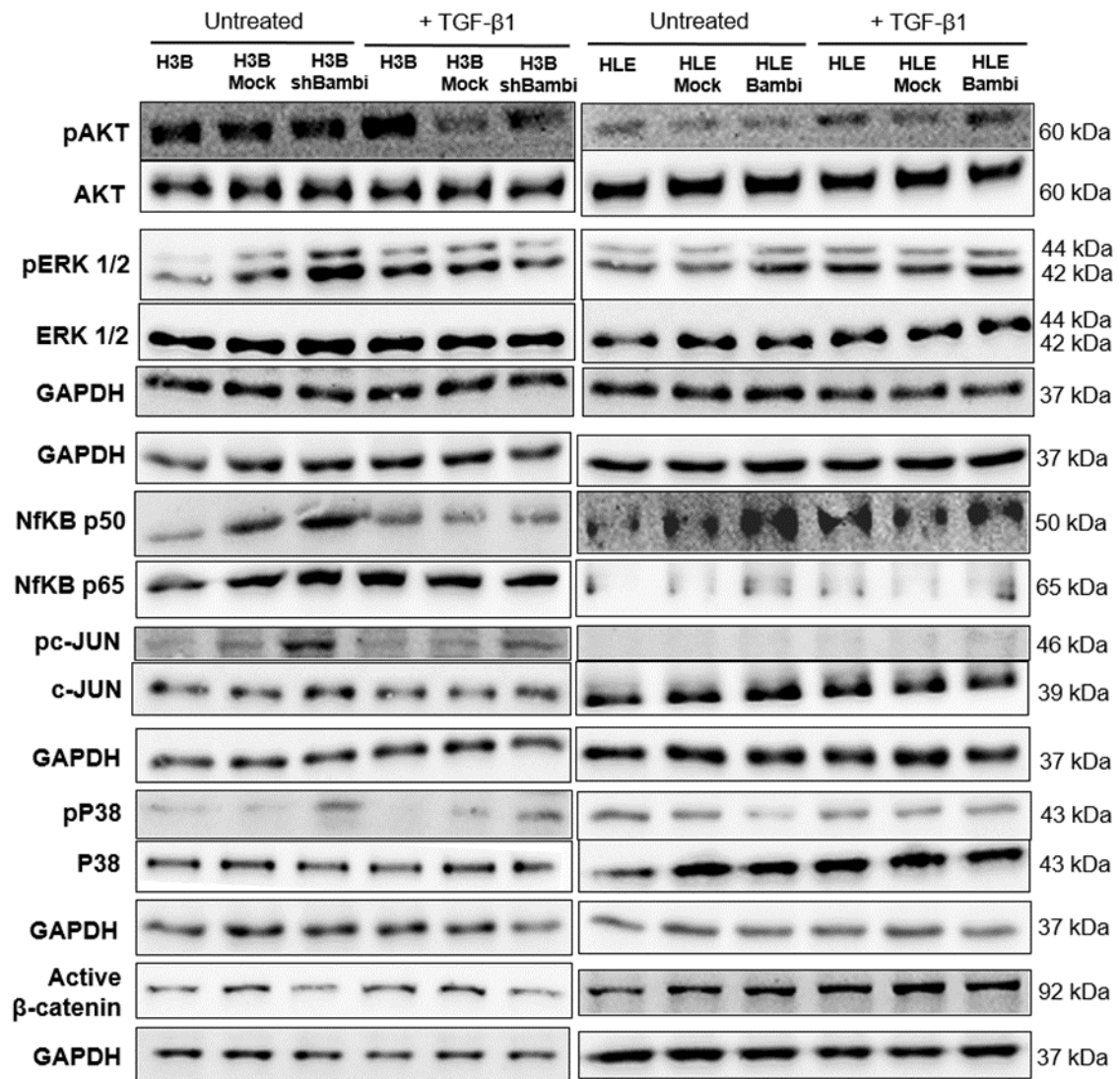


Figure 3.32: BAMBI modulation affects other signalling pathways. Immunoblot analyses of phosphorylated Akt, ERK1/2, c-JUN, p38, as well as p50, p65 and active β -catenin with and without 48h TGF- β 1 treatment were performed using GAPDH as loading control.

Interestingly, ERK1/2 phosphorylation increased upon BAMBI downregulation but decreased when the H3B shBAMBI cells were treated with TGF- β 1. What seems contradictory initially may be explained by the full release of all repressed signalings by BAMBI when the cytokine is not present. Once TGF- β 1 enters the picture, the enhanced apoptosis is higher than any tumour promotor effect, resulting in the death of the malignant cells. In addition, the HLE BAMBI cell line showed higher ERK1/2 phosphorylation with and without TGF- β 1 treatment, favouring the TGF- β tumour promotor effects.

As explained in chapter 1.2.3, non-canonical TGF- β signalling is able to activate some stress response signals such as JNK and p38 MAPK to induce apoptosis.

The increments in JNK, c-Jun (downstream target of JNK) and p38 phosphorylation are good indicatives of stress pathway activation [210-213]. As can be observed in Figure 3.32, the stress response pathways are activated upon BAMBI downregulation as represented by the increment of the c-JUN and P38 phosphorylated forms. This result was expected due to the increment of apoptosis in the H3B shBAMBI cells and confirms once again BAMBI's effect on non-canonical TGF- β signalling. Despite the absence of c-JUN signalling, the diminished P38 phosphorylation found corresponds to the anti-apoptotic effect upon BAMBI overexpression in HLE BAMBI cells.

The phosphorylation of AKT increases upon TGF- β 1 treatment and is even greater in BAMBI overexpressing cells (HLE BAMBI), which again emphasises that the aggressiveness of TGF- β is enhanced by BAMBI in late signature cells. In contrast, pAKT is reduced upon BAMBI downregulation and TGF- β 1 stimulation, which results in reduced aggressiveness. In this case it is clear that BAMBI does not modify AKT phosphorylation per se but through modulation of TGF- β signalling.

On the other hand, the NF κ B components p50 and p65 showed different results in the H3B shBAMBI and HLE BAMBI cells. The pro-inflammatory and anti-apoptotic functions of NF κ B need to be highly controlled since an excess or lack of its activation has been related to hepatocarcinogenesis [209]. As explained at the beginning of this chapter, p50 can repress BAMBI expression during fibrogenesis; therefore, it is not surprising to find it enhanced in H3B shBAMBI cells. Thus, in accordance with the p50 anti-apoptotic and pro-inflammatory responses, the protein levels of this component were reduced in H3B shBAMBI cells upon TGF- β 1 treatment and enhanced in HLE BAMBI cells with and without TGF- β 1. These results suggest a possible bypass of BAMBI repression by p50 and the consequent use of its anti-apoptotic function. In the case of the p65 component, which has been associated with bad prognosis and HBV infection, there were no changes in the protein levels upon BAMBI modulation and TGF- β 1 treatment in Hep3B cells. Nonetheless, BAMBI enhanced the p65 protein levels in HLE cells regardless of the presence of TGF- β 1, suggesting that the use of the NF κ B pathway on its own advantage in order to promote hepatocarcinogenesis.

In conclusion, due to the crosstalk existing between many pathways involved in hepatocarcinogenesis, the modification of a single component can unbalance the whole network. This is the case with BAMBI, whose modulation was found to affect not only the canonical and non-canonical TGF- β signalling but also other pathways such as Wnt/ β -catenin, JNK/p38 MAPK, ERK1/2, AKT and NF κ B. Malignant cells use them for their own advantage to promote their aggressiveness. In H3B cells, the downregulation of BAMBI in synergism with the TGF- β 1 cytokine reduced the malignancy of the cells by increasing apoptosis (as seen by the increment of the pc-JUN and pP38 protein levels) and decreasing cell proliferation (pERK1/2). Moreover, the Wnt/ β -catenin pathway seemed to be affected negatively by the reduction of active β -catenin, which translates into less cell proliferation. In HLE cells, BAMBI upregulation resulted in the increment of several molecules associated with invasion, metastasis and aggressiveness, such as pAKT, pERK1/2, β -catenin, p50 and p65, which explains the enhanced rates of migration, invasion and proliferation found in these cells.

4 DISCUSSION

4.1 Upregulated BAMBI expression in human hepatocellular carcinoma tissues and mice models

Bone morphogenetic protein and activin membrane-bound inhibitor (BAMBI), a transmembrane glycoprotein without the serine/threonine-kinase domain that plays a role in early embryogenesis and regulates several biological activities through TGF- β signalling inhibition (chapter 1.3) was found to have increased expression in colorectal, gastric and ovarian cancers, where it correlated with metastasis, invasion and poor prognosis. Several investigations confirmed BAMBI's effects on TGF- β signalling; however, there were also reports implicating the Wnt/ β -catenin pathway in driving the metastatic and invasive potential in osteosarcoma, colorectal and gastric cancers (chapter 1.3.1). In HCC, BAMBI was reported to be upregulated, but no molecular and functional studies had been performed to date to unravel its participation in hepatocarcinogenesis.

Our meta-analysis performed on publicly available HCC data cohorts confirmed BAMBI overexpression in $\approx 78\%$ of HCC patients compared to normal liver or surrounding tissues, with upregulation also being present in cirrhotic and stroma samples compared to normal liver in the GSE1898/4024 cohorts. Additional evidence was found after analysing the Oncomine® database, where three out of five HCC cohorts showed significant BAMBI overexpression (Figure 4.1, A). The cirrhotic samples in two of these cohorts showed BAMBI overexpression (Figure 4.1, B), suggesting a possible increment of BAMBI throughout disease progression from normal liver to cirrhosis and finally HCC. These results suggest a possible influence of the microenvironment (stroma) on the enhancement of BAMBI expression and on cancer progression. This hypothesis is supported by MDR2-KO mice analysis, where BAMBI was significantly overexpressed at early time points of the disease (3 and 6 months), without tumour formation. On the other hand, DEN-treated mice showed upregulation in the tumours (9 and 12 months) and in the surrounding tissues. In particular, BAMBI levels that were higher in the surrounding tissues than in the tumours were found after 9 months of treatment, and the levels became comparable after 12 months.

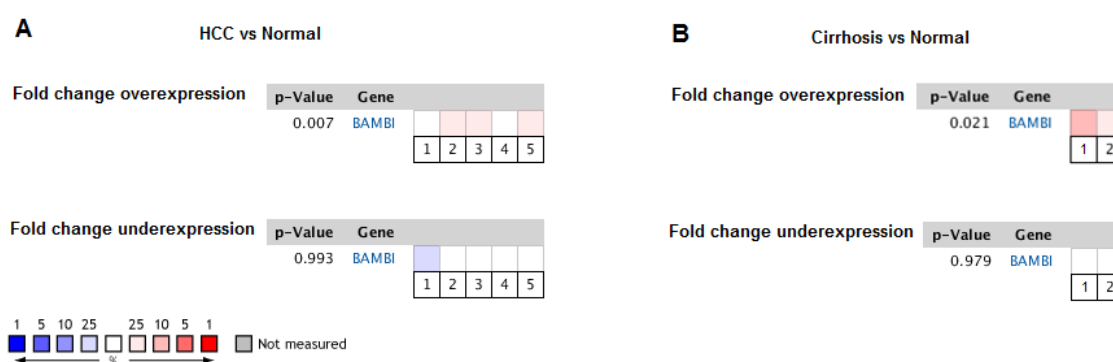


Figure 4.1: BAMBI expression in human HCC and cirrhosis stages in Oncomine® Research database. (A, B) The numbers represent different cohorts. A) Gene expression in HCC vs normal liver was analysed. B) Gene expression in cirrhosis vs normal liver was analysed. Median ranked analysis was performed under p-value < 0.05.

In parallel to these results, the IHC staining of human HCC tissue microarrays revealed upregulation in 76% of the patients, with positive staining for BAMBI in the surrounding tissues. In addition, we found infiltrated cells with a strong BAMBI signal that resembled inflammatory cells. This would make sense, as inflammation-related cytokines, such as TGF- β 1, are actively involved in the progression of chronic liver disease [161, 222].

4.2 BAMBI expression correlation with clinical-pathological characteristics of HCC patients

As presented in chapter 3.1.3, BAMBI expression in the GSE14520 HCC cohort was not found to influence the survival rate of the patients. This result is comparable to the one presented by Pils *et al.* [154], where BAMBI overexpression in ovarian cancer tissues did not affect the overall survival rates even though BAMBI overexpression conferred SKOV3 ovarian cancer cell line oncogenic characteristics *in vitro*. On the other hand, Zhang *et al.* [153] demonstrated significant associations between BAMBI expression and invasion depth, histologic differentiation, lymphatic node invasion and metastasis, and the TNM stage. In line with these results, I found positive correlations with age, BCLC staging, hepatitis B antigen and antibody (HBeAg and HBeAb), TNM stage and cirrhosis (chapters 3.1.3 and 3.4.2) on the mRNA and protein levels. Collectively, these evidences indicate that BAMBI is involved in the hepatocarcinogenesis process influencing the aggressiveness of HCC *in vivo*.

4.3 Differential BAMBI expression in HCC cell lines

Gene expression profiling shed new light on the pathogenesis of HCC and its heterogeneous origin. Given the dual role of TGF- β as a tumour suppressor and promotor, Coulouarn *et al.* [62] hypothesised that the identification of a gene signature linked to this pathway could help to find clinically relevant groups in liver cancer patients. They discovered two subsets of tumours within TGF- β -positive HCC samples characterised by the expression of early or late TGF- β signature that correlated with differences in survival status and recurrence. The late signature patients presented higher recurrence and less survival time compared to those with early TGF- β gene expression signature. In our qRT-PCR analysis of HCC cell lines, BAMBI expression appeared only in the early TGF- β signature cells (Hep3B, HepG2 and HUH7), which corresponds to an epithelial phenotype and less aggressiveness. Furthermore, BAMBI knockdown in Hep3B cells showed strong TGF- β -mediated apoptosis, which affected the proliferation and migration in these cells, suggesting that the major function of BAMBI in the early stage is to bypass the TGF- β tumour suppressor effects, such as cell growth arrest and apoptosis. In a therapeutic context, HCC patients with TGF- β early signature would benefit from BAMBI knockdown.

The fact that late-stage HCC cell lines (HLE, HLF and FLC4) do not express BAMBI, even though it would give them proliferative and invasive advantages, could be explained by the influence of the microenvironment (chapter 1.1.3). Furthermore, the lack of activation of their malignant potential by the stroma may explain why HLE cells fail to produce tumours when injected into animal models [176].

4.4 BAMBI effects on apoptosis

When I examined the functional effects of BAMBI modulation in HLE and Hep3B cells, apoptosis was found to be affected, as confirmed by Caspase 3 assays and immunoblot examination of the JNK/p38MAPK components, Mcl1 and pBcl2 proteins. Higher levels of phosphorylated JNK, p38 and Bcl2 forms as well as higher Cas3 activation levels after 24 and 48 hours confirmed the release of TGF- β -mediated apoptosis upon BAMBI downregulation in Hep3B cells. In contrast, the activation of apoptosis was blocked by BAMBI overexpression in HLE cells as shown by increased levels of Mcl1, decreased pP38 and pBcl2 proteins and Caspase 3 activity. Interestingly, no pJNK signal was found. This situation was already reported by Iyoda *et al.* in their study [213], where JNK contributed much less to apoptosis than p38 MAPK. Another plausible explanation is that transitory activation of JNK is considered anti-apoptotic while constant activation is pro-apoptotic [211]; therefore, we cannot see it while BAMBI is present. These evidences show the major role of BAMBI as a repressor of TGF- β -mediated apoptosis during early stages of the diseases. Another intriguing result was obtained when the phosphorylated ERK1/2 forms of this pro-survival pathway were checked. BAMBI downregulation increased the levels of pERK1/2, but this increment was lost upon TGF- β 1 stimulation, suggesting that the enhanced apoptosis is higher than any TGF- β tumour promotor activity released upon BAMBI knockdown. This result implies that tumorous cells with early TGF- β signature are using BAMBI to their own advantage to block and bypass TGF- β tumour suppressor activity, which further supports postulating BAMBI as a potential therapeutic target.

Finally, Seki *et al.* [159] reported BAMBI repression through NF κ B p50 by TLR4 signalling, leading to enhanced TGF- β signalling. Thus, they confirmed BAMBI's implication in inflammation-mediated fibrosis progression. In my research, H3B shBAMBI cells displayed an increment of p50 expression upon BAMBI knockdown and a decrement after TGF- β 1 stimulation. Interestingly, HLE-BAMBI cells exhibited enhanced p50 levels independent of TGF- β 1 stimulation. These results suggest a switch or bypass of BAMBI repression by p50 aimed at taking advantage of the NF κ B anti-apoptotic response in HCC. This result is supported by p65 upregulation upon BAMBI overexpression, with this NF κ B component being associated with bad prognosis.

4.5 BAMBI effects on proliferation, migration and invasion

Interestingly, the elevated invasion upon BAMBI overexpression was not further increased by TGF- β 1 stimulation, suggesting collaboration from another pathway. As mentioned above, BAMBI is known to interact with Wnt/ β -catenin [23, 145, 155], a pathway implicated in the proliferation, migration and invasiveness of cancer cells. Moreover, two major publications on gastric cancer [156] and osteosarcoma [157] showed reduced levels of β -catenin and aggressiveness after in vitro BAMBI knockdown. Similar to this result, I found reduced active β -catenin levels in Hep3B shBAMBI cells and slightly enhanced levels in HLE, suggesting that BAMBI may play a role during epithelial-mesenchymal transition and metastasis by participating in the upregulation of β -catenin. These data show that one function of BAMBI in the late stages of the disease is to enhance the TGF- β tumour promotor effects in synergy with the Wnt pathway.

Furthermore, the activation of AKT and ERK1/2 has been shown to correlate with aggressiveness in HCC [214] as well as with invasion and metastasis through MMP9 upregulation [215]. The increased rates of migration and invasion in HLE BAMBI cells are accompanied by enhanced levels of phosphorylated AKT and ERK1/2 proteins as well as a higher MMP9 expression level upon BAMBI overexpression. Moreover, SERPINE1 (PAI1) positively correlated with BAMBI expression in the HCC patient cohorts and showed increased expression levels in HLE BAMBI cells. Since the plasminogen activator inhibitor-1 (PAI-1) is known to be induced by TGF- β during EMT in hepatocytes, I expected to see a decrement in its expression due to the blockage of TGF- β signalling upon BAMBI overexpression. This confirms again that BAMBI is not blocking but rather enhancing the EMT effect of TGF- β signalling, which provides an advantage to tumour cells.

4.6 BAMBI in cholangiocarcinoma

Additionally to the HCC samples, the TMA used for BAMBI expression assessment (chapter 3.4.2) presented 15 cholangiocarcinomas (CCA). Those CCA samples showed BAMBI upregulation in 93.3% (n=14) of them, and only one patient presented BAMBI downregulation (6.67%; n=1) when tumour tissues were compared to their matching surrounding tissues (Figure 4.2). Just as in the HCC samples, the tissues presented a high number of infiltrated structures that resembled inflammatory cells (Figure 4.2, white arrows). Thus, I searched for possible correlations between BAMBI expression and the clinical-pathological data. Surprisingly, BAMBI overexpression correlated with less vascular invasion and smaller tumours (Table 4.1). Sato *et al.* [224] already reported that TGF- β /Snail activation was associated with an increment in the aggressiveness of CCA, resulting in poor prognosis. In this context, BAMBI may be exerting a protective function by blocking TGF- β tumour promoter effects such as EMT. Taking together the results in HCC and CCA, it seems that BAMBI is modulating rather than inhibiting TGF- β signalling, and that this modulation may depend on cell type and context.

BAMBI's potential role in CCA has not been studied to date [223], so this is a potential area for further investigations.

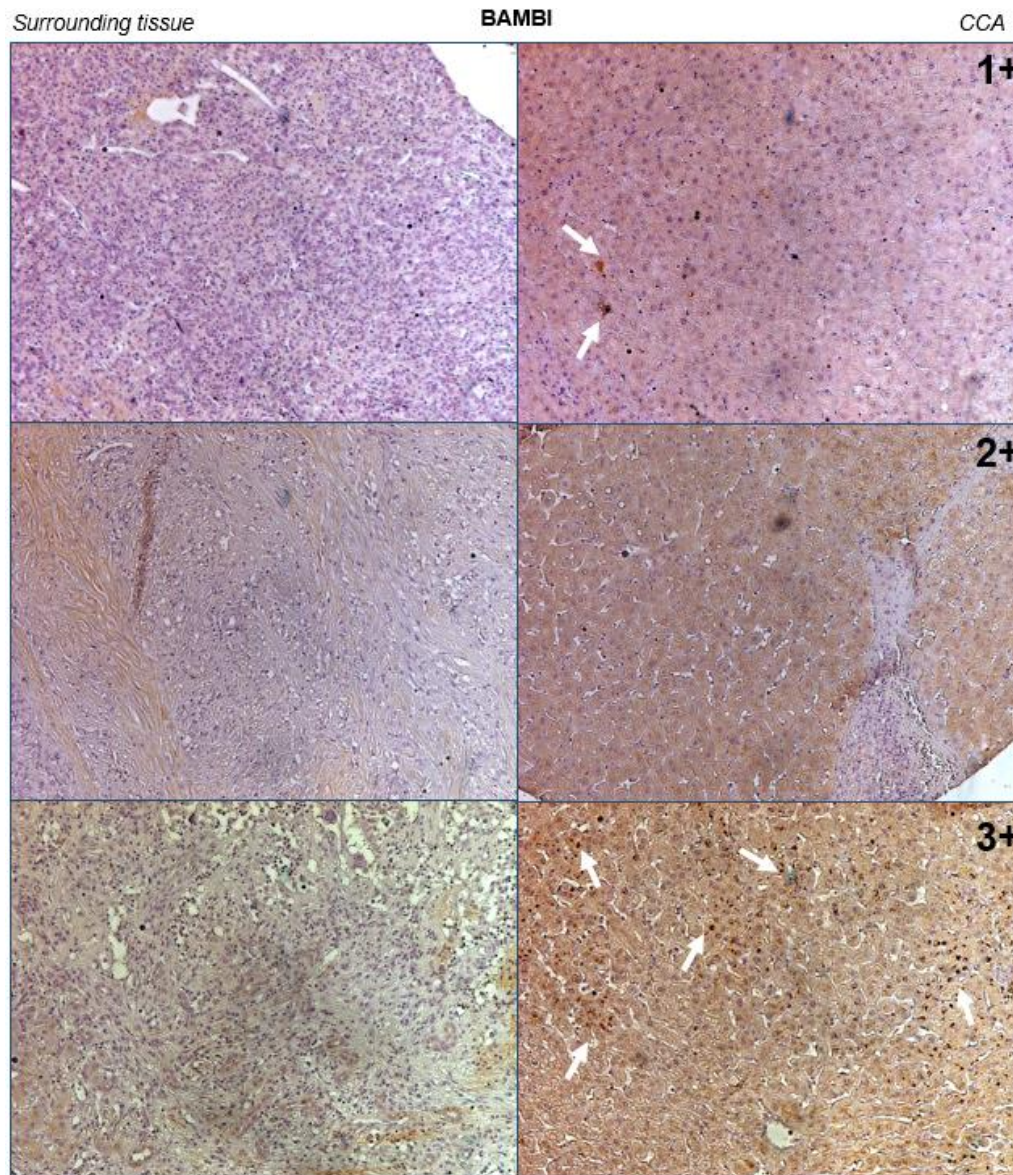


Figure 4.2: Immunohistochemical staining of BAMBI in the CCA samples from the tissue microarray (TMA). The BAMBI-staining intensity of CCA tumour tissues was classified into three groups according to the level of intensity (1+, 2+ and 3+) (magnification 10x). The images represent tumour and surrounding tissue samples from three CCA patients.

| Clinical-pathological factors | Low Bambi (n=5, %) | High Bambi (n=4, %) | P-value ^a | Clinical-pathological factors | Middle Bambi (n=5, %) | High Bambi (n=4, %) | P-value ^a |
|-------------------------------|-----------------------|------------------------|----------------------|-------------------------------|--------------------------|------------------------|----------------------|
| Vascular invasion | | | 0.047* | Vascular invasion | | | 0.21 |
| 0 | 0 (0) | 3 (75) | | 0 | 1 (20) | 3 (75) | |
| 1 | 5 (100) | 1 (25) | | 1 | 4 (80) | 1 (25) | |
| Main tumor size | | | 0.047* | Main tumor size | | | 0.047* |
| <5 | 0 (0) | 3 (75) | | <5 | 0 (0) | 3 (75) | |
| >5 | 5 (100) | 1 (25) | | >5 | 5 (100) | 1 (25) | |

Table 4.1: Correlation of BAMBI expression level with the clinical-pathological characteristics of cholangiocarcinoma tissues present in the TMA. ^a Fishers’ exact test.

4.7 BAMBI, a potential therapeutic target for personalized HCC therapies

This study indicates that the overexpression of BAMBI in HCC tissues may contribute to cancer progression. BAMBI loss activated TGF- β -mediated apoptosis in Hep3B cells, while its overexpression induced cell proliferation, migration and invasion in HLE cells. The data shown suggest the activation of the tumour promoter activity of the TGF- β and Wnt/ β -catenin pathways as well as the modulation of the JNK/p38MAPK stress-related pathways and the ERK1/2 and NF κ B pro-survival pathways by BAMBI. The activation of these functions depends on the TGF- β signature stage and the cell context. The results presented in this research postulate BAMBI as a potential candidate for personalised and targeted therapies in human hepatocellular carcinoma.

REFERENCES

1. Wong MCS, Jiang JY, Chan HLY, *et al.* International incidence and mortality trends of liver cancer: a global profile. *Nature Scientific Reports* 2017, 7, Article number: 45846 (2017)
2. Lee JG, Kang CM, Park JS, *et al.* The actual five-year survival rate of hepatocellular carcinoma patients after curative resection. *Yonsei Med. J.* 2006, 47, 105-112.
3. Altekruse SF, McGlynn KA, Reichmann ME. Hepatocellular carcinoma incidence, mortality and survival trends in the United States from 1995 to 2005. *J. Clin. Oncol.* 2009, 27, 1487-1491.
4. El-Serag HB, Rudolph KL. Hepatocellular carcinoma: epidemiology and molecular carcinogenesis. *Gastroenterology* 2007; 132(7), 2557-76.
5. Omer RE, Kuijsten A, Kadaru AM, *et al.* Population-attributable risk of dietary aflatoxins and hepatitis B virus infection with respect to hepatocellular carcinoma. *Nutr. Cancer* 2004, 48, 15-21.
6. Fattovich G, Stroffolini T, Zagni I, Donato F. Hepatocellular carcinoma in cirrhosis: Incidence and risk factors. *Gastroenterology* 2004, 127, S35-S50.
7. Zucman-Rossi J, Nault JC, Zender L. Primary liver carcinomas can originate from different cell types: A new level of complexity in hepatocarcinogenesis. *Gastroenterology* 2013, 145, 53-55.
8. Roskams T, Desmet VJ, Verslype C. Development, structure and function of the liver. *MacSween's Pathology of the Liver*, 5th ed.; Burt AD, Portmann BC, Ferrell LD, Eds.; Churchill Livingstone Elsevier: Philadelphia, PA, USA, 2007; Volume 1, pp. 1-74.
9. Lee JS, Heo J, Libbrecht L, *et al.* A novel prognostic subtype of human hepatocellular carcinoma derived from hepatic progenitor cells. *Nat. Med.* 2008, 12, 410-416.
10. Ishak K, Anthony PP, Sobin LH. *Histological Typing of Tumours of the Liver*, 2nd ed., Springer-Verlag: Berlin, Germany, 1994; Volume 1, pp. 5-7.
11. Goodman ZD, Terracciano L. Tumours and tumour-like lesions of the liver. *MacSween's Pathology of the Liver*, 5th ed.; Burt AD, Portmann BC, Ferrell LD, Eds.; Churchill Livingstone Elsevier: Philadelphia, PA, USA, 2007; Volume 1, pp. 761-814.
12. Sugihara S, Nakashima O, Kojiro M, *et al.* The morphologic transition in hepatocellular carcinoma. A comparison of the individual histologic features disclosed by ultrasound-guided fine-needle biopsy with those of autopsy. *Cancer* 1992, 70, 1488-1492.
13. Sugihara S, Kojiro M, Nakashima T. Ultrastructural study of hepatocellular carcinoma with replacing growth pattern. *Acta Pathol. Jpn.* 1985, 35, 549-559.
14. Rodrigues RR, Barry CT. Gene pathway analysis of hepatocellular carcinoma genomic expression datasets. *J. Surg. Res.* 2011, 170, e85-e92.
15. Jia D, Wei L, Guo W, *et al.* Genome-wide copy number analyses identified novel cancer genes in hepatocellular carcinoma. *Hepatology* 2011, 54, 1227-1236.

16. Wang K, Lim HY, Shi S, *et al.* Genomic landscape of copy number aberrations enables the identification of oncogenic drivers in hepatocellular carcinoma. *Hepatology* 2013, 58, 706-717
17. Tischoff I, Tannapfe A. DNA methylation in hepatocellular carcinoma. *World J. Gastroenterol.* 2008, 14, 1741-1748.
18. Yang SF, Wang SN, Wu CF, *et al.* Altered p-STAT3 (tyr705) expression is associated with histological grading and intratumour microvessel density in hepatocellular carcinoma. *J. Clin. Pathol.* 2007, 60, 642-648.
19. He G, Karin M, NF-kappaB and STAT3-Key players in liver inflammation and cancer. *Cell. Res.* 2011, 21,159-168.
20. Kisseleva T, Bhattacharya S, Braunstein J, Schindler CW. Signaling through the JAK/STAT pathway, recent advances and future challenges. *Gene* 2002, 285, 1-24.
21. Tu T, Budzinska MA, Maczurek AE, *et al.* Novel aspects of the liver microenvironment in hepatocellular carcinoma pathogenesis and development. *Int. J. Mol. Sci.* 2014, 15, 9422-9458.
22. Edamoto Y, Hara A, Biernat W, *et al.* Alterations of RB1, p53 and Wnt pathways in hepatocellular carcinomas associated with hepatitis C, hepatitis B and alcoholic liver cirrhosis. *Int. J. Cancer* 2003, 106, 334-341.
23. Waisberg J, Saba GT. Wnt/- β -catenin pathway signaling in human hepatocellular carcinoma. *World J. Hepatol.* 2015, 7(26): 2631–2635.
24. Huang S, He J, Zhang X, *et al.* Activation of the hedgehog pathway in human hepatocellular carcinomas. *Carcinogenesis* 2006, 27, 1334-1340.
25. Cheng WT, Xu K, Tian DY, *et al.* Role of Hedgehog signaling pathway in proliferation and invasiveness of hepatocellular carcinoma cells. *Int. J. Oncol.* 2009, 34, 829-836.
26. Marquardt JU, Seo D, Thorgeirsson SS, *et al.* Sequential transcriptome analysis of human liver cancer indicates large stage acquisition of malignant traits. *J. Hepatol.* 2014, 60, 346-353.
27. Brodt P. Review: Role of the Microenvironment in Liver Metastasis: From Pre- to Prometastatic Niches. *Clin. Cancer Res.* 2016,10.1158/1078-0432.CCR-16-0460.
28. Wang JS, Groopman JD. DNA damage by mycotoxins. *Mutat. Res.* 1999, 424, 167-181.
29. Besaratinia A, Kim SI, Hainaut P, Pfeifer GP. *In vitro* recapitulation of TP53 mutagenesis in hepatocellular carcinoma associated with dietary aflatoxin B1 exposure. *Gastroenterology* 2009, 137, 1127-1137.
30. Loguercio C, Federico A, Oxidative stress in viral and alcoholic hepatitis. *Free Radic. Biol. Med.* 2003, 34, 1-10.
31. Okuda M, Li K, Beard MR, *et al.* Mitochondrial injury, oxidative stress, and antioxidant gene expression are induced by hepatitis C virus core protein. *Gastroenterology* 2002, 122, 366-375.
32. Navasumrit P, Ward TH, O'Connor PJ, *et al.* Ethanol enhances the formation of endogenously and exogenously derived adducts in rat hepatic DNA. *Mutat. Res.* 2001, 479, 81-94.

33. Plentz RR, Caselitz M, Bleck JS, *et al.* Hepatocellular telomere shortening correlates with chromosomal instability and the development of human hepatoma. *Hepatology* 2004, *40*, 80-86.
34. Giron-Gonzalez JA, Martinez-Sierra C, Martin-Herrera L, *et al.* Implication of inflammation-related cytokines in the natural history of liver cirrhosis. *Liver Int.* 2004, *24*, 437-445.
35. De Lalla C, Galli G, Porcelli SA, *et al.* Production of profibrotic cytokines by invariant NKT cells characterizes cirrhosis progression in chronic viral hepatitis. *J. Immunol.* 2004, *173*, 1417-1425.
36. Folkman J. Tumor angiogenesis: Therapeutic implications. *N. Engl. J. Med.* 1971, *285*, 1182-1186.
37. Yamaguchi R, Yano H, Iemura A, *et al.* Expression of vascular endothelial growth factor in human hepatocellular carcinoma. *Hepatology* 1998, *28*(1), 68-77.
38. Wu XZ, Xie GR, Chen D. Hypoxia and hepatocellular carcinoma: The therapeutic target for hepatocellular carcinoma. *J. Gastroenterol. Hepatol.* 2007, *22*, 1178-1182.
39. Gao Q, Wang XY, Qiu SJ, *et al.* Tumor stroma reaction-related gene signature predicts clinical outcome in human hepatocellular carcinoma. *Cancer Sci.* 2011, *102*, 1522-1531.
40. Van Zijl F, Mair M, Mikulits W, *et al.* Hepatic tumor-stroma crosstalk guides epithelial to mesenchymal transition at the tumor edge. *Oncogene* 2009, *28*, 4022-4033.
41. Zhao XL, Sun T, Che N, *et al.* Promotion of hepatocellular carcinoma metastasis through matrix metalloproteinase activation by epithelial-mesenchymal transition regulator Twist1. *J. Cell Mol. Med.* 2011, *15*, 691-700.
42. Thieringer FR, Maass T, Teufel A, *et al.* Liver-specific overexpression of matrix metalloproteinase 9 (MMP-9) in transgenic mice accelerates development of hepatocellular carcinoma. *Mol Carcinog.* 2012, *51*(6):439-48.
43. Matsumura T, Makino R, Mitamura K. Frequent down-regulation of E-cadherin by genetic and epigenetic changes in the malignant progression of hepatocellular carcinomas. *Clin. Cancer Res.* 2001, *7*, 594-599.
44. Sicklick JK, Li YX, Torbenson MS, *et al.* Role of hedgehog signaling in hepatic stellate cells activation and viability. *Lab. Investig.* 2005, *85*, 1368-1380.
45. Maida M, Orlando E, Cammà C and Cabibbo G. Staging systems of hepatocellular carcinoma: A review of literature. *WJG* 2014, *20*(15): 4141-4150.
46. Okuda K, Obata H, Ohnishi K, *et al.* Prognosis of primary hepatocellular carcinoma. *Hepatology* 1984, *4*: 3S-6S.
47. Llovet JM, Bruix J. Novel advancements in the management of hepatocellular carcinoma in 2008. *J. Hepatology* 2008, *48*, S20-S37.
48. Villanueva A, Hernandez-Gea V, Llovet JM. Medical therapies for hepatocellular carcinoma: a critical view of the evidence. *Nat. Rev. Gastroenterol. Hepatol.* 2013, *10*, 34-42.
49. Leung TW, Tang AM, Zee B, *et al.* Construction of the Chinese University Prognostic Index for hepatocellular carcinoma and comparison with the TNM staging system, the Okuda staging system, and the Cancer of the Liver Italian Program staging system: a study based on 926 patients. *Cancer* 2002, *94*, 1760-1769.

50. The Cancer of the Liver Italian Program (CLIP) Investigators. Prospective validation of the CLIP score: a new prognostic system for patients with cirrhosis and hepatocellular carcinoma. *Hepatology* 2000, 31, 840-845.
51. Kudo M, Chung H, Seki T, *et al.* Validation of a new prognostic staging system for hepatocellular carcinoma: the JIS score compared with the CLIP score. *Hepatology* 2004, 40, 1396-1405.
52. Chevret S, Trinchet JC, Chastang C, *et al.* A new prognostic classification for predicting survival in patients with hepatocellular carcinoma. *J Hepatology* 1999, 31: 133-141.
53. Tateishi R, Yoshida H, Omata M, *et al.* Proposal of a new prognostic model for hepatocellular carcinoma: an analysis of 403 patients. *Gut* 2005, 54: 419-425.
54. Leung TW, Tang AM, Johnson PJ, *et al.* Construction of the Chinese University Prognostic Index for hepatocellular carcinoma and comparison with the TNM staging system, the Okuda staging system, and the Cancer of the Liver Italian Program staging system: a study based on 926 patients. *Cancer* 2002, 94: 1760-1769.
55. Marrero JA, Fontana RJ, Lok AS, *et al.* Prognosis of hepatocellular carcinoma: comparison of 7 staging systems in an American cohort. *Hepatology* 2005, 41: 707-716.
56. Kim BK, Kim SU, Han KH, *et al.* Applicability of BCLC stage for prognostic stratification in comparison with other staging systems: single centre experience from long-term clinical outcomes of 1717 treatment-naïve patients with hepatocellular carcinoma. *Liver Int.* 2012, 32: 1120-1127.
57. Hsu CY, Hsia CY, Lee SD, *et al.* Selecting an optimal staging system for hepatocellular carcinoma: comparison of 5 currently used prognostic models. *Cancer* 2010, 116: 3006-3014.
58. Cammà C, Di Marco V, Craxì A, *et al.* Survival of patients with hepatocellular carcinoma in cirrhosis: a comparison of BCLC, CLIP and GRETCH staging systems. *Aliment Pharmacol Ther.* 2008, 28: 62-75.
59. Villanueva A, Newell P, Llovet JM, *et al.* Genomics and signaling pathways in hepatocellular carcinoma. *Semin. Liver Dis.* 2007, 27, 55-76.
60. Pei Y, Zhang T, Renault V, Zhang X. An overview of hepatocellular carcinoma study by omics-based methods. *Acta Biochim. Biophys. Sin.* 2009, 41, 1-15.
61. Lemmer E, Friedman S, Llovet JM. Molecular diagnosis of chronic liver disease and hepatocellular carcinoma: the potential of gene expression profiling. *Semin. Liver Dis.* 2006, 26, 373-384.
62. Coulouarn C, Factor VM, Thorgeirsson SS. Transforming Growth Factor- β gene expression signature in mouse hepatocytes predicts clinical outcome in human cancer. *Hepatology* 2008, 47, 2059-2067.
63. Ye QH, Qin LX, Peng AC, *et al.* Predicting hepatitis B virus-positive metastatic hepatocellular carcinomas using gene expression profiling and supervised machine learning. *Nat. Med.* 2003, 9, 416-423.
64. Iizuka N, Oka M, Mori N, *et al.* Oligonucleotide microarray for prediction of early intrahepatic recurrence of hepatocellular carcinoma after curative resection. *Lancet* 2003, 361, 923-929.
65. Kurokawa Y, Matoba R, Nakamori S, *et al.* Molecular-based prediction of early recurrence in hepatocellular carcinoma. *J. Hepatol.* 2004, 41, 284-291.

66. Zucman-Rossi J, Villanueva A, Llovet JM, *et al.* Genetic landscape and biomarkers of hepatocellular carcinoma. *Gastroenterology* 2015, 149: 1226-1239.
67. Llovet JM, Montal R, Sia D and Finn RS. Molecular therapies and precision medicine for hepatocellular carcinoma. *Nat Rev Clin Oncol.* 2018, 15: 599-616.
68. Hoshida Y, *et al.* Molecular classification and novel targets in hepatocellular carcinoma: recent advancements. *Semin Liver Dis.* 2010, 30: 35-51.
69. Chiang DY, *et al.* Focal gains of VEGFA and molecular classification of hepatocellular carcinoma. *Cancer Res.* 2008, 68: 6779-6788.
70. Lachenmayer A, *et al.* Wnt-pathway activation in two molecular classes of hepatocellular carcinoma and experimental modulation by sorafenib. *Clin Cancer Res.* 2012, 18: 4997-5007.
71. Hoshida Y, *et al.* Gene expression in fixed tissues and outcome in hepatocellular carcinoma. *N Engl J Med.* 2008, 359: 1995-2004.
72. Pikarsky E, *et al.* NF- κ B functions as a tumour promoter in inflammation-associated cancer. *Nature* 2004, 431: 461-466.
73. Sia D, *et al.* Identification of an immune-specific class of hepatocellular carcinoma, based on molecular features. *Gastroenterology* 2017, 153: 812-826.
74. Huang J, Zeng Y. Current clinical uses of the biomarkers for hepatocellular carcinoma. *Drug Discoveries & Therapeutics* 2014, 8, 98-99.
75. Abou-Shady M, Baer HU, Büchler MW, *et al.* Transforming Growth Factor Betas and their signaling receptors in human hepatocellular carcinoma. *The American Journal of Surgery* 1999, 177, 209-215.
76. ten Dijke P, Goumans MJ, Itoh F, Itoh S. Regulation of cell proliferation by Smad proteins. *J. Cell. Physiol.* 2002, 191, 1-16.
77. Derynck R, Jarrett JA, Chen EY, *et al.* Human transforming growth factor-beta complementary DNA sequence and expression in normal and transformed cells. *Nature* 1985, 316, 701-705.
78. Gentry LE, Lioubin MN, Purchio AF, Marquardt H. Molecular events in the processing of recombinant type 1 pre-pro-transforming growth factor beta to the mature polypeptide. *Mol. Cell. Biol.* 1988, 8, 4162-4168.
79. Sato Y, Rifkin DB. Inhibition of endothelial cell movement by pericytes and smooth muscle actin: activation of a latent transforming growth factor-beta 1-like molecule by plasmin during co-culture. *J. Cell. Biol.* 1989, 109, 309-315.
80. Schultz-Cherry S, Murphy-Ullrich JE. Thrombospondin causes activation of latent transforming growth factor-beta secreted by endothelial cells by a novel mechanism. *J. Cell. Biol.* 1993, 122, 923-933.
81. Munger JS, Huang X, Kawakatsu H, *et al.* The integrin alpha v beta 6 binds and activates latent TGF beta 1: a mechanism for regulating pulmonary inflammation and fibrosis. *Cell* 1999, 96, 319-328.
82. Miyazono K, Olofsson A, Colosetti P, Heldin CH. A role of the latent TGF-beta 1-binding protein in the assembly and secretion of TGF-beta 1. *EMBO J* 1991, 10, 1091-1101.
83. ten Dijke P, Arthur HM. Extracellular control of TGFbeta signalling in vascular development and disease. *Nat. Rev. Mol. Cell. Biol.* 2007, 8, 857-869.
84. Deli A, Kreidl E, Grusch M, *et al.* Activins and activin antagonists in hepatocellular carcinoma. *W. J. Gastroenterol.* 2008, 14, 1699-1709.

85. Wrana JL, Attisano L, Carcamo J, *et al.* TGF beta signals through a heteromeric protein kinase receptor complex. *Cell* 1992, 71, 1003-1014.
86. Shi Y, Massague J. Mechanisms of TGF-beta signaling from cell membrane to the nucleus. *Cell* 2003, 113, 685-700.
87. Feng XH, Derynck R. Specificity and versatility in tgf-beta signaling through Smads. *Annu. Rev. Cell. Dev. Biol.* 2005, 21, 659-693.
88. ten Dijke P, Yamashita H, Ichijo H, *et al.* Characterization of type I receptors for transforming growth factor-beta activin. *Science* 1994, 264, 101-104.
89. Daly AC, Randall RA, Hill CS. Transforming growth factor beta-induced Smad1/5 phosphorylation in epithelial cells is mediated by novel receptor complexes and is essential for anchorage-independent growth. *Mol. Cell. Biol.* 2008, 28, 6889-6902.
90. Heldin CH, Moustakas A. Role of Smads in TGFbeta signalling. *Cell Tissue Res.* 2012, 347, 21-36.
91. Shi Y, Wang YF, Jayaraman L, *et al.* Crystal structure of Smad MH1 domain bound to DNA: insights on DNA binding in TGF-beta signaling. *Cell* 1998, 94, 585-594.
92. Chacko BM, Qin BY, Tiwari A, *et al.* Structural basis of heteromeric smad protein assembly in TGF-beta signaling. *Mol Cell.* 2004, 15, 813-823.
93. Dennler S, Itoh S, Vivien D, *et al.* Direct binding of Smad3 and Smad4 to critical TGF beta-inducible elements in the promoter of human plasminogen activator inhibitor-type 1 gene. *EMBO J.* 1998, 17, 3091-3100.
94. Oh SP, Seki T, Goss KA, *et al.* Activin receptor-like kinase I modulates transforming growth factor-beta 1 signaling in the regulation of angiogenesis. *Proc. Natl. Acad. Sci. USA* 2000, 97, 2626-2631.
95. Higashi K, Inagaki Y, Fujimori K, *et al.* Interferon-gamma interferes with transforming growth factor-beta signaling through direct interaction of YB-1 with Smad3. *J. Biol. Chem.* 2003, 278, 43470-43479.
96. Imamura T, Takase M, Nishihara A, *et al.* Smad6 inhibits signaling by the TGF-beta superfamily. *Nature* 1997, 389, 622-626.
97. Nakao A, Afrakhte M, Moren A, *et al.* Identification of Smad7, a TGFbeta-inducible antagonist of TGF-beta signalling. *Nature* 1997, 389, 631-635.
98. Luo K, Stroschein SL, Zhou Q, *et al.* The Ski oncoprotein interacts with the Smad proteins to repress TGFβ signaling. *Genes Dev.* 1999, 13, 2196-2206.
99. Sun Y, Liu X, Weinberg RA. SnoN and Ski protooncoproteins are rapidly degraded in response to transforming growth factor β signaling. *Proc. Natl. Acad. Sci. USA* 1999b, 96, 12442-12447.
100. He W, Dorn DC, Erdjument-Bromage H, Massagué J, *et al.* Hematopoiesis controlled by distinct TIF1gamma and Smad4 branches of the TGFbeta pathway. *Cell* 2006, 125, 929-941.
101. Descargues P, Sil AK, Karin M, *et al.* IKKalpha is a critical coregulator of a Smad4-independent TGFbeta-Smad2/3 signaling pathway that controls keratinocyte differentiation. *Proc. Natl. Acad. Sci. USA* 2008, 105, 2487-2492.
102. Lu T, Tian L, Stark GR, *et al.* Dose-dependent cross-talk between the transforming growth factor-beta and interleukin-1 signaling pathways. *Proc. Natl. Acad. Sci. USA* 2007, 104, 4365-4370.

103. Ozdamar B, Bose R, Wrana JL, *et al.* Regulation of the polarity protein Par6 by TGFbeta receptors controls epithelial cell plasticity. *Science* 2005, 307, 1603–1609.
104. Wilkes MC, *et al.* Transforming Growth Factor-beta activation of Phosphatidylinositol 3-Kinase is independent of Smad2 and Smad3 and regulates fibroblast responses via p21-activated kinase-2. *Cancer Res.* 2005, 65, 10431-10440.
105. Bhowmick NA, Ghiassi M, Moses HL, *et al.* Transforming growth factor-beta1 mediates epithelial to mesenchymal transdifferentiation through a RhoA-dependent mechanism. *Mol. Biol. Cell.* 2001, 12, 27-36.
106. Suzuki K, Wilkes MC, Leof EB, *et al.* Transforming growth factor beta signaling via Ras in mesenchymal cells requires p21-activated kinase 2 for extracellular signal-regulated kinase-dependent transcriptional responses. *Cancer Res.* 2007, 67, 3673–3682.
107. Edlung S, Landstrom M, Heldin CH, Aspenstrom P. Smad7 is required for TGF-beta-induced activation of the small GTPase Cdc42. *J. Cell. Sci.* 2004, 117, 1835-1847.
108. Wilkes MC, Murphy SJ, Garamszegi N, Leof EB. Cell-type-specific activation of PAK2 by transforming growth factor beta independent of Smad2 and Smad3. *Mol. Cell. Biol.* 2003, 23, 8878-8889.
109. Matsuura I, Denissova NG, Wang G, *et al.* Cyclin-dependent kinases regulate the antiproliferative function of Smads. *Nature* 2004, 430, 226-231.
110. Hellerbrand C, Stefanovic B, Brenner DA, *et al.* The role of TGFβ1 in initiating hepatic stellate cell activation in vivo. *J Hepatol.* 1999, 30, 77–87.
111. Dooley S, Delvoux B, Gressner AM, *et al.* Modulation of transforming growth factor β response and signaling during transdifferentiation of rat hepatic stellate cells to myofibroblasts. *Hepatology* 2000, 31, 1094–1106.
112. Dooley S, Hamzavi J, Dijke P, Gressner AM, *et al.* Smad7 prevents activation of hepatic stellate cells and liver fibrosis in rats. *Gastroenterology* 2003, 125, 178–191.
113. Schnabl B, Kweon YO, Brenner DA, *et al.* The role of Smad3 in mediating mouse hepatic stellate cell activation. *Hepatology* 2001, 34, 89–100.
114. Seyhan H, Hamzavi J, Dooley S, *et al.* Liver fibrogenesis due to cholestasis is associated with increased Smad7 expression and Smad3 signaling. *J. Cell. Mol. Med.* 2006, 10, 922–932.
115. Yoshida K, Matsuzaki K, M, Okazaki K, *et al.* Transforming growth factor-β and platelet-derived growth factor signal via c-Jun N-terminal kinase-dependent Smad2/3 phosphorylation in rat hepatic stellate cells after acute liver injury. *Am. J. Pathol.* 2005, 166, 1029–1039.
116. Matsuzaki K, Murata M, Seki T, *et al.* Chronic inflammation associated with hepatitis C virus infection perturbs hepatic transforming growth factor β signaling, promoting cirrhosis and hepatocellular carcinoma. *Hepatology* 2007, 46, 48–57.
117. Moustakas A, Kardassis D. Regulation of the human p21/WAF1/Cip1 promoter in hepatic cells by functional interactions between Sp1 and Smad family members. *Proc. Natl. Acad. Sci. USA* 1998, 95, 6733–6738.

118. Fausto N, Mead JE, Shank PR, *et al.* Proto-oncogene expression and growth factors during liver regeneration. *Symp. Fundam. Cancer Res.* 1986, 39, 69–86.
119. Perlman R, Schiemann WP, Weinberg RA, *et al.* TGF- β -induced apoptosis is mediated by the adapter protein Daxx that facilitates JNK activation. *Nat. Cell. Biol.* 2001, 3, 708–714.
120. Becker C, Fantini MC, Neurath MF. TGF- β as a T cell regulator in colitis and colon cancer. *Cytokine Growth Factor Rev.* 2006, 17, 97–106.
121. Bierie B, Moses HL. TGF β : the molecular Jekyll and Hyde of cancer. *Nature Rev. Cancer* 2006, 6, 506-520.
122. Massagué J. TGF β in Cancer. *Cell* 2008, 134, 215-230.
123. Nagathihalli SN, Pran KD. Targeting the transforming growth factor- β signaling pathway in human cancer. *Expert Opin. Investig. Drugs* 2010, 19, 77-91.
124. Bissell DM. Chronic liver injury, TGF- β , and cancer. *Exp. Mol. Med.* 2001, 33, 179-190.
125. Kim SJ, Im YH, Markowitz SD, Bang YJ. Molecular mechanisms of inactivation of TGF- β receptors during carcinogenesis. *Cytokine and Growth Factor Rev.* 2000, 11, 159-168.
126. Rodgarkia-Dara C, Vejda S, Grusch M, *et al.* The activin axis in liver biology and disease. *Mutat. Res.* 2006, 613, 123–137.
127. Kang Y, Siegel PM, Massagué J, *et al.* A multigenic program mediating breast cancer metastasis to bone. *Cancer Cell* 2003b, 3, 537–549.
128. Sneddon JB, Zhen HH, Brown PO, *et al.* Bone morphogenetic protein antagonist gremlin 1 is widely expressed by cancer-associated stromal cells and can promote tumor cell proliferation. *Proc. Natl. Acad. Sci. USA* 2006, 103, 14842–14847.
129. Ebisawa T, Fukuchi M, Miyazono K, *et al.* Smurf1 interacts with transforming growth factor- β type I receptor through Smad7 and induces receptor degradation. *J. Biol. Chem.* 2001, 276, 12477-12480.
130. Hata A, Lagna G, Massagué J, Hemmati-Brivanlou A. Smad6 inhibits BMP/Smad1 signaling by specifically competing with the Smad4 tumor suppressor. *Genes Dev.* 1998a, 12, 186-197.
131. Ulloa L, Doody J, Massagué J. Inhibition of transforming growth factor- β /SMAD signalling by the interferon- γ /STAT pathway. *Nature* 1999, 397, 710-713.
132. Bitzer M, von Gersdorff G, Böttinger EP, *et al.* A mechanism of suppression of TGF- β /SMAD signaling by NF- κ B/RelA. *Genes Dev.* 2000, 14, 187-197.
133. Itoh F, Asao H, ten Dijke P, Itoh S, *et al.* Promoting bone morphogenetic protein signaling through negative regulation of inhibitory Smads. *EMBO J.* 2001, 20, 4132-4142.
134. Calonge MJ, Massagué J. Smad4/DPC4 silencing and hyperactive Ras jointly disrupts transforming growth factor- β antiproliferative responses in colon cancer cells. *J. Biol. Chem.* 1999, 274, 33637-33643.
135. Alexandrow MG, Kawabata M, Aakre M, Moses HL. Over-expression of the c-Myc oncoprotein blocks the growth-inhibitory response but is required for the mitogenic effects of transforming growth factor β 1. *Proc. Natl. Acad. Sci.* 1995, 92, 3239-3243.
136. Izutsu K, Kurokawa M, Hirai H, *et al.* The corepressor CtBP interacts with Evl-1 to repress transforming growth factor β signaling. *Blood* 2001, 97, 2815-2822.

137. Verrecchia F, Pessah M, Atfi A, Mauviel A. Tumor necrosis factor- α inhibits transforming growth factor- β /Smad signaling in human dermal fibroblasts via AP-1 activation. *J. Biol. Chem.* 2000, 275, 30226-30231.
138. Bianco C, Strizzi L, Salomon DS, *et al.* Cripto-1: an oncofetal gene with many faces. *Curr. Top Dev. Biol.* 2005, 67, 85-133.
139. Gray PC, Harrison CA, Vale W. Cripto forms a complex with activin and type II activin receptors and can block activin signaling. *Proc. Natl. Acad. Sci. USA* 2003, 100, 5193-5198.
140. Gray PC, Shani G, Vale W, *et al.* Cripto binds transforming growth factor beta (TGF- β) and inhibits TGF- β signaling. *Mol. Cell Biol.* 2006, 26, 9268-9278.
141. Onichtchouk D, Chen YG, Niehrs C, *et al.* Silencing of TGF- β signalling by the pseudoreceptor BAMBI. *Nature* 1999, 401, 480-485.
142. Tsang M, Kim R, Dawid IB, *et al.* Zebrafish nma is involved in TGF β family signaling. *Genesis.* 2000, 28, 47-57.
143. Higashihori N, Song Y, Richman JM. Expression and regulation of the decoy bone morphogenetic protein receptor BAMBI in the developing avian face. *Dev. Dyn.* 2008, 237, 1500–1508.
144. Sekiya T, Adachi S, Higuchi O, *et al.* Identification of BMP and activin membrane-bound inhibitor (BAMBI), an inhibitor of transforming growth factor- β signaling, as a target of the beta-catenin pathway in colorectal tumor cells. *J. Biol. Chem.* 2004, 279, 6840–6846.
145. Lin Z, Gao C, Chen YG, *et al.* The pseudoreceptor BMP and activin membrane-bound inhibitor positively modulates Wnt/ β -catenin signaling. *J. Biol. Chem.* 2008, 283, 33053-33058.
146. Guillot N, Kollins D, Schlondorff D, *et al.* BAMBI regulates angiogenesis and endothelial homeostasis through modulation of alternative TGF β signaling. *PLoS ONE* 2012, 7(6): e39406.
147. Wanninger J, *et al.* Adiponectin induces the transforming growth factor decoy receptor BAMBI in human hepatocytes. *FEBS Letters* 2011, 585: 1338-1344.
148. Seki E, De Minicis S, Schwabe RF, *et al.* TLR4 enhances TGF- β signaling and hepatic fibrosis. *Nat. Med.* 2007, 13, 1324-1332.
149. Fritzmann J, Morkel M, Birchmeier W, *et al.* A colorectal cancer expression profile that includes transforming growth factor β inhibitor BAMBI predicts metastatic potential. *Gastroenterology* 2009, 137, 165-175.
150. Yan X, Lin Z, Chen YG, *et al.* Human BAMBI cooperates with Smad7 to inhibit transforming growth factor- β signaling. *J. Biol. Chem.* 2009, 284, 30097-30104.
151. Degen WG, Weterman MA, Bloemers HP, *et al.* Expression of nma, a novel gene, inversely correlates with the metastatic potential of human melanoma cell lines and xenografts. *Int. J. Cancer* 1996, 65, 460-465.
152. Khin SS, Kitazawa R, Kitazawa S, *et al.* BAMBI gene is epigenetically silenced in subset of high-grade bladder cancer. *Int. J. Cancer* 2009, 125, 328-338.
153. Zhang Y, Yu Z, Sun M, *et al.* Expression of BAMBI and its combination with Smad7 correlates with tumor invasion and poor prognosis in gastric cancer. *Tumor Biol.* 2014, 35, 7047-7056.
154. Pils D, Wittinger M, Krainer M, *et al.* BAMBI is overexpressed in ovarian cancer and co-translocates with Smads into the nucleus upon TGF- β treatment. *Gyn. Oncol.* 2010, 117, 189-197.

155. Cavard C, Colnot S, Terris B & Perret C, *et al.* Wnt/ β -catenin pathway in hepatocellular carcinoma pathogenesis and liver physiology. *Future Oncology*, 2008, 4(5): 647-660.
156. Liu K, Song X, Hu S, *et al.* Knockdown of BAMBI inhibits β -catenin and transforming growth factor β to suppress metastasis of gastric cancer cells. *Mol. Med. Rep.* 2014, 10, 874-880.
157. Zhou L, Park J, Kim JR, *et al.* The overexpression of BAMBI and its involvement in the growth and invasion of human osteosarcoma. *Oncol. Rep.* 2013, 30, 1315-1322.
158. Seki E, De Minicis S, Schwabe RF, *et al.* TLR4 enhances TGF-beta signaling and hepatic fibrosis. *Nat. Med.* 2007, 13, 1324-1332.
159. Liu C, Chen X, Seki E, *et al.* Transcriptional repression of the transforming growth factor β (TGF- β) Pseudoreceptor BMP and activin membrane-bound inhibitor (BAMBI) by Nuclear Factor κ B (NF- κ B) p50 enhances TGF- β signaling in hepatic stellate cells. *J. Biol. Chem.* 2014, 289, 7082-7091.
160. Lou X, Hutley LJ, Whitehead JP, *et al.* Identification of BMP and activin membrane-bound inhibitor (BAMBI) as a potent negative regulator of adipogenesis and modulator of autocrine/paracrine adipogenic factors. *Diabetes* 2012, 61: 124-136.
161. Dooley S, ten Dijke P. TGF- β in progression of liver disease. *Cell Tissue Res.* 2012, 347, 245-256.
162. Dzieran J, Fabian J, Dooley S, Meindl-Beinker NM, *et al.* Comparative Analysis of TGF- β /Smad Signaling Dependent Cytostasis in Human Hepatocellular Carcinoma Cell Lines. *PLoS One* 2013, 8(8): e72252.
163. Meyer C, Liu Y, Kaul A, Peipe I, Dooley S. Caveolin-1 abrogates TGF- β mediated hepatocyte apoptosis. *Cell Death Dis.* 2013, 4(1): e466
164. Dropmann A, Dediulia T, Katja Breilkopf-Heinlein, Dooley S, Meindl-Beinker NM, *et al.* TGF- β 1 and TGF- β 2 abundance in liver diseases of mice and men. *Oncotarget* 2016, 7, 19499–19518.
165. Zhang L, Huang H, ten Dijke P, *et al.* RNF12 controls embryonic stem cell fate and morphogenesis in zebrafish embryos by targeting Smad7 for degradation. *Mol. Cell.* 2012, 46, 650-661.
166. Derynck R, Akhurst RJ. Differentiation plasticity regulated by TGF-beta family proteins in development and disease. *Nat. Cell Biol.* 2007, 9, 1000–1004.
167. Dalal BI, Keown PA, Greenberg AH. Immunocytochemical localization of secreted transforming growth factor-beta 1 to the advancing edges of primary tumors and to lymph node metastases of human mammary carcinoma. *Am. J. Pathol.* 1993, 143, 381–389.
168. Arteaga CL. Inhibition of TGFbeta signaling in cancer therapy. *Curr. Opin. Genet. Dev.* 2006, 16, 30–37.
169. Wrzesinski SH, Wan YY, Flavell RA. Transforming growth factor- beta and the immune response: implications for anticancer therapy. *Clin. Cancer Res.* 2007, 13, 5262–5270
170. Loeys BL, Schwarze U, Manouvrier S, *et al.* Aneurysm syndromes caused by mutations in the TGF-beta receptor. *N. Engl. J. Med.* 2006, 355, 788–798.

171. Aden DP, Fogel A, Plotkin S, *et al.* Controlled synthesis of HBsAg in a differentiated human liver carcinoma-derived cell line. *Nature* 1979, 282, 615-616.
172. Knowles BB, Howe CC, Aden DP. Human hepatocellular carcinoma cell lines secrete the major plasma proteins and hepatitis B surface antigen. *Science* 1980, 209, 497-499.
173. Doi I. Establishment of a cell line and its clonal sublines from a patient with hepatoblastoma. *Gann* 1976, 67, 1-10.
174. Laurent T, Murase D, Tsukioka S, *et al.* A novel human hepatoma cell line, FLC-4, exhibits highly enhanced liver differentiation functions through the three-dimensional cell shape. *J. Cell. Physiol.* 2012, 227, 2898-2906.
175. Hasumura S, Sujino H, Nagamori S, Kameda H. Establishment and characterization of a human hepatocellular carcinoma cell line JHH-4. *Hum. Cell.* 1988, 1, 98-100.
176. Doi I, Namba M, Sato J. Establishment and some biological characteristics of human hepatoma cell lines. *Gann* 1975, 66, 385-392.
177. DuBridges RB, *et al.* Analysis of mutation in human cells by using an Epstein-Barr virus shuttle system. *Mol. Cell Biol.* 1987, 7, 379-387.
178. Pear WS, *et al.* Production of high-titer helper-free retroviruses by transient transfection. *Proc. Natl. Acad. Sci. USA.* 1993, 90, 8392-8396.
179. Korchynskiy O, ten Dijke P. Identification and functional characterization of distinct critically important bone morphogenetic protein-specific response elements in the Id1 promoter. *JBC* 2002, 277, 4883-4891.
180. Roessler S, Jia HL, Budhu A, Forgues M, Ye QH, Lee JS, Thorgeirsson SS, Sun Z, Tang ZY, Qin LX, Wang XW. A unique metastasis gene signature enables prediction of tumor relapse in early-stage hepatocellular carcinoma patients. *Cancer Res.* 2010, 70, 10202-10212.
181. Jia HL, Ye QH, Wang XW, *et al.* Gene expression profiling reveals potential biomarkers of human hepatocellular carcinoma. *Clin. Cancer Res.* 2007, 13, 1133-1139.
182. Lee JS, Chu IS, Thorgeirsson SS, *et al.* Application of comparative functional genomics to identify best-fit mouse models to study human cancer. *Nat. Genet.* 2004, 36, 1306-1311.
183. Neumann O, Kesselmeier M, Longerich T, *et al.* Methylome analysis and integrative profiling of human HCCs identify novel protumorigenic factors. *Hepatology* 2012, 56, 1817-1827.
184. Shimokawa K, Mogushi K, Tanaka H, *et al.* iCOD: an integrated clinical omics database based on the systems-pathology view of disease. *BMC Genomics* 2010, 11, S19.
185. Lee JS, Heo J, Libbrecht L, Thorgeirsson SS, *et al.* A novel prognostic subtype of human hepatocellular carcinoma derived from hepatic progenitor cells. *Nat. Med.* 2006, 12, 410-416.
186. De Minicis S, Seki E, Schwabe RF, *et al.* Gene expression profiles during hepatic stellate cell activation in culture and in vivo. *Gastroenterology* 2007, 132, 1937-1946.

187. Camp RL, Dolled-Filhart M, Rimm DL. X-tile: a new bio-informatics tool for biomarker assessment and outcome-based cut-point optimization. *Clin. Cancer Res.* 2004, 10, 7252-7259.
188. Staib F, Thorgeirsson SS, Teufel A, *et al.* CellMinerHCC: a microarray-based expression database for hepatocellular carcinoma cell lines. *Liver Int.* 2014, 34, 621-631.
189. Ghafoory S, Dooley S, Wöfl S, *et al.* A fast and efficient polymerase chain reaction-based method for the preparation of in situ hybridization probes. *Histopathology* 2012, 61, 306-313.
190. Dooley S, Hamzavi J, Ciuculan L, *et al.* Hepatocyte-specific Smad7 expression attenuates TGF-beta-mediated fibrogenesis and protects against liver damage. *Gastroenterology* 2008, 135, 642-659.
191. van Zijl F, Zulehner G, Petz M, *et al.* Epithelial-mesenchymal transition in hepatocellular carcinoma. *Future Oncol.* 2009, 5, 1169-1179.
192. Godoy P, Hengstler JG, Ilkavets I, *et al.* Extracellular matrix modulates sensitivity of hepatocytes to fibroblastoid dedifferentiation and transforming growth factor beta-induced apoptosis. *Hepatology* 2009, 49, 2031-2043.
193. Schuster N, Kriegstein K. Mechanisms of TGF-beta-mediated apoptosis. *Cell Tissue Res.* 2002, 307, 1-14.
194. Mamiya T, Yamazaki K, Masugi Y, *et al.* Reduced transforming growth factor-beta receptor II expression in hepatocellular carcinoma correlates with intrahepatic metastasis. *Lab. Invest.* 2010, 90, 1339-1345.
195. Zhang H, Ozaki I, Mizuta T, *et al.* Involvement of programmed cell death 4 in transforming growth factor-beta1-induced apoptosis in human hepatocellular carcinoma. *Oncogene* 2006, 25, 6101-6112.
196. Inagaki M, Moustakas A, Lin HY, *et al.* Growth inhibition by transforming growth factor beta (TGF-beta) type I is restored in TGF-beta-resistant hepatoma cells after expression of TGF-beta receptor type II cDNA. *Proc. Natl. Acad. Sci. USA* 1993, 90, 5359-5363.
197. Lee D, Chung YH, Kim JA, *et al.* Transforming growth factor beta 1 overexpression is closely related to invasiveness of hepatocellular carcinoma. *Oncology* 2012, 82, 11-18.
198. Matsuzaki K, Date M, Furukawa F, *et al.* Autocrine stimulatory mechanism by transforming growth factor beta in human hepatocellular carcinoma. *Cancer Res.* 2000, 60, 1394-1402.
199. Ciribilli Y, Singh P, Borlak J, *et al.* Decoding c-Myc networks of cell cycle and apoptosis regulated genes in a transgenic mouse model of papillary lung adenocarcinomas. *Oncotarget* 2015, 6, 31569-31592.
200. Wang HG, Reed JC. Mechanisms of Bcl-2 protein function. *Histol. Histopathol.* 1998, 13, 521-530.
201. Martin TA, Ye L, Jiang WG, *et al.* Cancer invasion and metastasis: molecular and cellular perspective. *Metastatic Cancer: Clinical and Biological Perspectives edited by Rahul Jandial.* 2013, Landes Bioscience.
202. Ono M, Torisu H, Fukushi J, *et al.* Biological implications of macrophage infiltration in human tumor angiogenesis. *Cancer Chemo. Pharmacol.* 1999, Volume 43, Supplement 1, pp S69–S71.

203. Chu CY, Chang CC, Prakash E, Kuo ML. Connective tissue growth factor (CTGF) and cancer progression. *J. Biomed. Sci.* 2008, 15, 675-685.
204. Mazzocca A, Fransvea E, Giannelli G, *et al.* Down-regulation of connective tissue growth factor by inhibition of transforming growth factor beta blocks the tumor-stroma cross-talk and tumor progression in hepatocellular carcinoma. *Hepatology* 2010, 51, 523-534.
205. Yamaguchi R, Yano H, Kojiro M, *et al.* Expression of vascular endothelial growth factor in human hepatocellular carcinoma. *Hepatology* 1998, 28, 68-77.
206. Thieringer FR, Maass T, Teufel A, *et al.* Liver-specific overexpression of matrix metalloproteinase 9 (MMP-9) in transgenic mice accelerates development of hepatocellular carcinoma. *Mol. Carcinog.* 2012, 51, 439-448.
207. Chen R, Cui J, Ren Z, *et al.* The significance of MMP-9 over MMP-2 in HCC invasiveness and recurrence of hepatocellular carcinoma after curative resection. *Ann. Surg. Oncol.* 2012, 19, Suppl. 3, S375-384.
208. Fischer AN, Herrera B, Mikula M, *et al.* Integration of Ras subeffector signaling in TGF-beta mediated late stage hepatocarcinogenesis. *Carcinogenesis* 2005, 26, 931-942.
209. Luedde T, Schwabe RF. NF- κ B in the liver--linking injury, fibrosis and hepatocellular carcinoma. *Nat. Rev. Gastroenterol. Hepatol.* 2011, 8, 108-118.
210. Luedde T, Trautwein C. Intracellular survival pathways in the liver. *Liver Int.* 2006, 26, 1163-1174.
211. Lin A. Activation of the JNK signalling pathway: breaking the brake on apoptosis. *Bioessays* 2003, 25, 17-24.
212. Kennedy NJ, Davis RJ. Role of JNK in tumour development. *Cell Cycle* 2003, 2, 199-201.
213. Iyoda K, Sasaki Y, Hayashi N, *et al.* Involvement of the p38 mitogen-activated protein kinase cascade in hepatocellular carcinoma. *Cancer* 2003, 97, 3017-3026.
214. Schmitz KJ, Wohlschlaeger J, Baba A, *et al.* Activation of the ERK and AKT signalling pathway predicts poor prognosis in hepatocellular carcinoma and ERK activation in cancer tissue is associated with hepatitis C virus infection. *J. Hepatol.* 2008, 48, 83-90.
215. Chen JS, Wang Q, Zhang LJ, *et al.* Involvement of PI3K/PTEN/AKT/mTOR pathway in invasion and metastasis in hepatocellular carcinoma: Association with MMP-9. *Hepatol. Res.* 2008, 39, 177-186.
216. Bertran E, Crosas-Molist E, Sancho P, Caja L, Lopez-Luque J, Navarro E, Egea G, Lastra R, Serrano T, Ramos E and Fabregat I. Overactivation of the TGF- β pathway confers a mesenchymal-like phenotype and CXCR4-dependent migratory properties to liver tumor cells. *Hepatology*, 2013, 58: 2032-2044.
217. Pikarsky E, Porat RM, Stein I, Abramovitch R, Amit S, Kasem S, Gutkovich-Pyest E, Urieli-Shoval S, Galun E, Ben-Neriah Y. NF- κ B functions as a tumour promoter in inflammation-associated cancer. *Nature* 2004, 431:461-466.
218. Pusterla T, Nemeth J, Stein I, Wiechert L, Knigin D, Marhenke S, Longerich T, Kumar V, Arnold B, Vogel A, Bierhaus A, Pikarsky E, Hess J, *et al.* Receptor for advanced glycation endproducts (RAGE) is a key regulator of oval cell activation and inflammation-associated liver carcinogenesis in mice. *Hepatology* 2013, 58:363-373.

219. Murakami H, Sanderson ND, Nagy P, Marino PA, Merlino G, Thorgeirsson SS. Transgenic mouse model for synergistic effects of nuclear oncogenes and growth factors in tumorigenesis: interaction of c-myc and transforming growth factor alpha in hepatic oncogenesis. *Cancer Res.* 1993, *53*:1719–1723.
220. Hauptenthal J, Bihrer V, Korkusuz H, Kollmar O, Schmithals C, Kriener S, Engels K, Pleli T, Benz A, Canamero M, Longerich T, Kronenberger B, Richter S, et al. Reduced efficacy of the Plk1 inhibitor BI 2536 on the progression of hepatocellular carcinoma due to low intratumoral drug levels. *Neoplasia* 2012, *14*:410–419.
221. Ghafoory S, Mehrabi A, Hafezi M, Cheng X, Breitkopf-Heinlein K, Hick M, Huichalaf M, Herbel V, Saffari A, Wöfl S. Nuclear accumulation of CDH1 mRNA in hepatocellular carcinoma cells. *Oncogenesis* 2015, *1*, 4:e152.
222. Sanjabi S, Zenewicz LA, Kamanaka M, Flavell RA. Anti- and Pro-inflammatory Roles of TGF- β , IL-10, and IL-22 In Immunity and Autoimmunity. *Current opinion in pharmacology* 2009, *9*(4):447-453.
223. Torre LA, Bray F, Siegel RL, Ferlay J, Lortet-Tieulent J and Jemal A. Global cancer statistics, 2012. *CA: A Cancer Journal for Clinicians*, 2012, *65*: 87–108.
224. Sato Y, Harada K, Nakanuma Y, et al. Epithelial-Mesenchymal Transition Induced by Transforming Growth Factor- β 1/Snail Activation Aggravates Invasive Growth of Cholangiocarcinoma. *Am J Pathol.* 2010, *177*(1): 141–152.
225. Feuer R, Vlaic S, Arlt J, Sawodny O, Dahmen U, Zanger UM, Thomas M. LEMming: A Linear Error Model to Normalize Parallel Quantitative Real-Time PCR (qPCR) Data as an Alternative to Reference Gene Based Methods. *PLoS One.* 2015;*10*:e0135852.

LIST OF FIGURES

| | | |
|-------------|---|----|
| Figure 1.1 | Schematic representation of liver cancer formation | 1 |
| Figure 1.2 | TGF- β 1 production | 9 |
| Figure 1.3 | Canonical and non-canonical TGF- β signalling | 10 |
| Figure 1.4 | The ambiguous role of TGF- β in cancer | 13 |
| Figure 1.5 | BAMBI silencing mechanism | 16 |
| Figure 2.1 | PCR for detection of mycoplasma contamination | 35 |
| Figure 2.2 | Figure from Corning protocol | 37 |
| Figure 2.3 | Disposition of the wounds in the plate | 38 |
| Figure 2.4 | Illustration of the cell migration assay protocol | 40 |
| Figure 2.5 | Illustration of the cell invasion assay protocol | 41 |
| Figure 2.6 | Schematic overview of the screening | 52 |
| Figure 3.1 | BAMBI is upregulated in HCC publicly available cohorts | 54 |
| Figure 3.2 | Fluidigm qRT-PCR assessed BAMBI expression levels in MDR2-KO murine model | 56 |
| Figure 3.3 | Fluidigm qRT-PCR assessed BAMBI expression levels in DEN murine model | 57 |
| Figure 3.4 | qRT-PCR assessed BAMBI expression levels in the MDR2-KO model .. | 58 |
| Figure 3.5 | Kaplan-Meier survival analysis of patients in the GSE14520 cohort | 59 |
| Figure 3.6 | BAMBI expression in HCC cell lines from Cell Miner database..... | 60 |
| Figure 3.7 | BAMBI mRNA levels correlate with early TGF- β gene signature cell lines | 61 |
| Figure 3.8 | ISH and IHC images of HCC patient serial sections at different levels of magnification | 62 |
| Figure 3.9 | HLE cells infected with lentiviral constructs showed BAMBI mRNA accumulation in the nucleus | 63 |
| Figure 3.10 | HLE cells infected with adenoviral constructs showed BAMBI mRNA accumulation in the nucleus | 64 |
| Figure 3.11 | BAMBI modulation in HLE and Hep3B cells affected SMAD2, SMAD3 and p38 phosphorylation | 65 |
| Figure 3.12 | BMP6, BMP9 and TGF- β 1 induced BAMBI expression in Hep3B cells... | 66 |
| Figure 3.13 | BMP6, BMP9 and TGF- β 1 induced BAMBI expression in a different patron in HLE cells | 67 |

| | | |
|-------------|---|----|
| Figure 3.14 | BAMBI expression significantly correlates with TGF- β -mediated signalling downstream genes | 68 |
| Figure 3.15 | TGF- β -mediated Smad3 activation is reduced by BAMBI overexpression in HLE cells | 69 |
| Figure 3.16 | TGF- β -mediated Smad3 activation is enhanced by BAMBI downregulation in Hep3B cells | 70 |
| Figure 3.17 | Immunohistochemical staining of BAMBI in tumour and surrounding HCC tissues..... | 72 |
| Figure 3.18 | Immunohistochemical staining of BAMBI in the HCC tissue microarray (TMA) | 73 |
| Figure 3.19 | HCC samples classification by BAMBI staining intensity in TMA | 74 |
| Figure 3.20 | BAMBI blocks SMAD2 phosphorylation in HCC patients | 77 |
| Figure 3.21 | BAMBI downregulation decreased proliferation and viability in Hep3B cells | 79 |
| Figure 3.22 | BAMBI upregulation increased proliferation and viability in HLE cells..... | 80 |
| Figure 3.23 | Apoptosis is increased upon BAMBI downregulation in Hep3B cells | 82 |
| Figure 3.24 | BAMBI overexpression reduced the apoptosis in HLE cells..... | 83 |
| Figure 3.25 | Wound closure increases upon BAMBI overexpression and TGF- β 1 treatment..... | 85 |
| Figure 3.26 | Migration capacity increases with BAMBI overexpression and TGF- β 1 treatment..... | 86 |
| Figure 3.27 | Migration capacity accompanies BAMBI overexpression and higher PAI1 levels..... | 87 |
| Figure 3.28 | Migration decreases upon BAMBI downregulation and TGF- β 1 treatment | 88 |
| Figure 3.29 | High apoptosis levels reduce the migration capacity of H3B shRNA cells | 89 |
| Figure 3.30 | The invasive capacity of HLE cells increased upon BAMBI overexpression and TGF- β 1 treatment..... | 90 |
| Figure 3.31 | MMP9 overexpression and CTGF and VEGF induction accompany BAMBI overexpression and TGF- β 1 treatment | 91 |
| Figure 3.32 | BAMBI modulation affects other signalling pathways..... | 93 |
| Figure 4.1 | BAMBI expression in human HCC and cirrhosis stages in Oncomine® Research database | 95 |
| Figure 4.2 | Immunohistochemical staining of BAMBI in the CCA samples from the tissue microarray (TMA) | 99 |

LIST OF TABLES

| | | |
|-----------|---|----|
| Table 1.1 | TGF- β signalling regulator (TSR) candidates..... | 19 |
| Table 2.1 | Primers sets for gene specific SYBR Green real time PCR | 27 |
| Table 2.2 | Primary and secondary antibodies used for immunoblot analysis | 32 |
| Table 2.3 | Primary and secondary antibodies used for immunohistochemistry..... | 33 |
| Table 2.4 | Composition of SYBR Green Master mix for real time PCR..... | 45 |
| Table 2.5 | Composition of separating and stacking gels for SDS-PAGE gel electrophoresis | 48 |
| Table 2.6 | HCC publicly available microarray data cohorts used in the meta-analysis of TSRs expression | 53 |
| Table 3.1 | BAMBI expression in publicly available HCC cohorts | 55 |
| Table 3.2 | BAMBI expression in HCC-significant patients | 55 |
| Table 3.3 | Correlation of BAMBI expression levels with clinical-pathological characteristics in the GSE14520 cohort..... | 59 |
| Table 3.4 | BMP and TGF- β -mediated signalling downstream genes correlations with BAMBI expression in the GSE5975 and GSE14520 cohorts | 67 |
| Table 3.5 | List of inflammatory markers used for correlation with BAMBI expression | 75 |
| Table 3.6 | Positive correlations with BAMBI expression in the GSE1898, GSE5975 and GSE14520 cohorts | 75 |
| Table 3.7 | Correlation of BAMBI expression level with clinical-pathological characteristics in the tissue microarray (TMA) | 76 |
| Table 4.1 | Correlation of BAMBI expression level with the clinical-pathological characteristics of cholangiocarcinoma tissues present in the TMA | 99 |

DECLARATION

I hereby declare that this dissertation is, to the best of my knowledge and belief, a presentation of my own work, except where otherwise acknowledged.

Heidelberg, Signature

(Date)

ACKNOWLEDGEMENT

First, I wish to thank Professor Dr. Steven Dooley (Molecular Hepatology-Alcohol Associated Diseases, II. Medical Clinic, Medical Faculty of Mannheim, University of Heidelberg) for giving me the opportunity to work on several interesting topics.

I would also like to thank Dr. Isabel Fabregat (TGF- β and cancer, IDIBELL, Barcelona, Spain) for introducing me into the Marie Curie Initial Training Network and, together with Prof. Dr. Dooley, giving me the chance to work with high class specialists in the field of hepatology. The vivid discussions and the creative environment during IT-Liver meetings made the work very enjoyable.

Thanks to my colleagues from the research group Molecular Hepatology, who helped to create a wonderful atmosphere. Special thanks to Anne Dropmann for your support and many joyful professional, and personal, conversations during and outside working hours. You made my start at a new work in a foreign country easier and became a good friend. Our talks really helped me in my lowest moments during this PhD and made me rethink anytime I wanted to drop out. Thank you, Christoph Meyer. You were very helpful in my last months at work and, without being aware of it, you gave me a confirmation of my high professionalism and honesty.

Many thanks to Prof. Dr. Stefan Wöflf and all my collaborators: Prof. Dr. Cédric Coulouarn, Prof. Dr. Andreas Teufel, Prof. Dr. Peter ten Dijke, Dr. Stephanie Rössler, Dr. Shahrouz Ghafoory and Dr. Timo Itzel.

I would like to thank my fellow colleagues from the IT-Liver consortium, in particular Dr. Annalisa Addante, for filling each meeting/secondment/conference with an extremely gratifying and pleasant atmosphere. I hope we will keep in contact and build strong and profitable collaborations.

My deepest gratitude goes to my family. Thank you Marina and Vladislav (Mama and Papa) for your unconditional support and encouragement, and for providing me resources during my whole career. I really appreciate that you could give me the opportunity to follow my dreams and support me in doing so.

Last but not least, I would not have been able to write this thesis without the kind support of my husband Simon Ballmann. Thank you for your love, for your cheerful mood and for providing me a home during the writing of this thesis.

*“These are better days baby
These are better days it's true
These are better days
There's better days shining through”*

Better Days - Bruce Springsteen

